Electrodeposition of tin and tin based alloys from ionic liquids: Nanowires, thin films and macroporous structures

Doctoral thesis

To be awarded the degree
Doctor rerum naturalium (Dr. rer. nat.)

Submitted by
Amr Mohamed Wahba Elbasiony
from El-Dakahlia / Egypt

Approved by the faculty of
Natural and Materials Sciences
Clausthal University of Technology

Date of Oral Examination
23 July 2015

Chairperson of the Board of Examiners
Prof. Dr. D. E. Kaufmann

Chief Reviewer
Prof. Dr. Frank Endres

Reviewer
Prof. Dr. Arnold Adam

Electrodeposition of tin and tin based alloys from ionic liquids: Nanowires, thin films and macroporous structures

Amr Elbasiony

Abstract

During the past decade, Ionic liquids have gained massive attention as interesting electrolytes in electrochemical processes and in industry due to their unique physicochemical properties.

Tin is an important metal known for its corrosion resistance, optical properties and silver-like finish that makes it suitable for many applications such as decorations, corrosion protecting coatings, and also in lithium-ion batteries. However, the electrodeposition of tin from aqueous solutions is complicated.

- The results presented in this thesis show, for the first time, a comparative study on the electrodeposition of tin from two different ionic liquids containing the same cation namely, 1-butyl-1-methylpyrrolidinium dicyanamide ($[Py_{1,4}]$DCA) and 1-butyl-1-methylpyrrolidinium trifluoromethylsulfonate ($[Py_{1,4}]$TfO). The effect of the ionic liquid anion on the morphology of the obtained deposits was also studied by cyclic voltammetry, scanning electron microscopy (SEM), infrared (IR) spectroscopy and X-ray diffraction. The results showed that the morphology of the tin deposits changes upon changing the IL. Agglomerated tin deposits are obtained on gold and copper from $[Py_{1,4}]$TfO. Tin dendrites were obtained both from $[Py_{1,4}]$DCA and [EMIm]DCA. This study reveals that a change in the ionic composition (anion) of the IL can influence the morphology of electrodeposits of tin and presumably of other elements and compounds.
- Sn nanowires are electrodeposited from two different air- and water stable ionic liquids [EMIm]DCA and $[Py_{1,4}]$TfO each containing 0.1 M $SnCl_2$ as Sn precursor. The tin nanowires were synthesized at room temperature via a template-assisted electrodeposition

process using track etched polycarbonate membranes as templates. Gold or copper thin films were sputtered on one side of the track-etched polycarbonate template to make it conductive to be used as a working electrode. A copper layer was deposited on the sputtered side from 1 M CuCl/[EMIm]DCA to act as a supporting layer for the Sn nanowires.

- The electrodeposition of Zn-Sn films as well as of free-standing nanowires from $[Py_{1,4}]TfO$ ionic liquid is reported. The nanowire arrays were obtained by using polycarbonate membranes. The study includes cyclic voltammetry, chronoamperometry, X-ray diffraction, and scanning electron microscopy/energy-dispersive X-ray analyses. The results reveal that the morphology of Zn-Sn deposits shows coarse Zn particles on a Sn-rich layer, indicating the formation of Zn/Sn co-deposits. The XRD results reveal the co-deposition of Zn-Sn films. Zn-Sn nanowires with average diameters of approximately 100 nm and lengths of 5 µm were synthesized. Free-standing Zn-Sn nanowires with different lengths and a diameter of approximately 200 nm were also synthesized.
- Macroporous CuSn films as well as free standing nanowires were electrodeposited from [EMIm]DCA. A uniform periodicity of macroporous CuSn films is obtained through potentiostatic deposition at -1 V for 10 minutes. Higher potentials destroy the obtained deposits and lead to a honeycomb structure. The electrodeposition at -1 V for 15 minutes produces a three dimensional macroporous structure. Free standing CuSn nanowires were obtained via a template-assisted electrodeposition process using polycarbonate membranes as templates. The produced nanowires have an average diameter of 100 nm and an average length of 7 µm.
- Si, Sn and SiSn thin films were electrodeposited from $[Py_{1,4}]TfO$. Microcrystals of Sn were obtained by the potentiostatic deposition at -1.3 V vs Pt. White greyish Si deposits

were obtained galvanostatically at -20 μA. SiSn thin films containing tiny particles were obtained at -2 V for 1 hr while hair-like SiSn nanowires are produced when the electrodeposition process is done after running CV. Increasing the applied potential leads to the synthesis of free standing nanowires.

Content

1. Introduction

1.1 Ionic liquids

1.1.1 Definition and classifications [1-5]

An ionic liquid can be defined as an organic salt in the liquid state whose melting point is commonly below 100℃. The fact that a salt can be a liquid at low temperature can be well understood such that the charge on these ions is delocalized, causing a reduction in the crystal lattice energy of the entire salt and lowering the melting point [1,2].

Due to their physical properties such as high thermal stability, high ionic conductivity, low vapor pressure and their wide electrochemical windows, ionic liquids are considered as promising electrolytes in electrochemical processes and in industry. The ability of ionic liquids to dissolve many chemical substances makes them widely used in the fundamental electrodeposition of different metals and semiconductors [3].

Table 1.1 shows different kinds of some ionic liquid cations and anions.

Ionic liquids are often classified into several categories [4] (figure 1.1)

A) Task-specific ionic liquids [TSIL] [4,5]

They are sometimes named as multi-functional ionic liquids due to the incorporation of additional functional groups, giving new properties to the basic liquid.

The incorporation of NH_2, urea, SH or OH to the imidazolium cation can introduce catalytical activity, to mention one example [5].

Fig. 1.1. *Various classes of ionic liquids*

B) Protic ionic liquids [4]

Nowadays, this kind of ionic liquids has attracted great interest because they contain protons which make such a liquid suitable as electrolyte in fuel cells.

C) Chiral ionic liquids [4]

These ionic liquids are characterized by the presence of a chiral center in anion or cation or both. They are used usually as chiral solvents in organic synthesis.

D) Switchable polarity solvents [4]

Carbamate salts are a kind of switchable polarity solvents which have intermediate polarity between higher and lower polarity solvents, so they are very important for chemical processes that require different solvent polarity in different chemical steps.

E) Metal salt ionic liquids [4]

$AlCl_3$ combined with pyrrolidinium or imidazolium halides give liquids that are often regaded as the first generation of ionic liquids. Other systems have complexs like $[CuCl_3]^-$, $[NiCl_4]^{2-}$ as anion.

Table 1.1. *Different kinds of ionic liquids cations and anions*

Cations	Anions
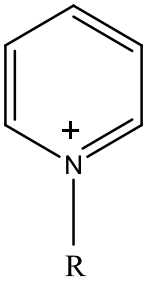 N-alkyl pyridinium 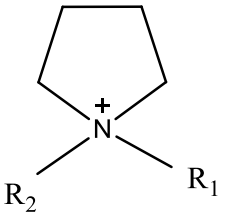 N-alkyl-N-alkyl pyrrolidinium	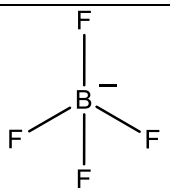 tetrafluoroborate $[BF_4]^-$ 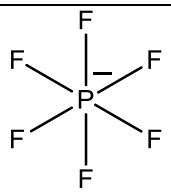 hexafluorophosphate $[PF_6]^-$
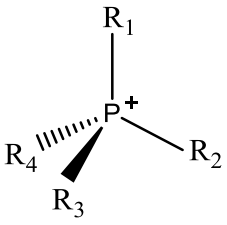 tetraalkyl phosphonium 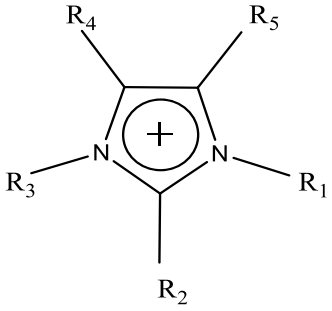 1-alkyl-3-alkylimidazolium	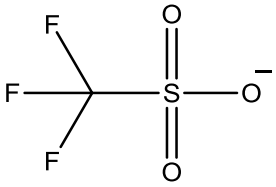 trifluoromethylsulfonate $[TFO]^-$ 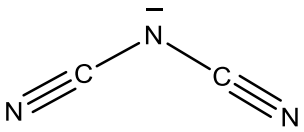 dicyanamide $[DCA]^-$
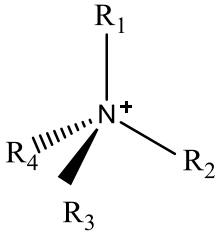 tetraalkylammonium 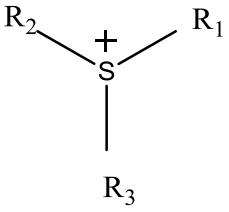 trialkylsulfonium	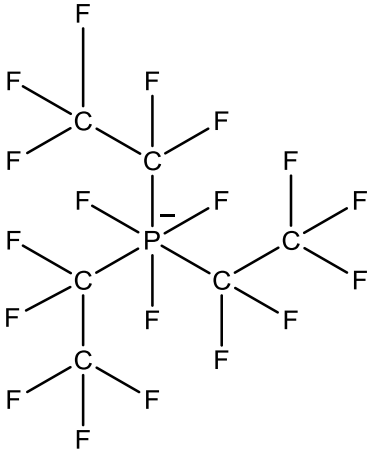 tris(pentafluoroethyl)trifluorophosphate [FAP] 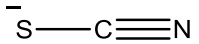 thiocyanate $[SCN]^-$

1.1.2 History of ionic liquids [6-23]

The history of ionic liquids started –more or less- in 1914 when Walden [6] succeeded to synthesise ethylammonium nitrate with the chemical formula ($[C_2H_5NH_3][NO_3]$), having a

melting point of 12 ℃. He described the physical properties of this material, made by the reaction of concentrated nitric acid with ethylamine. Of course, there was no idea -at that time- about the great potential of these new materials as variable temperature solvents for electrochemistry and many other applications.

In 1951, low temperature molten salts with haloaluminate ions were developed by Hurley and Wier [7] by the combination of 1-ethylpyridinium bromide (EtPyBr) with anhydrous aluminum chloride ($AlCl_3$). The prepared molten salt with a eutectic composition 1:2 of EtPyBr to $AlCl_3$ was used for the electroplating of aluminum at ambient temperature. However, it was highly hygroscopic and the electrodepostion process needs a dry atmosphere. Due to experimental limitations this liquid was almost forgotten for about 30 years.

In the 1970s and the 1980s $AlCl_3$ based room temperature ionic liquids [RTILs] gained a lot of interest in the field of electrochemistry. Hussey et al. and Osteryoung et al. [8–13] focused their research on the synthesis of "chloroaluminate ionic liquids" with 1-ethyl-3-methylimidazolium chloride ([EMIm]Cl) or 1-butylpyridinium chloride ($BP^+ Cl^-$) mixed with $AlCl_3$.

Such $AlCl_3$ based ionic liquids are often considered as the first generation of ionic liquids and the Lewis acidity of the liquid is controlled by changing the ratio of $AlCl_3$ to the organic salt [14]. With a molar surplus of $AlCl_3$ the liquid is a Lewis acid, it is a Lewis base with a molar surplus of the organic salt.

Koronaios et al. quantitatively measured the latent acidity of these ionic liquids and mentioned that in Lewis acid liquids, complexes of polynuclear chloroaluminates are found. Chloride and tetrachloroaluminate are present in Lewis basic systems. Neutral solutions which have a difficult to achieve equimolar ratio of $AlCl_3$ and the organic salt, have to be buffered by alkali halides like NaCl or $CaCl_2$ due to the variation in species concentration during electrochemical deposition or dissolution [15]. This change in Lewis acidity makes them suitable for different applications.

In the mid of the 1980s, the described low melting $AlCl_3$ based ionic liquids were also used as solvents for the organic synthesis [16,17], without considerable success:

Both $AlCl_3$ and the organic species are hygroscopic and absorb water rapidly leading to the formation of hydrochloric acid and oxochloroaluminates in the liquid [18].

In the case of electrochemistry elements such as Si, Ti, Ge, Ta and Nb cannot be electrodeposited as a single phase from $AlCl_3$ based ionic liquids. In acidic liquids alloys with Al will be formed, and in basic liquids the potential of deposition will be shifted due to complex formation below the cathodic limit of the liquid.

In 1992 Wilkes and Zaworotko reported on the synthesis of the first more or less air- and water stable ionic liquid [19] consisting of 1-ethyl-3-methylimidazolium cations and tetrafluroborate (BF_4^-) or hexaflurophosphate (PF_6^-) anions. These ionic liquids are often called the second generation of ionic liquids, as they are nearly Lewis neutral since the employed organic cation is considered as weak acid and the inorganic anions are considered as weak bases. In addition, they are comparably insensitive to water and can be handled under air. Later it was found that the physical and chemical properties are affected by the long time exposure to moisture, especially at higher temperature due to the hydrolysis of the anions and formation of HF [20]. Thus, the development of hydrophobic and more stable anions has attracted great interest. Trifluoromethylsulfonate ($CF_3SO_3^-$), bis(trifluoromethylsulfonyl)amide [$(CF_3SO_2)_2N^-$] and tris(trifluoromethylsulfonyl)methide [$(CF_3SO_2)_3C^-$] are more stable anions and have been developed for different ionic liquids [21–23].

This class of ionic liquids has received an extensive interest because of extraordinary physical properties, low reactivity towards water and versatility.

The low vapor pressure, chemical and thermal stability, conductivity and solubility of most elements in these ionic liquids attracted the interest of many researchers to use them in different

applications; however, the higher electrochemical window (up to 6 V) is one of the most important physical properties of ionic liquids for electrochemistry which opens the door, e.g., for the electrochemical deposition of less noble elements such as Si, Ge, Ta, Se, Al and many other ones that cannot be obtained from aqueous solutions at ambient temperatures.

1.1.3 Significant importance of ionic liquids [24-27]

Nowadays, there are more than 1000 of synthesized RTILs available in literature and the research activities are still increasing [24,25]. During the 1990s there were only 40 articles per year about ionic liquids [26], in 2002 there were about 500 articles while in 2005 the number exceeded 1500 articles per year. The research area of ionic liquids expanded more and more till it reached about 5,000 articles per year in 2010 and more than 6,500 articles in 2012 and in 2013 it's almost nearby 7,000 articles related to ionic liquid per year [27].

Figure 1.2 shows the annual growth of ionic liquids related articles per year from 2000 till 2014.

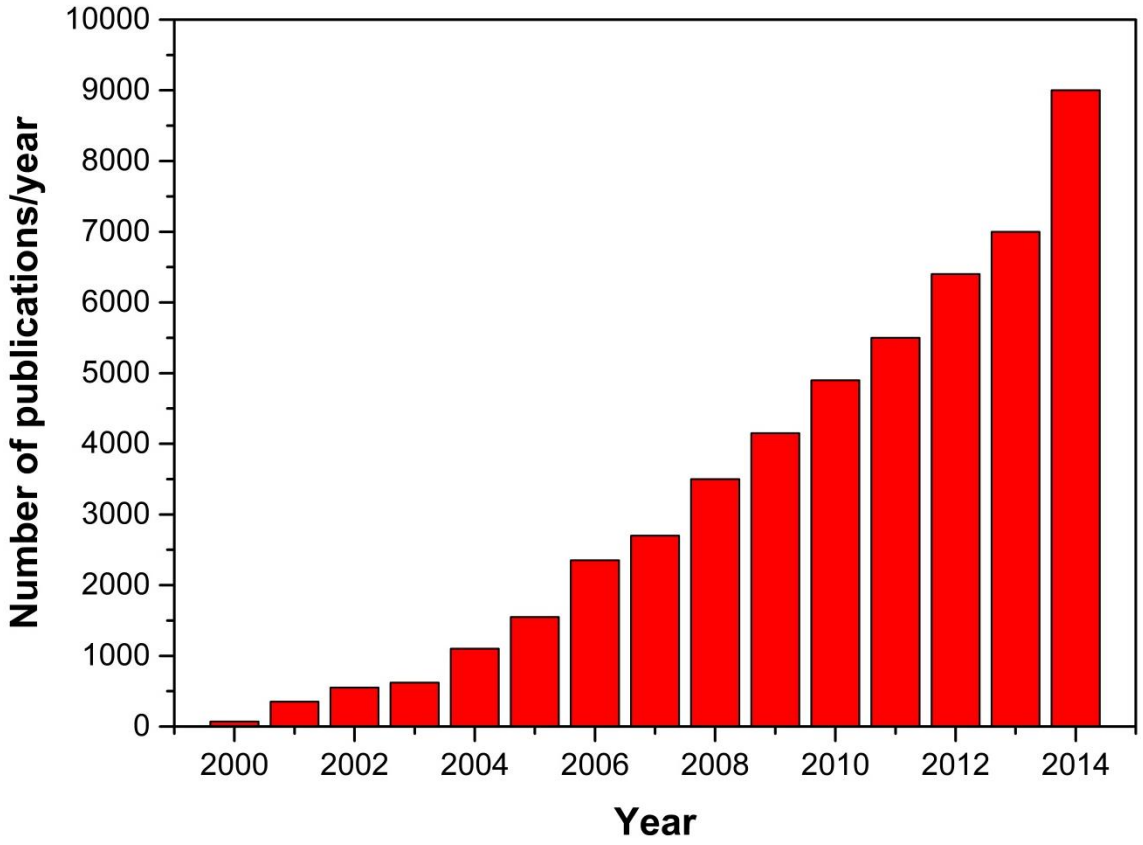

Fig. 1.2. *Annual growth of the ILs publication from 2000 till 2014 updated by the ISI web of science*

1.1.4 **Properties of ionic liquids** [28-31]

Ionic liquids, as solvents, exhibit a unique variety of physicochemical properties, such as low melting points, low vapor pressures, high chemical and thermal stability and good conductivity. Some ionic liquids are used in both organic and inorganic synthesis, some are considered as "green solvents". The application of ionic liquids in green chemistry was first introduced by Seddon et al. [28] as he wrote *"its implementation will lead to cleaner environment and more cost-effective use of starting materials"*. Due to their low vapor pressure they can be used under high-vacuum in purification and distillation processes of organic/organometallic compounds overcoming the - to some extent - problems of organic solvents volatility that's why they are environmentally friendly solvents [29–31].

Currently, ionic liquids are widely used in different chemical applications. They are of great interest in the field of electrochemistry as novel solvents due to their wide electrochemical window (up to ~ 6V), high thermal stability and good conductivity.

From ionic liquids, metals, their alloys and semiconductors can be electrodeposited.

The properties of ionic liquids are shortly summarized in the following sub-sections.

1.1.4.1 **Thermal stability** [26, 30, 32, 33]

The thermal stability of ionic liquids depends on their ion structure and is limited by the strength of their heteroatom-carbon and their heteroatom-hydrogen bonds, respectively [30]. It was reported that some ionic liquids which contain tetrafluoroborate anions are thermally stable at high temperatures, depending on the alky chain length. For example, 1-ethyl-3-methylimidazolium tetrafluoroborate and 1-butyl-3-methylimidazolium tetrafluoroborate were reported to be stable up to 445 and 423 ℃ respectively, and 1,2-dimethyl-3-propylimidazolium bis(trifluoromethylsulfonyl) is thermally stable up to 457 ℃ [32] a least for a short time. Today it is known that the tolerance of these ionic liquids to such high temperatures is limited to a short time only, and decomposition will occur if they are exposed to such temperatures for a longer time [26]. Nevertheless, thermal stability together with a negligible vapor pressure makes ionic liquids suitable solvents for the electrodeposition of elements such as Nb, V, Ta that cannot be deposited from aqueous or organic solutions. Due to its high thermal stability combined with low vapor pressure, Wilkes et al suggested ionic liquids to be used as heat transfer fluids in large scale solar energy collectors [33].

1.1.4.2 Low melting points [34, 35]

The melting point of any salt is determined by the electrostatic forces between its cations and anions. In the case of molten salts such as NaCl the interactions between Na^+ and Cl^- is very high leading to a high melting point. This interaction can be expressed by the lattice energy of the salts [34].

$$E = K\frac{Q1Q2}{d}$$

Where K is the Madelung constant, Q1 and Q2 are the charges of ions and d is the interionic distance between ions. With larger ion size such as in ionic liquids, the interionic distance d is large which leads to a lower lattice energy and low melting points [34].

The chemical composition of ionic liquids plays an important role to keep them liquid at room temperature or even at lower temperatures. The melting points of ionic liquids often decreases with the increase in the alkyl chain length and increases with the increase of the degree of symmetry [35]. Molten salts such as sodium chloride and lithium chloride have high melting points 801 and 614 ℃, respectively as they contain symmetric inorganic ions compared to the asymmetric organic cations of ionic liquids.

1.1.4.3 Viscosity [21, 36]

The viscosity of any solvent depends on the size of its molecules or ions. Since ionic liquids contain ions of large size in most cases, they are generally more viscous than common molecular solvents. Their viscosity varies between 10 mPa·s and 500 mPa·s at room temperature [36]. In electrochemical studies the viscosity of solvents is a very important factor as it has a very strong effect on the mass transfer in the solution.

The temperature is also an important factor that affects the viscosity of ionic liquids. An increase from 20 ℃ to 100 ℃ usually decreases the viscosity by factor of 10, see example [36].

The viscosity is also determined by hydrogen bonding and Van der Waals forces. As an example for the effect of hydrogen bonding on the viscosity of ionic liquids Bonhôte et al. reported [21] that ionic liquids based on the weakly basic bis(trifluoromethylsulfonyl)amide $[TFSA]^-$ are less viscous than those with BF_4^- and PF_6^- anions because of their high relative basicity and their ability to form hydrogen bonds.

Due to Van der Waal forces longer alkyl chains in the cation leads to an increase in the viscosity [21].

1.1.4.4 Ionic conductivity [23, 37]

The conductivity of solvents that are used in electrochemical processes has quite a high importance. As mentioned in the definition section, ionic liquids are entirely consisting of ions which are capable of carrying and transporting charges, thus all ionic liquids are conductive with the ions acting as charge carrier. The degree of conductivity depends on the ionic liquid viscosity and thus it's highly dependent on the temperature. At room temperature the conductivity of ionic liquids is in the range between 0.1–18 mS/cm [37].

Since the ion mobility of ionic liquids is often low at room temperature, the conductivity of ionic liquids is usually lower than the one of concentrated aqueous solutions.

Ionic liquids with imidazolium cations have a higher conductivity (10 mS/cm) than those with tetraalkylammonium, pyrrolidinium, piperidinium or pyridinium cations (0.1-5 mS/cm). As an explanation the imidazolium cation increases the conductivity due to its ring flatness [23]. Some details about the ionic liquid conductivity and the parameters affecting it are summarized in [37].

1.1.4.5 Electrochemical window [1, 23, 38]

The potential window of any electrolyte solution is an important factor for electrochemical processes. The electrochemical window is determined by the oxidation-reduction of the electrolyte species at an electrode or by the electrodes, so it's not only controlled by the chemical structure but also governed by the electrode substrate materials and many other factors such as temperature, pressure and impurities.

For aqueous solutions, the electrochemical window is thermodynamically only 1.23 V at 25 ℃. Thus there is a limitation in the electrodeposition process of many elements due to the evolution of hydrogen and oxygen. The electrochemical windows of ionic liquids are usuallydetermined by the reduction of the organic cation in the cathodic regime and by the oxidation of the anion or the oxidation of the substrate in the anodic regime. Some ionic liquids have electrochemical windows of up to 6V which is much wider than in aqueous solutions, making them suitable for the electrodeposition of many metals, semiconductors, alloys and conductive polymers [1].

The purity of ionic liquids is an important factor that affects oxidation-reduction processes, as a consequence the presence of halides or alkali metal ions such as Li^+ in the ionic liquid would reduce its electrochemical window. Moreover, the reference / quasi reference electrode which is often used in electrochemical processes plays an important role in the determination of the potential values in addition to the working substrate material.

Borissenko et al. [38] reported that 1-butyl-1-methylpyrrolidinium bis(trifluoromethylsulfonyl)amide $[Py_{1,4}]$TFSA has an electrochemical window of 6 V on Au(111) substrate. However, the authors in [23] showed that the electrochemical window of the same ionic liquid on glassy carbon is 5.5 V using Pt as quasi reference electrode with a lower limit of -3.2 V vs. ferrocene/ferrocinium as quasi reference electrode.

This electrochemical stability of ionic liquids makes them - in contrast to many other solvents - suitable electrolytes for the electrochemical deposition of metals and semiconductors such as Ta, Ge or Si which cannot be deposited as pure elements from aqueous or organic solutions.

A brief summary on the electrochemical windows of ionic liquids and materials or elements which can be electrochemically synthesized in them is shown in figure 1.3.

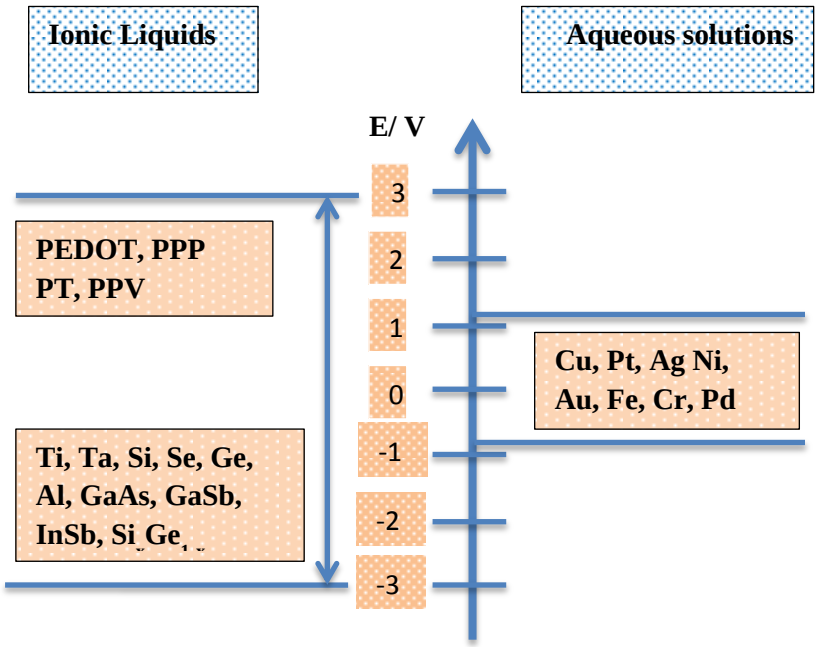

Fig. 1.3 *The electrochemical windows of aqueous solutions (water) and ionic liquids with the possible conducting polymers, elements or alloys that can be electrochemically synthesized in them. PPP: poly(paraphenylene), PT: polythiophene, PPV: poly(p-phenylene vinylene), PEDOT poly(3,4-ethylenedioxythiophene).*

1.1.4.6 Solvation and solubility [5, 39]

The solvation power of ionic liquids is very important for both fundamental and applied studies. Ionic liquids can be regarded as polar solvents as they solely consist of ions. However, they both dissolve polar and non-polar solutes.

The polarity of solvents is a very important factor which enables to determine their ability to dissolve a certain solute; therefore it can be defined as the overall solvation capability of solvent. In a chemical meaning this expresses the ability of solvent molecules (or ions) to associate with solute molecules (or ions).

In some cases, the solubility of some salts in ionic liquids is low due to the weak coordinating ability of the bulky cations and anions forming ionic liquids which hinder the breakdown of the electrostatic interactions between metal salts. However, if the temperature of the system is increased the solubility of salts is often enhanced.

Changing the ionic liquid polarity is also an important factor which helps to increase the solvation power. By reducing e.g. the alkyl chain length in the cation the polarity of the ionic liquid will increase and its ability to dissolve polar compounds will also increase. Using ionic liquids with long alkyl chains will reduce the polarity and the liquids become more suited to dissolve non-polar compounds.

Task specific ionic liquids [TSIL], as has been mentioned before, are a class of ionic liquids in which e.g. an additional functional group will complex metal ions and thus increase the solubility of metal salts [5].

$AlCl_3$ based ionic liquids have been reported to have a flexible solvating ability because of their capability to be either Lewis acid or Lewis base according to the molar ratio of $AlCl_3$ to the organic salt. By adding an excess of the organic salt the overall mixture becomes a Lewis base, as mentioned above. An excess of $AlCl_3$ would render the mixture Lewis acid due to the formation

of coordinately unsaturated aluminum species and the buffering of 1:1 molar ratio of the mixture with NaCl would produce neutral liquids [39].

This change in the Lewis acidity and basicity of ionic liquids enables them to dissolve a wide range of both organic and inorganic salts.

1.1.4.7 **Density** [1, 40]

The density of ionic liquids is usually higher than the density of water and the values are in the range of 1.0-1.6 g cm^{-3} depending on the individual ions.

Dzyuba et al. [40] reported that the density decreases by increasing the alkyl chain length of imidazolium cations. The density also varies with the type of the ions where the density of aromatic onium salts is e.g. higher than that one of aliphatic ammonium salts.

As an example, the densities of liquids with 1-ethyl-3-methylimidazolium $[EMIm]^+$ having different anions is in the order

$CH_3SO_3^- < BF_4^-$ and $CF_3COO^- < CF_3SO_3^- < (CF_3SO_2)_2N^- < (C_2F_5SO_2)_2N^-$ [1].

1.1.4.8 **Effect of impurities in ionic liquids** [36, 41, 42]

For electrochemical studies, the presence of impurities even in low concentrations is an important issue due to a great influence on electrochemical processes. The presence of some halides or organic impurities in ionic liquids affects significantly their physical properties. Therefore, it is important to purify ionic liquids and remove such impurities.

From the synthesis process of ionic liquids halide impurities can be introduced. They can affect the viscosity of ionic liquids and their electrochemical windows.

Seddon et al. studied the effect of impurities on the physical properties of several imidazolium tetrafluoroborate ionic liquids and they reported that even a low concentration of halide ions

causes a considerable increase in the viscosity [41]. However, the presence of water or molecular solvents rather decreases the viscosities of the mentioned ionic liquids [41]. They also noted that the melting point of these ionic liquids which has been reported in earlier studies in the range 5.8-15℃ is clearly varied by impurities [41].

Moreover, the reduction and oxidation of water will narrow the electrochemical window of the ionic liquid and the oxidation of halide ions in the anodic regime can have an impact on the quality of deposits.

The presence of water, chloride and 1-methylimidazole in 1-butyl-3-methylimidazolium tetrafluoroborate ([BMIm]BF_4) alters size and shape of silver nanoparticles made in the liquid. Trace amount of these impurities create polydisperse and irregularly shaped ensembles of both large and small particles and also negatively impact the stabilization of the resulting silver nanoparticles [42].

Ionic liquids are unlike other molecular organic solvents: they cannot be purified by distillation due to their negligible vapor pressures. Therefore other techniques must be used to remove these impurities. One early example is the precipitation of such halides with silver nitrate. Another technique for the purification of ionic liquids is chromatography.

For water immiscible ionic liquids the impurity level can be lowered by extracting the ionic liquid with an organic solvent and washing the whole solution with deionized water. Subsequently the solvent can be removed by evaporation using a rotary evaporator and finally the ionic liquid can be heated under vacuum to remove water traces.

In water miscible ionic liquids such as imidazolium tetrafluoroborates, alkylation reactions using halide free alkylating agents are used to get halide free ionic liquids [36].

Although the presence of small amounts of water may not always have a significant effect, the amount of water should at least be determined and reported. To allow comparability Karl Fischer titration is a common technique to determine the water amount.

1.1.5 Applications of ionic liquids [43-72]

Ionic liquids are discussed to many different applications such as pharmaceuticals [43,44], food and bioproducts [45,46] and fundamental research [47] because of their physico-chemical properties. They are suitable for many applications such as catalysis and surface chemistry [48–53], nuclear fuel reprocessing [54–59], liquid/liquid extractions, photochemistry [60–62], electroanalytical applications and different processes in chemical industry [63–69].

The potential of ionic liquids as electrolytes in electrochemistry is based on their non-flammability, high ionic conductivity, viscosity and electrochemical and thermal stability. Thus ionic liquids are discussed for batteries, capacitors, fuel cells, photovoltaics, actuators and electrochemical sensors [70].

Furthermore, ionic liquids enable the electrochemical deposition of noble metals, alloys and also of conducting polymers [71,72].

1.1.5.1 Electrodeposition of metals and alloys [71, 73-123]

The electrodeposition of aluminum from the so called first generation ionic liquids, also known as “room-temperature molten salts” or “ambient temperature molten salts” is comparably easy [73–78]. Also many relatively noble elements such as copper, silver, gold and platinum can be deposited from these first generation ionic liquids. However reactive elements such as silicon, lithium, germanium and others cannot be electrodeposited from these ionic liquid without the codeposition of aluminum.

Lipsztajn and Osteryoung reported the first electrochemical deposition of Li from 1-ethyl-3-methyl-imidazolium chloride/$AlCl_3$ [79]. Li was later also electrodeposited from 1-ethyl-3-methyl-imidazolium tetrachloroaluminate by Piersma et al. on platinum, glassy carbon and tungsten using molybdenum and platinum foils as counter electrodes [80].

Sodium [81,82], indium [83,84], gallium [85], tin [86], antimony [87,88] and tellurium [89] were also electrodeposited from $AlCl_3$ based ionic liquids

After the introduction of air- and water-stable ionic liquids in 1990s which possess wide electrochemical windows up to 6V combined with extremely low vapor pressures, many reactive elements such Li, Si, Ta, Ge, Nb and other elements could be electrodeposited as pure elements. These ionic liquids are often called the second and third generation of ionic liquids, as mentioned above.

Zinc and zinc alloys were electrodeposited from $ZnCl_2$/[EMIm]Cl where the concentration of $ZnCl_2$ is more than 33% [90–92]. Some types of steel cannot be zincated in aqueous solution due to hydrogen embrittlement. Such ionic liquid baths, however, suggest a viable alternative route. Urea and ethylene glycol/choline chloride ionic liquid like electrolytes were proposed by Abbott et al. for the deposition of Zn [93].

Copper which is one of the most widely used elements with several industrial applications, has been electrochemically deposited from different ionic liquids such as 1-ethyl-3-methyl imidazolium tetrafluoroborate ([EMIm]BF_4), trimethyl-n-hexylammonium bis (trifluoromethylsulfonyl)amide ([TMHA]TFSA) and 1-butyl-1-methylpyrrolidinium bis (trifluoromethylsulfonyl) amide ([$Py_{1,4}$]TFSA) [94–96].

Very pure and adherent cadmium was electrodeposited from [EMIM]BF_4 containing $CdCl_2$ on tungsten [97]. The codeposition of Cd and Zn can be obtained from acidic zinc chloride-1-ethyl-

3-methylimidazolium chloride ($ZnCl_2$–[EMIm]Cl) ionic liquids where the content of cadmium can be increased by increasing the $CdCl_2$ concentration [98].

In 2004 Abbott et al. reported the electrochemical deposition of chromium in a mixture of choline chloride and chromium(III) chloride hexahydrate and the addition of LiCl lead to nanocrystalline black chromium films [99,100] .

Palladium is well known for its absorbtion of hydrogen; therefore the deposition of palladium from aqueous solutions yields only brittle deposits. The deposition from ionic liquids prevents the hydrogen embrittlement, thus compact adherent deposits of Pd and many of its alloys such as Pd–Ag [101], Pd–Au [102] and Pd–In [103] can be electrodeposited from basic 1-ethyl-3-methylimidazolium chloride/tetrafluoroborate. Antimony and its alloys can be electrodeposited from the same basic ionic liquid ([EMIm]Cl-BF_4) [104,105].

The electrodeposition of silver from $AlCl_3$ based ionic liquids has been reported in many papers [106–108]. However, as mentioned before, the contamination of Al in the final deposits makes these ionic liquids not suitable enough for silver deposition. ([EMIm]BF_4) was considered as a better alternative for silver electroplating producing pure silver deposits [109].

Electrodeposition of silver from 1-butyl-3-methylimidazolium hexafluorophosphate ([BMIm]PF_6) has also been reported [71].

Shiny and dense deposits of Pt with a tiny particle size were reported from [BMIm]BF_4 and [BMIm]PF_6 [110]. The electrodeposition of Al from ionic liquids which contains more hydrophobic anions such as $[TFSA]^-$ has also been studied [111,112]. Magnesium electrodeposition from [BMIm]BF_4 and 1-butyl-1-methylpyrrolidinium trifluoromethylsulfonate ([$Py_{1,4}$]TfO) was reported [113–117].

Other reactive elements such as lithium [118,119] and tantalum [120] were deposited from [$Py_{1,4}$]TFSA. In situ STM measurements give a hint that ultrathin layers of Ti can be obtained by

the electrodeposition from 1-butyl-3-methyl-imidazolium bis (trifluoromethylsulfonyl) amide [BMIm]TFSA containing $TiCl_4$ as a source of titanium [121]. However, later studies [122,123] showed that there is huge increase in viscosity during $TiCl_4$ electroreduction combined with TFSA breakdown which might hinder Ti deposition. More efforts are needed to find a suitable ionic liquid and suitable Ti precursors for the electrodeposition of thick film.

1.1.5.2 **Electrodeposition of semiconductors** [20, 38, 124-132]

Owing to their wide applications in different field such as electronics, optical devices and solar cells, semiconductors are of great interest in both fundamental and industrial applications. Aqueous solutions are rarely suitable solvents for the electrodeposition of semiconductors as hydrogen evolution disturbs the deposition process. The electrochemical deposition of germanium from ([BMIm]PF_6) saturated with GeI_4, $GeBr_4$ and $GeCl_4$ was reported in [20,124–126].

Nanocrystalline silicon with crystal diameters between 50 and 150 nm were electrochemically deposited from 1-butyl-1-methyl-pyrrolidinium bis(trifluoromethylsulfonyl) amide at room temperature [38,127].

Recently, silicon nanowires and nanotubes were obtained by electrodeposition in ionic liquids at room temperature [128,129] and the effect of the anion on the interfacial processes during silicon deposition from three different ionic liquids was also studied [130].

Ionic liquids are not only used for the electrochemical synthesis of elemental semiconductors but they can also be employed to get compound semiconductors such as InSb [105], CdTe [131] and recently GeSn [132].

1.1.5.3 Electrodeposition of conductive polymers [72, 133-138]

The optical, magnetic and electrical properties of conducting polymers make them interesting for several applications. The conductivity of these polymers enables them to be produced by the electropolymerization of their appropriate monomers. Conventional organic solvents are not always suitable for the electrochemical synthesis of conductive polymers due to their vapor pressure, degradation and low thermal stability. Such problems can be circumvented by ionic liquids.

Zein El Abedin et al [72] reported the electrodeposition of poly(paraphenylene) in 1-hexyl-3-methylimidazolium tris(pentafluoroethyl)trifluorophosphate ([HMIM]FAP). Other conductive polymers were electrochemically synthesized in different ionic liquids such as polypyrrole in [BMIm]PF_6 and in [EMIm]TfO [133–135], poly-(3,4-ethylenedioxythiophene) in [EMIm]TFSA [136] and poly(3-(4-fluorophenyl)thiophene) in 1-ethyl-2,3-dimethylimidazolium bis(trifluoromethylsulfonyl)amide ([EMMIm]TFSA) and in 1,3-diethyl-5-methylimidazolium bis(trifluoromethylsulfonyl)amide ([EEMIm]TFSA) [137].

A further advantage of ionic liquids is, that in situ scanning tunneling microscopy (STM) measurements are easily available in ionic liquids, whereas practically impossible in highly aggressive media such as H_2SO_4 formerly needed for benzene polymerization. Carstens et al. [138] reported in situ-STM measurements of the initial stage of benzene polymerization in [HMIM]FAP and they showed that the band gap of the electrodeposited polymer on Au(111) is 2.9 ± 0.2 eV, in good agreement with the reported value in literature.

1.2 Tin and its electrodeposition

1.2.1 Tin as element [139, 153]

Tin is one of the oldest soft and pliable metals known by man in the ore cassiterite (SnO_2) [139]. This ore does not occur in mineral veins but in extensive alluvial deposits where the concentration does not exceed 4%. Tin ring and pilgrim bottle has been found in an Egyptian tomb of the eighteenth dynasty (1580–1350 BC) [139]. The mining of tin around 700 BC in the province of Yunnan was done by Chinese. Pure tin has also been found at Machu Picchu, the mountain citadel of the Incas [139].

Tin is flabby, ductile and a highly crystalline silvery white element. There are two main allotropic forms of tin: α-Sn which is gray, brittle and only stable below 13.2 ℃. It has a diamond cubic crystal structure with no metallic properties due to the formation of covalent bonds between atoms, thus electrons cannot move freely. The α-Sn can be used in few semiconductors applications [140]. The second form is β-Sn which is more stable at room temperature and above with metallic properties. At higher temperature ~ 160℃ and higher pressure two more forms (γ-Sn and σ-Sn) exist [141].

Tin has important chemical and physical properties such as corrosion resistivity and silver like finish. Therefore, it can be used in several applications such as corrosion protection, decorations, soldering, batteries [142], electronic components, integrated circuits and many other ones.

Tin salts and alloys are also used widely, for example tin salts are sprayed over glass to produce electrically conductive glass and tin(II) chloride is used as reducing agent. Niobium-tin alloys are used for superconducting magnets and electric power machinery [143,144]. There are many other tin alloys of different applications.

Due to the formation of several inter-metallic phases with Li, Sn is an attractive material to be used in Li ion batteries as a Li/Sn anode has a theoretical capacity of 990 $mAhg^{-1}$ compared to 370 $mAhg^{-1}$ for graphite [145–147].

There are different routes for the synthesis of tin and tin based compounds such as sol-gel precipitation [148], ball milling [149,150] and electrochemical synthesis [147,151,152]. The easiest, cheapest and most controllable technique for obtaining thin films with optimized morphology might be electrodeposition [153].

1.2.2 Electrodeposition of tin [1, 154-164]

Electrodeposition of tin from aqueous solutions has been studied for at least a hundred years. Tin deposition is usually carried out from acidic Sn(II) solutions or from alkaline Sn(IV) solutions. However, both acidic and alkaline solutions have several disadvantages. The major drawback of alkaline solutions is that the deposition of tin must be carried out at elevated temperatures. Acidic solutions have a low maximum deposition current density for the deposition of tin. Furthermore, the composition is difficult to control and satisfactory deposits were not obtained from acidic solutions of Sn(II) salts [154–158], especially because hydrogen is evolved during the electrolysis process. Moreover, acidic and alkaline baths result in the precipitation of hydroxides of tin, and hence additives such as oxidation inhibitors and surfactants must be used to prevent hydroxide formation, which makes the electrodeposition processes even more difficult to control [159,160]. Organic solvents were also used as electrolytes to avoid the aforementioned problems. Dimethyl sulfoxide was e.g. used as an electrolyte for the deposition of tin [161]. However, aprotic organic solvents often do not provide adequate conductivity and solubility of metal salts. Furthermore, the volatility and flammability of these organic solvents raise some safety issues. In this context, ILs may circumvent the above problems owing to their negligible/low vapor pressure and the

good solubility of tin salts therein [1,162–164]. In the following sections the electrodepostion baths for tin are explained in more detail.

1.2.2.1 Electrodeposition of tin from acidic baths [165-173]

Acidic deposition baths of tin consist of divalent stannous salts. They are consuming less electricity than alkaline solutions, thus they can be used in microelectronic packaging. The advantages of simple acidic stannous baths are that they are environmentally friendly and working at reasonable rates at room temperature. Acidic stannous solutions produce less adherent and non-uniform deposits, therefore additives must be introduced to the deposition bathes to improve the morphology and adhesion of the deposits. Different additives have been used to improve the deposition. The addition of gelatine to acidic tin solutions has been reported to improve the morphology and adherence of the produced tin films [165,166]. In two British patents from Schloetter [167,168] the addition of hydroxyl aromatic compounds to the stannous based solution is reported. The addition of acids was reported by other authors: Alexander et al. introduced sulphonic acid to the acidic deposition bath [169] and the addition of cresylic acid was also reported [170]. In some cases the authors tried to combine more than one component in the acid deposition baths to get more prominent results [171–173]. Although these organic additives were used to improve the quality of the tin deposits, the deposition systems became more complicated and difficult to be controlled.

1.2.2.2 Electrodeposition of tin from alkaline baths [174-178]

Alkaline deposition baths of tin are based on tetravalent tin salts, sodium stannate or potassium stannate and the corresponding alkali metal hydroxides are the main salts that are used in these baths. The main advantages of such systems are that they are non-corrosive and easy to control as

they can be used simply without any additive. However, such baths cannot be used at room temperature and have low maximum deposition current density in addition to a restrictive anode current density range [174]. At lower temperature a spongy precipitate is formed in the deposition bath which passivates the anode even at lower current densities and the temperature has to be higher than 65 ℃ to get more satisfactory deposits. Since the deposition from alkaline tin baths is based on tetravalent stannate solutions, the required electrical charge to plate the same mass of tin is twice higher than that which is used in divalent stannous acidic baths.

One of the most important disadvantages of alkaline plating baths is the diffusion of hydrogen inside the tin deposits whereas the obtained deposits from stannate solutions are uniform, those which are obtained from stannite $[HSnO_2]^-$ are not uniform, spongy and non-coherent [175–178]. Furthermore, the presence of oxygen in such aqueous solutions can promote further oxidation of $[HSnO_2]^-$ to $[SnO_3]^-$ showing the need for inhibitors or additives complicating baths.

1.2.2.3 **Electrodeposition of tin from organic solvents** [161, 179]

Due to the aforementioned problems that appear during the electrochemical deposition of tin in aqueous acidic or alkaline baths, organic solvents can be used as alternative deposition electrolytes.

Santato et al. reported the electrodeposition of tin wires using dimethyl sulfoxide (DMSO) as a plating medium [161]. The authors showed that there are two factors which can affect the morphology of the deposits, one of which is the amount of electrical charge passed through the cell prior to deposition in addition to the aging time of the electrolytic solutions. Spherical tin agglomerates are formed when the deposition solutions are not aged for enough time while tin wires are obtained if the electrolyte containing 0.1M $SnCl_2$ and 0.5M $NaNO_3$ is aged for two weeks after an electric charge of 20 C was passed through the cell.

Tin-nickel codeposition from organic solvents and mixed organic and aqueous solvents was also reported [179].

Such organic solvents involve safety issues due to their volatility and flammability, in addition to their low conductivity and solubility of metal salts which limits their use in the electrodeposition processes.

1.2.2.4 Electrodeposition of tin from ionic liquids [93, 180-193]

The electrodeposition of tin from ILs has been reported in literature [93,180–186]. Xu and Hussey [180] investigated the electrochemistry of Sn(II) and Sn(IV) in acidic and basic [EMIm]Cl/$AlCl_3$). The electrochemistry of tin was investigated by Huang and Sun in acidic and basic [EMIm]Cl/$ZnCl_2$ [181]. Ling and Koura also studied the electrochemistry of tin [182]. Tachikawa et al. investigated the electrochemical behavior of Sn species in 1-butyl-1-methylpyrrolidinium bis(trifluoromethylsulfonyl)amide ([$Py_{1,4}$]TFSA); tin species were introduced into the IL by anodic dissolution of a tin wire [183]. Morimitsu et al. studied the electrodeposition of tin and indium–tin alloys from [EMIm]BF_4/[EMIm]Cl [184,185]. Abbott et al. studied the deposition of tin, zinc and their alloys from a choline-chloride-based, IL-like deep eutectic solvent [93]. Fabrication of porous tin was achieved by template free deposition of tin nanowires from an IL containing the dicyanamide (DCA^-) anion [186]. Adsorption/solvation layers of ILs can play a significant role in the deposition process and influence the kinetics of the electrodeposition reaction [187]. It was reported that nanocrystalline Al deposits can be obtained from [$Py_{1,4}$]TFSA, whereas a microcrystalline Al deposit was obtained in the case of 1-ethyl-3-methyl imidazolium bis(trifluoromethylsulfonyl) amide [EMIm]TFSA. The difference in grain size seems to be due to the influence of the cation of the IL, although the exact mechanism is unclear [188,189]. The different grain size may thus be due to a difference in the adsorption of

the pyrrolidinium cation on the growing nuclei and, thus, hindered further growth of crystals. This assumption was supported by studying the interface of the two ILs ([$Py_{1,4}$]TFSA and [EMIm]TFSA) independently by atomic force microscopy and scanning tunnelling microscopy which revealed that, in the neat liquid, $[Py_{1,4}]^+$ cations interact with the substrate more strongly than $[EMIm]^+$ cations [190]. Thus, differences in surface adsorption/interaction can lead to dramatic effects. Interestingly, a nanocrystalline Al deposit was also obtained from partially decomposed ILs such as 5.5 M $AlCl_3$/[EMIm]TFSA and acidic [EMIm]Cl/$AlCl_3$ (60/40 mol%) [191]. The decomposition products of the $[EMIm]^+$ cations seem to act as a grain refiner. Furthermore, a nanocrystalline Al deposit was obtained from 1-(2-methoxyethyl)-3-methylimidazolium chloride/$AlCl_3$ [192]. In addition to the above results, nanocrystalline Al deposits were obtained from [$Py_{1,4}$]TfO (TfO = trifluoromethylsulfonate), but microcrystalline Al was obtained from [EMIm]TfO [193]. Thus, a change in the cation or anion of the IL has some influence on the morphology of the respective deposit.

2. Aim of the work

Tin plays an important role in many industrial fields such as decorations, electroplating of metals to protect them from corrosion, soldering, integrated circuits, electronics, batteries and many other applications. For Li ion batteries the Li/Sn anode has a theoretical capacity of 990 $mAhg^{-1}$ or a volumetric capacity of 7200 Ah/L which is almost three times higher than the capacitance of graphite (370 $mAhg^{-1}$ or 800 Ah/L).

The aim of the current thesis is to make several deposits of tin and tin based alloys from air- and water stable ionic liquids. Different structures such as nanowires, thin films and three-dimensionally ordered macroporous structures (3DOM) are aimed to be electrochemically synthesized from different ionic liquids, namely 1-ethyl-3-methylimidazolium dicyanamide ([EMIm]DCA), 1-butyl-1-methylpyrrolidinium dicyanamide ($[Py_{1,4}]$DCA) and 1-butyl-1-methylpyrrolidinium trifluoromethylsulfonate, $[Py_{1,4}]$TfO.

Nanowires and macroporous structures with smaller particle sizes ensure short Li-ion baths and introduce large interface areas between the electrode and electrolyte which correspondingly accelerate the reaction rate.

Alloying of tin with different metals can help to overcome the poor cyclability of pure Sn due to the volume expansion during the lithiation/delithiation processes.

Therefore the aim is to combine the advantages of alloying and structure designing to improve the performance of Sn based materials.

These materials with different structure morphologies would have a potential as anode host battery materials.

The effect of the ionic liquid composition on the deposition morphology of tin is also one aim of this thesis.

3. Experimental

3.1 Chemicals [1, 194]

Anhydrous $SnCl_2$ powder (Alfa Aesar; 99.99%) was used as tin source for electrochemical deposition of tin, CuSn and SiSn. Tin wire (99.999%) and foil (99.999%) were purchased from Alfa Aesar. Silicon tetrachloride (Fluka; >99.999 %) and CuCl (Sigma-Aldrich; 99.995%) were used as sources for Si and Cu for the electrochemical deposition of SiSn and CuSn, respectively. $Zn(TfO)_2$ powder (IO-LI-TEC, Germany, 99%) and tin trifluoromethylsulfonate [$Sn(TfO)_2$] (Sigma-Aldrich; 98%) were used as a source of copper and tin, respectively in the electrodeposition of ZnSn alloy.

Three different ionic liquids were used in this thesis, namely, 1-ethyl-3-methylimidazolium dicyanamide ([EMIm]DCA), 1-butyl-1-methylpyrrolidinium dicyanamide ([$Py_{1,4}$]DCA) and 1-butyl-1-methylpyrrolidinium trifluoromethylsulfonate, [$Py_{1,4}$]TfO. All the ionic liquids were purchased from IO-LI-TEC (Germany) and dried for 2 days at 373 K under vacuum, then stored in closed bottles in an argon-filled glove box. The water and oxygen contents in the glove box were less than 2 ppm (OMNI-LAB from Vacuum Atmospheres). The water contents of the dried [$Py_{1,4}$]TfO, [EMIm]DCA and [$Py_{1,4}$]DCA ILs were determined by Karl–Fischer titration (10, 15 and 7 ppm, respectively).

The chemical structure of each ionic liquid is shown in figure 3.1.

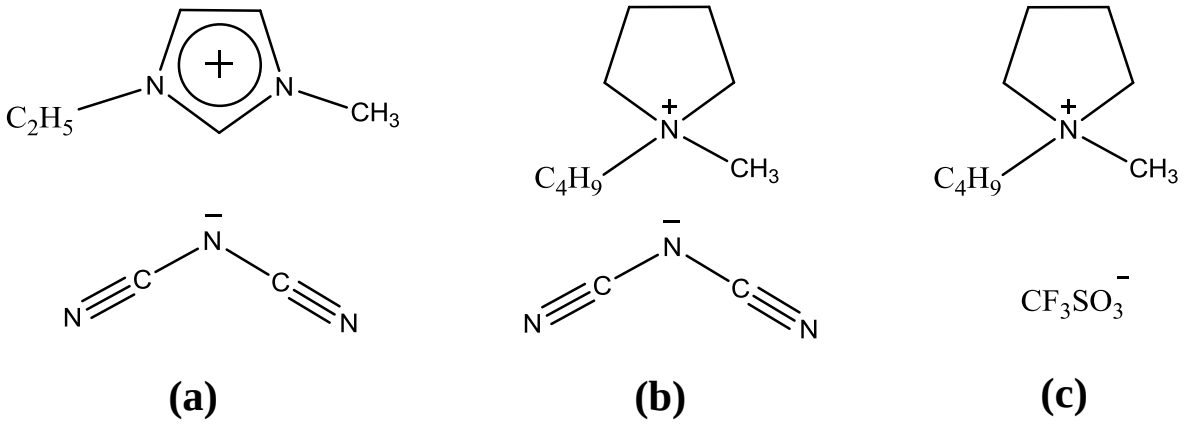

Fig.3.1. *Chemical structure of the ionic liquids (a) [EMIm]DCA, (b) [$Py_{1,4}$]DCA and (c) [$Py_{1,4}$]TfO*

These ionic liquids were selected for the electrodeposition of Sn nanowires, Sn films and different Sn based alloys such as ZnSn, SiSn and CuSn. They are thermally quite stable which enables an efficient drying by heating over 100 ℃ under vacuum; in addition they have a good conductivity compared to common organic solvents. Furthermore, their wide electrochemical windows makes them stable enough to deposit such materials. Some of their physical properities are summarized in table 3.1.

Table 3.1. *Some physical properties of the employed ionic liquids at room temperature.* [1,194]

Ionic liquid	**Density (g/cm)**	**Viscosity (mPa·s)**	**Melting point (℃)**	**Conductivity mS cm^{-1}**	**EC window (V) on platinum**
[EMIm]DCA	**1.08**	**19.4**	**-21**	**36**	**3**
[$Py_{1,4}$]DCA	**0.95**	**45**	**-55**	**n.a.**	**3.5**
[$Py_{1,4}$]TfO	**1.25**	**173.9**	**3**	**n.a.**	**5.75**

3.2 Electrodeposition baths

The chemical composition of the deposition baths that have been used for the electrodeposition of tin and its alloys in [EMIm]DCA, [$Py_{1,4}$]DCA, [$Py_{1,4}$]TfO are listed in table 3.2.

Table 3.2. *The chemical composition of baths used for tin and tin based alloys deposition in three air and water stable ionic liquids.*

Ionic liquid	$SnCl_2$	CuCl	$Zn(TfO)_2$	$Sn(TfO)_2$	$SiCl_4$	Notes
[EMIm]DCA	**0.1 and 0.05**	**1 and 0.25**	**-**	**-**	**-**	*** all the solutions are in molar concentration mol/L (M) * all the baths are monophasic**
[$Py_{1,4}$]DCA	**0.1 and 0.05**	**-**	**-**	**-**	**-**	
[$Py_{1,4}$]TfO	**0.1 and 0.05**	**-**	**0.05**	**0.05**	**0.1**	

3.3 Electrochemical cell

Two electrochemical cells were used in the electrodeposition processes. Figure 3.2 shows one of them which was made of polytetrafluoroethylene (Teflon), clamped over a Teflon covered O-ring onto the working electrode yielding a geometric surface area of 0.3 cm^2. This cell is only suitable for room temperature experiments delivering small area samples (only 0.3 cm^2). For obtaining deposits of higher surface area a 10 mL glass beaker with a Teflon holder was used for the electrochemical cell as shown in figure 3.3. Before running a new experiment the Teflon cell with the O-ring and all the parts in contact were cleaned in a mixture of 50/50 vol% H_2SO_4/H_2O_2 followed by rinsing in refluxing distilled water. The used electrodes are different according to each experiment; this will be explained in details in the following section.

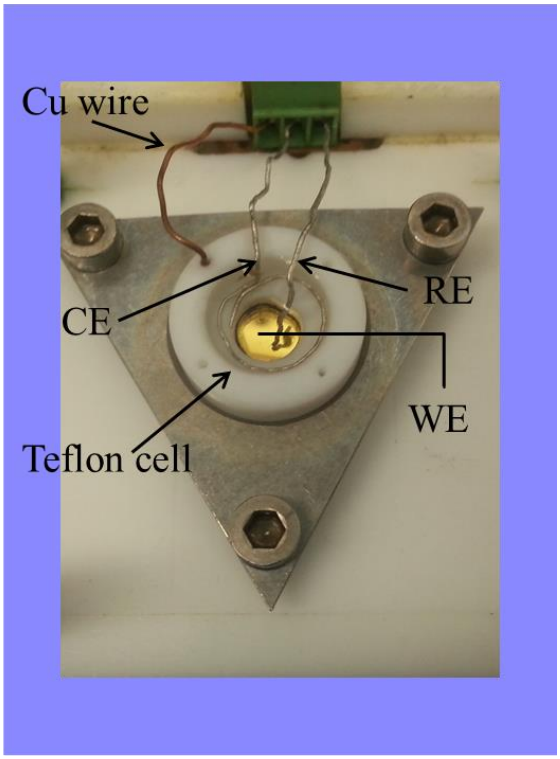

Fig. 3.2. *Photograph of the electrochemical cell used in this study for small area samples.*

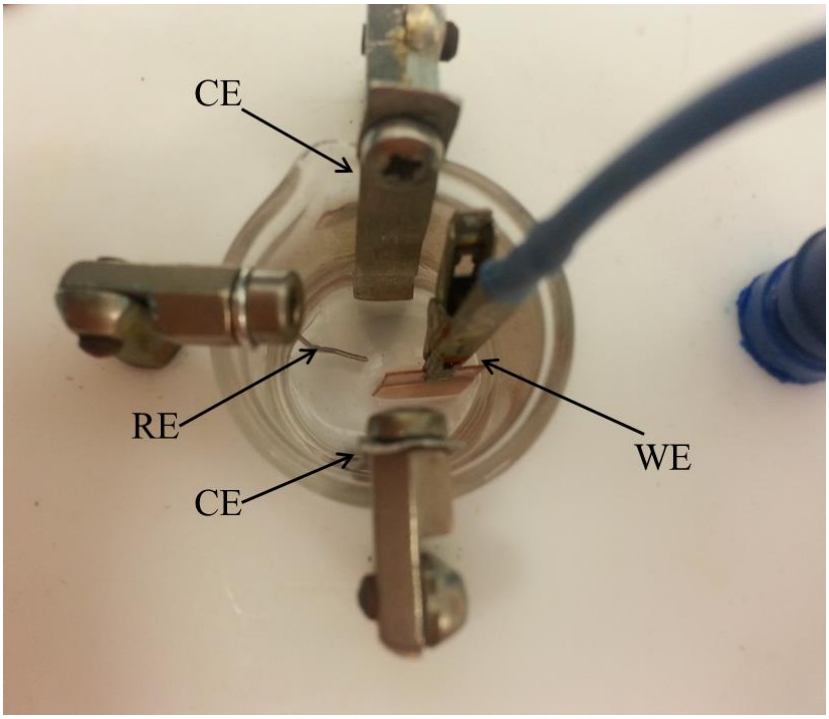

Fig. 3.3. *Photograph of the electrochemical cell used in this study for larger area samples.*

3.4 Electrodeposition of tin nanowires

For the electrochemical synthesis of freestanding tin nanowires from two different ionic liquids, namely, 1-ethyl-3-methylimidazolium dicyanamide and 1-butyl-1-methylpyrrolidinium dicyanamide via a template-assisted electrodeposition approach, track-etched polycarbonate (PC) membranes (Ion Track Technology for Innovative Products, IT4IP, Belgium) were used as templates. The templates have a thickness of 21 μm and a nominal pore diameter of 90 nm (pore density of 10^9 cm^{-2}). One side of the membrane was sputtered by approximately 100 nm thin films of either copper or gold to make it conductive and to serve as working electrode. The use of templates has the advantage of getting structures with predefined and controllable sizes and shapes in addition to the possibility to form vertically aligned nanowires, in principle. Sn was electrodeposited on both sides of the template to give a supporting Sn layer on the sputtered surface and Sn nanowires on the other side at the same time. Cu supporting layers were also deposited on the sputtered side instead of tin, which forms brittle dendrites. Consequently, Sn nanowires were deposited in a different step through the pores of the nonsputtered side. After dissolution of the PC membrane in dichloromethane, freestanding Sn nanowire structures on an electrodeposited Cu supporting layer were expected.

For bulk tin deposition on copper and gold (gold on glass, Arrandee Inc.) substrates, the small area electrochemical cell (figure 3.2) was used. Tin foil and tin wires (Alfa Aesar, 99.99 %) were used as counter (CE) and reference (RE) electrodes, respectively, for Sn deposition. A 10-ml-glass beaker (figure 3.3) was used as an electrochemical cell for Sn nanowire synthesis in which the sputtered membrane (working electrode) was placed between the counter and the reference electrodes, and the distance between the template and the counter electrode in all experiments is kept constant at 1 cm. In the case of Cu deposition, copper wires were used as counter and reference electrodes. All electrochemical measurements were performed using a PARSTAT 2263

potentiostat/galvanostat controlled by Power CV and PowerStep software. The deposits were washed by immersing the template in isopropanol to remove the ionic liquid residues; subsequently, the templates were dissolved in dichloromethane (CH_2Cl_2, AR, Merck). A schematic sketch of the free standing nanowire electrodeposition is shown in figure 3.4

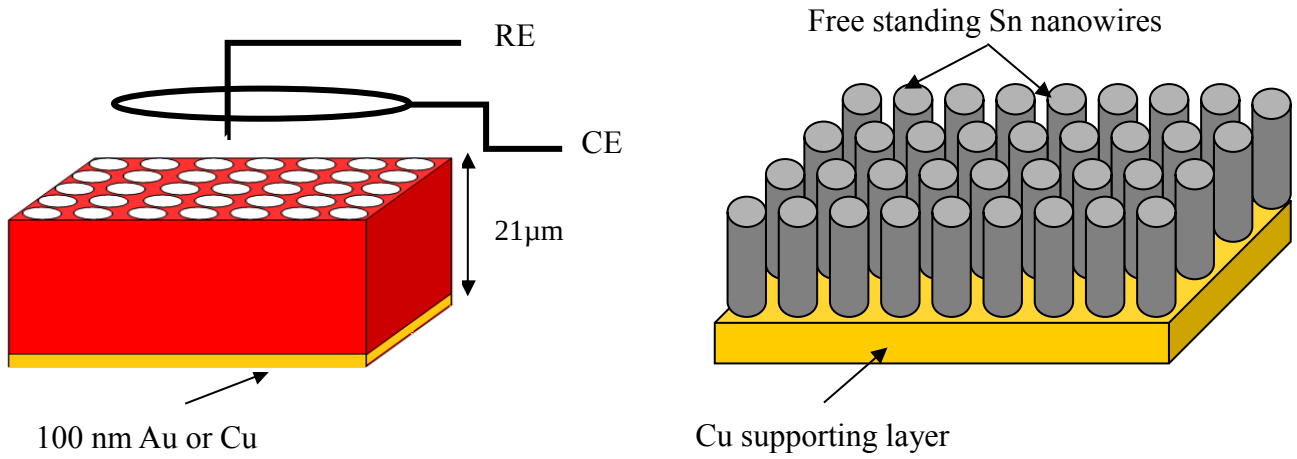

Fig. 3.4 *Schematic sketch explaining the electrochemical deposition of nanowires structure (a) Electrochemical cell including polycarbonate template as a working electrode. (B) Electrodeposited Sn nanowires after removal of the template by* CH_2Cl_2.

3.5 Influence of ILs anion on tin morphology

The change in the cation or anion of the IL has some influence on the morphology of the respective deposit. In the light of these results, the deposition of tin from ILs with the same $[Py_{1,4}]^+$ cation but two different anions, namely, TfO^- and DCA^-, was studied where the electrochemical deposition of tin from $[Py_{1,4}]TfO$ has not yet been reported. For comparison, tin electrodeposition was also studied in [EMIm]DCA. Gold and copper electrodes were employed to investigate the electrochemical behavior of $SnCl_2$ and the morphology of the tin deposits. IR

spectroscopy was employed to investigate the differences in the complexation of $SnCl_2$ in the three different ILs.

A 10 mL glass beaker was used for the electrochemical cell (figure 3.3), gold (200–300 nm-thick gold films on chromium covered borosilicate glass, procured from Arrandee Inc.) and copper plates were used as working electrodes (WEs) in different experiments. Prior to use, the gold WEs were annealed in a hydrogen flame to red glow for a few minutes. Copper plates were polished, rinsed in high purity acetone and then in ethanol in an ultrasonic bath to minimize possible surface contamination. Tin wires and tin foils were used as reference and counter electrodes, respectively.

3.6 Zinc–tin films and free-standing nanowire arrays

For the deposition of zinc-tin alloys, zinc trifluoromethylsulfonate [$Zn(TfO)_2$] and tin trifluoromethylsulfonate [$Sn(TfO)_2$] were used as sources of Zn and Sn, respectively. [$Sn(TfO)_2$] has a higher solubility in [$Py_{1,4}$]TfO than in [EMIm]TfO. Therefore, [$Py_{1,4}$]TfO was employed for Sn and Zn–Sn deposition. The electrochemical cell, which was made of polytetrafluoroethylene (Teflon), was clamped over a Teflon-covered Viton o-ring to yield an area of 0.3 cm^2 (figure 3.2). Gold substrates (gold on glass) from Arrandee Inc. were used as working electrodes. Track-etched polycarbonate (PC) membranes with a nominal thickness of 21 µm and an average pore diameter of 100 and 200 nm, respectively, were used as templates for synthesizing the nanowires. A thin layer of Au (about 100 nm thick) was sputtered on the reverse side of the templates serving as the working electrode. Platinum wires (Alfa, 99.99%) were used as counter and quasi reference electrodes, respectively. The reference and counter electrodes were directly immersed in the solutions without using a separate compartment. The Pt quasi reference electrode was the best compromise with respect to handling and electrochemical stability.

After deposition, the samples were rinsed with isopropanol to ensure removal of the ionic liquid, and the membranes were removed by dissolving in dichloromethane (CH_2Cl_2, AR, Merck).

3.7 Copper-tin macroporous films and free-standing nanowire arrays

Both CuSn nanowires and macroporous structures were electrochemically deposited from a mixture of 0.25M CuCl and 0.05M $SnCl_2$ in [EMIm]DCA.

The electrodeposition of macroporous CuSn structures from air and water stable ionic liquids was done through the voids of polystyrene opal structures on gold substrates. For this purpose, polystyrene spheres (PS) with an average diameter of about 600 nm (Thermo Scientific, USA) were applied onto the employed electrodes by a simple dipping process into polystyrene suspension (10 vol % PS dispersed in ethanol) for a few seconds at 40℃ and pulled out. The covered substrates with a PS layer thickness of about 10 μm were dried and heated at 100℃ for 2 h. Before the deposition of the polystyrene spheres, the gold substrates were annealed in a hydrogen flame to red glow for a few minutes then sonicated in highly pure acetone for a few minutes to remove any residual contamination and well dried before the deposition of polystyrene. After deposition, the PS template was removed by THF. A schematic sketch of the macroporous structure electrodeposition is shown in figure 3.5.

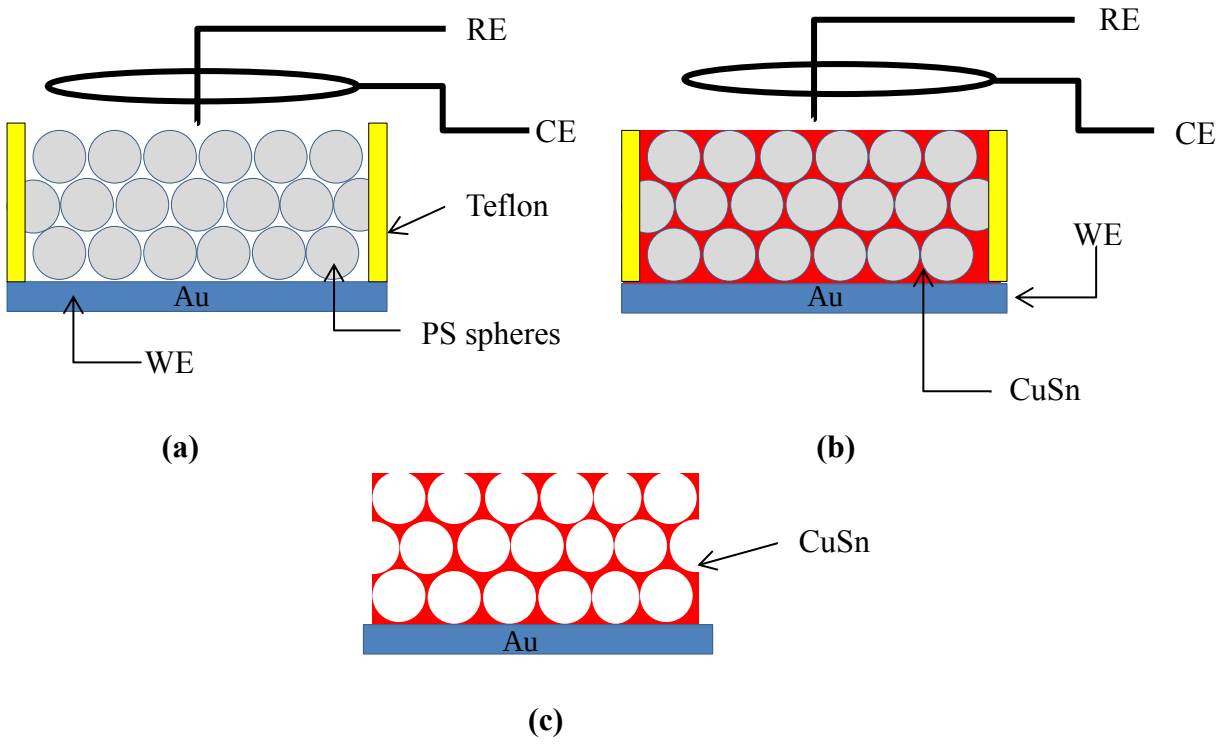

Fig. 3.5. *Schematic sketch explaining the electrochemical deposition of macroporous structures (a) Electrochemical cell to be filled with the electrolyte (0.25M CuCl and 0.05M $SnCl_2$ in [EMIm]DCA). (b) Electrodeposition of CuSn alloy (red). (c) After removal of PS spheres (grey) by tetrahydrofuran.*

For the CuSn nanowires, track-etched polycarbonate (PC) membranes were used as a template. The thickness of the membranes is 21 μm with an average pore diameter of 90 nm and a pore density of 10^9 cm^{-2}. One side of the membrane was sputtered with a ~100 nm thick film of copper to be used as a working electrode during the electrochemical synthesis for this study.

After the deposition was finished, the membrane, with the nanowires embedded inside, was carefully dissolved by CH_2Cl_2 to get free standing CuSn nanowires.

The small area electrochemical cell (figure 3.2) was used for the electrochemical deposition process. A platinum ring was used as a counter electrode, and a Pt wire was used as a quasi-reference electrode. A schematic sketch of the nanowire structure electrodeposition is shown in figure 3.4.

3.8 Electrodeposition of SiSn

Template free SiSn nanowires were electrochemically deposited from a mixture of 0.1M $SiCl_4$ and 0.1M $SnCl_2$ in $[Py_{1,4}]TFO$ on gold substrates. The small area electrochemical cell (figure 3.2) was used for the electrochemical deposition process. A Pt ring was used as a counter electrode, and a Pt wire was used as a quasi-reference electrode.

The final deposits were cleaned carefully in highly pure isopropanol and acetone before further analysis.

3.9 Experimental techniques

Each system has been investigated electrochemically by cyclic voltammetry using a PARSTAT 2263 potentiostat/galvanostat controlled by PowerCV and PowerStep software. The obtained deposits were washed thoroughly and then characterized by high-resolution scanning electron microscopy (HR-SEM) with energy dispersive X-ray spectroscopy (EDX) (Carl Zeiss DSM 982 Gemini), X-ray diffraction (XRD) analyses and a vacuum FTIR spectrometer (VERTEX 70V from Bruker Optics GmbH, Ettlingen, Germany) for recording IR spectra.

3.9.1 Cyclic voltammetry [195, 196]

Cyclic voltammetry (CV) is one of the standard analytical techniques that are used in electrochemistry. This technique often gives only qualitative information on the electrochemical reaction. Since it can provide a rapid allocation of the oxidation/reduction electrode potentials of the electroactive species which are dissolved in electrolytes, CV is usually the first experiment in an electrochemical experiment.

In this technique, the three electrodes electrochemical cell including the reference electrode (RE), working electrode (WE) and the auxiliary electrode (counter electrode CE), are connected to the

potentiostat. The potentiostat is scanning the potential of the working electrode linearly starting at the initial potential E_i where there is no electrode reaction, and therefore no Faradaic current flows, then swept between two given values E_{min} and E_{max} at a constant scan rate while the resulting current is recorded (figure 3.6). Single or multiple cycles can be recorded.

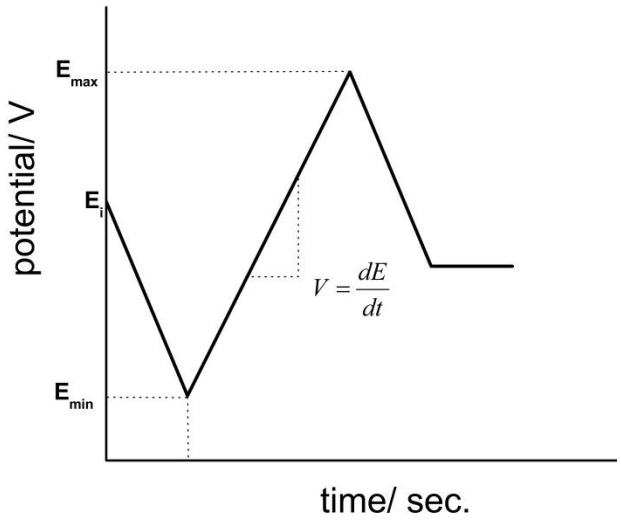

Fig. 3.6. *Potential-time signal in cyclic voltammetry sweep.*

For cyclic voltammetry there is a forward scan and a backward scan.

$E = E_i - \nu t$ (forward scan)

$E = E_{min} + \nu t$ and $E = E_{max} - \nu t$ (subsequent cycles)

Where E(t), E_i and E_{min} are final, initial and switching potentials in volt, respectively. And ν is the scan rate ($V\ s^{-1}$) and t is time (seconds).

The electrochemical reaction takes place at the working electrode and the electrical current due to the electron transfer at the working electrode is known as Faradaic current. The counter electrode closes the electrical circuit. It is important to mention that if a reduction process occurs at the working electrode, a corresponding oxidation process takes place at the counter electrode to

balance the electrochemical process and vice versa. The process that occurs at the counter electrode can affect the electrochemical process at the working electrode [195].

During the potential sweep, the potentiostat measures the potential (E) between the working electrode and the reference electrode while the current is measured between the working electrode and counter electrode. The output of the current-potential plot is known as a cyclic voltammogram (figure 3.7).

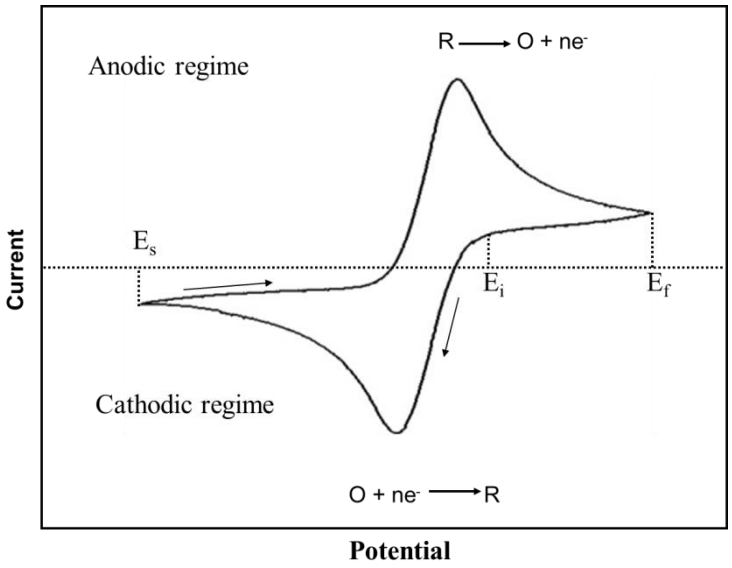

Fig. 3.7. *Typical voltammogram for a reversible system, 2nd cycle and above*

The scanning of the first half cycle starts at a potential value at which no reactions occur (E_i) then goes into the negative direction (forward scan) till it reaches a sufficient potential value for the reduction of the electroactive species. A cathodic current flows till a reduction peak is reached, then the direction of the potential sweep is reversed in the second half cycle (backward scan). In the backward scan the reduced species obtained in the forward scan either as a deposit or as active species near the electrode surface are re-oxidized and an anodic current flows till an anodic peak is reached.

For the redox reaction

$$\mathbf{O + ne^- \leftrightarrow R}$$

during the forward reaction the potential is scanned in the negative direction till the active species (O) is reduced at the electrode surface (reduction peaks are obtained). In the backward reaction the reduced form (R) is re-oxidized (anodic peaks are obtained). The characteristic peaks in the cyclic voltammogram are in most cases caused by diffusion limitation of the species to the surface.

The relationship between the applied potential and the concentration of the electroactive species is determined by the Nernst equation [196].

$$\mathbf{E = E^{\circ} + \frac{RT}{nF}\ ln\frac{a_o}{a_R}}$$

Where E^o is the standard electrode potential; R is the universal gas constant; T is the absolute temperature; F is Faraday's constant; a_o and a_R are the activities of the oxidants (O) and reductants (R) at the electrode surface, respectively.

According to Fick's first law of diffusion [196] the current flow during the redox reaction is proportional to the concentration gradient of the electroactive species at the electrode surface

$\mathbf{I = nFAD\left(\frac{dC}{dX}\right)}$, if diffusion is the slowest process.

n is the number of electrons transferred in the reaction; A is the area of the electrode surface; D is the diffusion coefficient of the electroactive species; c is the active species concentration and x is the distance from the electrode surface.

The peak current as function of scan rate for a fully reversible redox process with no other limitations is given by the Randles-Sevcik equation

$$\mathbf{I_p = \left(2.6 \times 10^5\right) n^{3/2}\ ACD^{1/2} \nu^{1/2}}$$

Where I_p is the peak current; n is the number of electrons transferred in the redox reaction; A is the surface area of the electrode; D is the diffusion coefficient of the electroactive species; C is the active species concentration and ν is the scan rate.

For an irreversible process the current peak is given by

$$\mathbf{I_p = \left(2.99 \times 10^5\right) n^{3/2}\, \alpha^{1/2} A C D^{1/2} \nu^{1/2}}$$

α is the transfer coefficient

However it's important to mention that these equations are mainly based on electrochemical studies in aqueous solutions and they can only rarely be applied to electrochemical reactions in ionic liquids.

In this study cyclic voltammetry were performed to study the electrochemical behavior of Sn and Sn based alloys. All the electrochemical measurements were carried out inside of an argon filled glove box with water and Oxygen contents below 2 ppm using a PARSTAT 2263 potentiostat/galvanostat controlled by PowerCV and PowerStep software.

3.9.2 SEM and EDX

The Scanning electron microscope (SEM) is one of the electron microscope types that produces an image of the surface of solid samples via scanning with a high energy beam of electrons.

The beam is interacting with the atoms of the samples and thus produces various signals which contain different information about the surface topography and composition.

In a typical SEM, an electron beam, with electron's energy up to 50 keV is emitted by heating a pin-shaped metallic cathode and accelerated by applying a high voltage between sample and cathode. The cathode is usually made of a metal with a high melting point and a low vapor pressure such as tungsten (figure 3.8).

The electron beam is focused by condenser lenses into a spot of 2 nm to 10 nm in diameter and passes through pairs of scanning coils or pairs of deflector plates in the electron column, typically in the final lens, which deflects the beam in the x and y axes so that it scans in a scanning fashion. When the primary electron beam interacts with the sample, the electrons lose energy by repeated random scattering and absorption within a teardrop-shaped volume of the specimen known as the interaction volume, therefore a series of elastic and inelastic interactions with the atoms of the sample results (figure 3.9).

Backscattered electrons are produced in the case of elastic interaction with the nucleus of the atoms while the inelastic interactions produced different signals depending on the part where the interaction takes place. The interaction with electrons induce secondary electron emission while the inelastic interaction with nuclei of the atoms induce the generation of Bremsstrahlung and may lead to ionization processes, which cause the generation of the characteristic X-rays. On the other hand, interactions of the primary electrons with the sample electrons may induce Auger electron emissions. Each of the backscattered and secondary electrons can be detected by specialized detectors. Figure 3.9 summaries the different types of emissions. The beam current absorbed by the specimen is corresponding to topography of the scan point (raster scan) and the sequence of the signals is used to give an image of the surface. Electronic amplifiers of various types are used to amplify the signals, which are displayed as variations in brightness on a computer monitor or on a cathode ray tube (in old versions).

In older microscopes images may be captured by photography from a high-resolution cathode ray tube, but in modern machines the image is saved to a computer data storage hard disc.

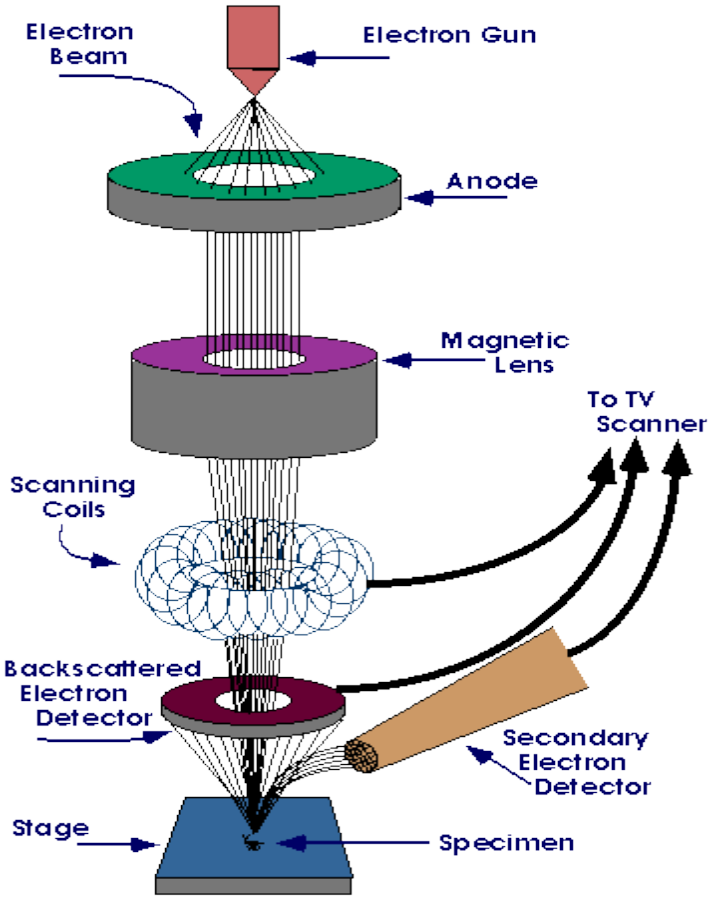

Fig. 3.8. *Schematic view of the scanning electron microscope (source: http://www.purdue.edu/ehps/rem/rs/sem.htm*

The backscattered electron signal intensity is strongly related to the atomic number of elements (intensity increase with increasing atomic number), thus backscattered electrons are used to detect contrast between areas with different chemical compositions and hence element distribution in the sample can be shown in the image.

The characteristic X-rays are used for qualitative elemental analysis of the samples. When a high-energy beam is focused into the sample it may excite an electron in an inner shell, emitting it from the shell while creating an electron hole where the electron was. Another electron from the higher-energy level shell fills the hole and an energy difference between the higher energy shell and the lower energy shell is created which may be released in the form of X-rays.

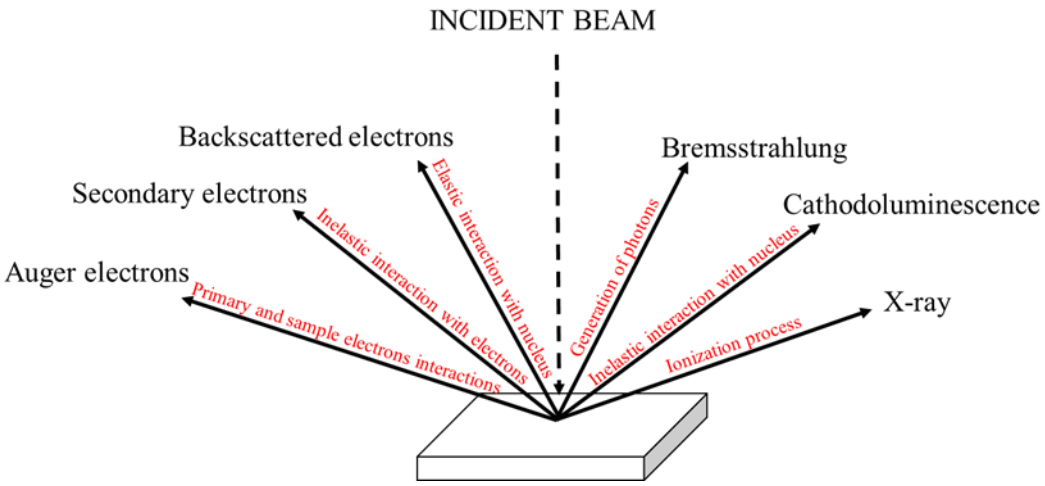

Fig. 3.9. *Interaction of the primary electron beam with the surface of the sample*

As the energy of the X-rays are characteristic for the difference in energy between the two shells, and for the atomic structure of the element from which they were emitted, this allows the elemental composition of the specimen to be measured. The X-ray spectrometer (EDX) which consists of a X-ray detector and a pulse processor with analyzer is able to measure the number and energy of the X-ray emitted from the sample. Figure 3.10 shows a graphical presentation of the EDX principle.

Therefore, SEM and EDX give useful information about the topography and morphology of the surface in addition to elemental composition of the investigated sample.

In this study, SEM and EDX were used for the analysis of the electrodeposited tin and tin based alloys. Before analysis, the working electrodes were removed from the electrochemical cell, washed with isopropanol to get rid of any ionic liquid residue and then finally dried and kept inside the glove box till they were given for analysis.

A high resolution field emission scanning electron microscope from Carl Zeiss (DSM 982 Gemini) was used for SEM and EDX analysis in this study.

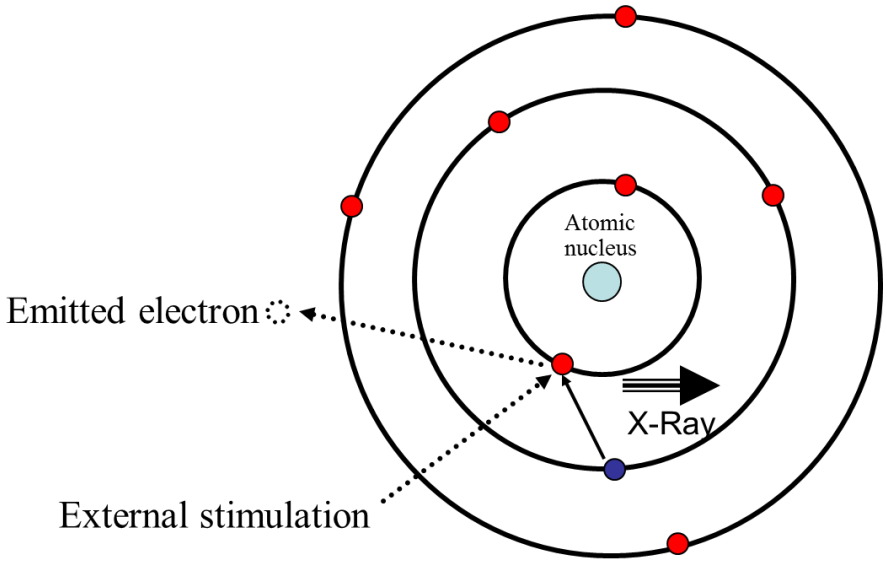

Fig. 3.10. *Schematic diagram explaining the principle of EDX*

3.9.3 X-Ray Diffraction (XRD) [197]

XRD is one of the most important techniques for solid material characterization where it is used for the determination of crystallographic structure of materials.

In such systems, electrons are emitted from a cathode and accelerated through a strong electric field of ~50 kV. Having reached a high speed, the electrons collide with a metal plate, emitting Bremsstrahlung (low intensity) as background when the bombarding electrons interact with the nucleus of the atoms while high intensity characteristic X-rays are emitted when the electrons collide with electrons of the inner shells of the atoms. This collision emits electrons from the inner shell and hence, electrons of higher energy fill the vacancies of the emitted electron and the excess energy is emitted as X-ray photons which is characteristic for this material.

During the measurement, a monochromatic beam illuminates the sample that has been set on the stage producing diffraction pattern. Figure 3.11 shows the reflection of X-rays in lattice planes.

Bragg's law :

$$n\lambda = 2d \sin \theta$$

where n is integer number, λ is the wavelength of X-ray, d is the distance between two adjacent lattice planes and θ is the diffraction peak angle.

The peaks of an XRD pattern can also be used for the average crystal size determination using Scherrer's equation [197].

$$D = 0.9\lambda/\beta \cos \theta$$

Where D is the crystallite size, λ is the radiation wavelength, θ is the diffraction peak angle and β is the line width at half peak intensity, that can be calculated using the following formula

$$\beta^2 = \beta_m^2 - \beta_s^2$$

where β_m and β_s are measured widths, at half maximum, of the diffraction lines from the sample and the standard, respectively.

Therefore, the crystal structure of the deposits from different ionic liquids on copper and Au (111) substrates were examined by X-ray diffraction analysis using a PANalytical Empyrean Diffractometer (Cabinet No. 9430 060 03002) with CuKα radiation.

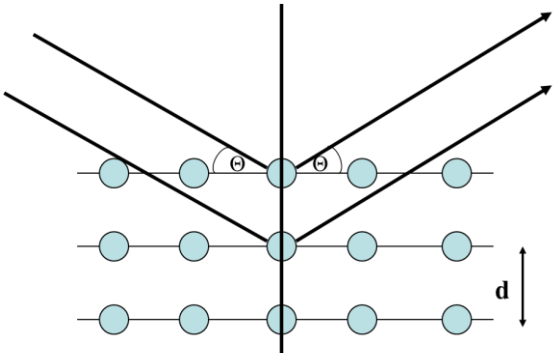

Fig. 3.11. *Schematic scetch showing the reflection of the X-rays in lattice planes.*

3.9.4 IR spectroscopy

In this thesis IR spectroscopy was employed to investigate the differences in the complexation of $SnCl_2$ in three different ILs. The IR spectra were recorded on a vacuum FTIR spectrometer (VERTEX 70V from Bruker Optics GmbH, Ettlingen, Germany) in the institute of inorganic chemistry of Tu-Clausthal university.

4 Results and discussion

4.1 Electrodeposition of tin nanowires [198]

The cyclic voltammograms of 0.1 M $SnCl_2$/[EMIm]DCA and of 0.1 M $SnCl_2$/[$Py_{1,4}$]DCA on gold and on copper sputtered membranes are shown in Figures 4.1.1 and 4.1.2, respectively. In the case of the Cu-sputtered membrane, the potential was scanned from the open circuit potential (OCP) till -0.5 V vs. Sn quasi ref. in the cathodic direction then up to only +0.1 V in the reverse scan to avoid the anodic dissolution of copper, and finally back to OCP.

In the case of a gold sputtered membrane the electrode potential was scanned from the open circuit potential (OCP) till -0.5 V in the cathodic direction, then up to +0.5 V in the reverse scan, and then finally back to OCP. The scan rate for all experiments was 10 mV/sec.

Fig. 4.1.1 shows that the cyclic voltammogram of 0.1 M $SnCl_2$/[EMIm]DCA on the gold sputtered template shows two reduction processes (C1, C2), while only one clear reduction process (C2) was observed in the case of the copper sputtered membrane. The reduction process (C1) might be correlated to surface alloying processes and underpotential deposition, respectively. The second peak (C2) is due to the bulk deposition of Sn. In the case of 0.1 M $SnCl_2$/[$Py_{1,4}$]DCA, the cyclic voltammogram (Fig. 4.1.2) shows another reduction process (C*) at about -0.1 V both on gold and copper sputtered membranes which, however, is difficult to allocate to a process. Four anodic peaks (A1, A2, A3, A4) appear in the backward scan on the gold sputtered membrane, Fig. 4.1.1. The peaks A1 and A2 are correlated with the stripping of the electrodeposited tin and the other peaks A3 and A4 might be due to dealloying process.

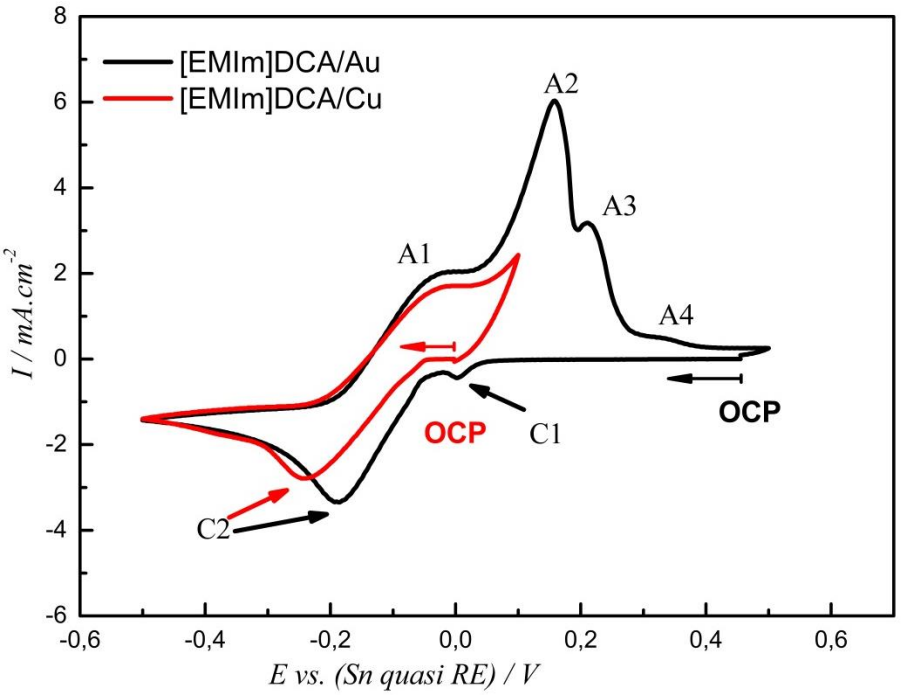

Fig. 4.1.1 *Cyclic voltammograms of Sn deposition on Au-sputtered and Cu sputtered membranes in 0.1 M $SnCl_2$/[EMIm]DCA at 25 °C at a scan rate of 10 mV s^{-1}*

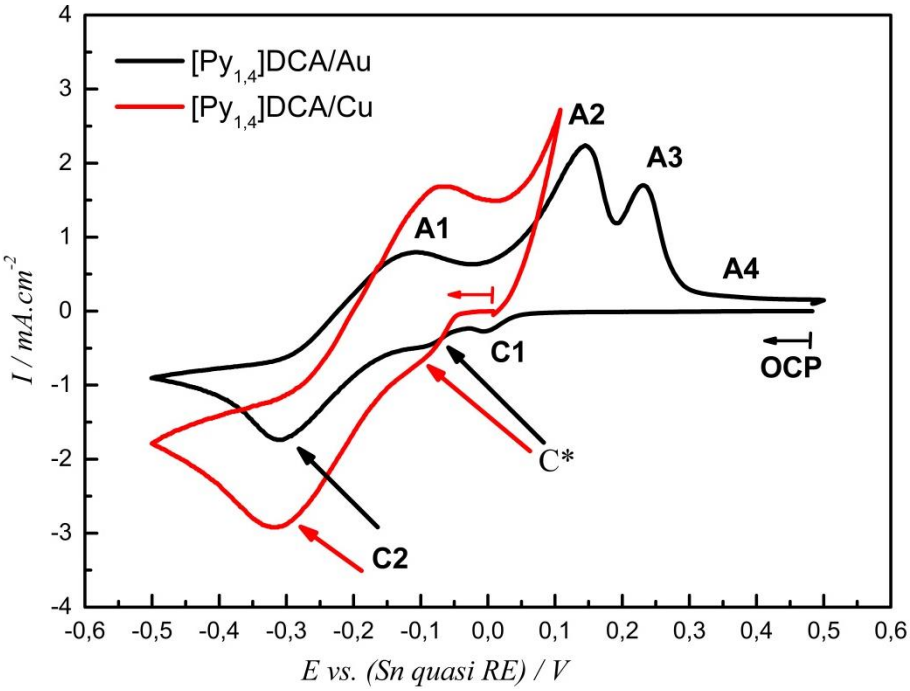

Fig. 4.1.2. *Cyclic voltammograms of Sn deposition on Au-sputtered (black) and Cu sputtered (red) membranes in 0.1 M $SnCl_2$/[$Py_{1,4}$]DCA at 25 ° C at a scan rate of 10 mV s^{-1}*

According to the equilibrium phase diagram, the Au-Sn system represents one of the more complicated and intriguing binary systems due to the existence of four different stable intermetallic compounds (see appendix).

Tin and gold atoms have almost the same atomic radius of approximately 0.16 nm, which allows their substitution [199]. Therefore, several surface alloys appear plausible. Thermodynamic measurements show that this compound has very strong bonds which is consistent with CV data. Sn atoms have a smaller surface free energy which led to the segregation of Sn to the surface of the alloy and create a Sn-rich surface layer that can be oxidized in the presence of any small amount of O_2. However this is not valid in ionic liquids [199–201].

In order to shed more light on these peaks, cyclic voltammetry of 0.1M $SnCl_2$/[EMIm]DCA on the Au substrate was performed at different switching potentials as shown in Figure 4.1.3.

When the switching potentials were -0.5 V and +0.5 V, the reduction peak C1 and also the four anodic peaks A1, A2, A3 and A4 were observed (fig. 4.1.3 black curve). The green curve of Fig. 4.1.3 shows the CV with applied switching potentials −0.15 V and +0.5 V, where the bulk deposition of Sn starts, the reduction peak C1 was observed, and also the other four anodic peaks A1, A2, A3, and A4 appeared.

By reducing the potential range to be between -0.03 V and +0.5 V (fig. 4.1.3 red curve) where Sn deposition has just not started, the reduction peak C1 appeared while the anodic peaks A1, A2 and A3 were not present and only the anodic process A4 was recorded as quite a broad peak, which clearly indicates that the anodic peaks A1, A2 and A3 are related to the oxidation of deposited bulk Sn. The cyclic voltammogram with switching potentials between +0.1 V and +0.5 V (fig. 4.1.3 blue curve) shows no Faradaic cathodic/anodic process confirming that the peak A4 must be due to dealloying/stripping of Sn considering that C1 is due to the alloying of Sn with Au

or due to an underpotential deposition process. A detailed answer would require an in situ STM experiment, which, for time reasons, could not be done in the framework of the present thesis.

In order to synthesize Sn nanowire films, constant potential and pulsed deposition experiments were performed. However, the sputtered layer on the membrane (gold or copper) was not thick enough to keep the nanowire arrays free standing. As a consequence, after removing of the template by dissolution in dichloromethane, rather a tiny fine powder of nanowires was obtained. Therefore, in order to keep the electrodeposited nanowires free standing, a thicker deposit was formed on the sputtered layer to serve as a supporting layer for the nanowires. As shown in [202], for the case of aluminum, strongly adherent free standing nanowire arrays can be obtained on an electrodeposited supporting layer of Al. Consequently, the same electrodeposition routine was employed for the synthesis of free standing Sn nanowires on either electrodeposited Sn or Cu supporting layers.

For Sn deposition in [EMIm]DCA the deposited bulk layer on the sputtered surface forms dendrites on both the Cu- and the Au-sputtered membrane, Figure 4.1.4.a shows the SEM micrograph for Sn deposition on a Au sputtered membrane at -0.2 V for 1 hour. This dendritic structure was also obtained by pulsed deposition at -0.3V for 2 hours (1 second on and 4 seconds off), Fig. 4.1.4b. Such dendritic structures cannot serve as a supporting layer for the growth of the nanowires as they are too brittle, completely collapsing during the dissolution of the membrane in dichloromethane as evidenced in figure 4.1.4.c. The deposition of Sn from $[Py_{1,4}]$DCA leads to a completely different, porous structure; figure 4.1.5a, b shows the grown nanowires through the template on the bulk porous Sn layer that was deposited on the Au sputtered surface.

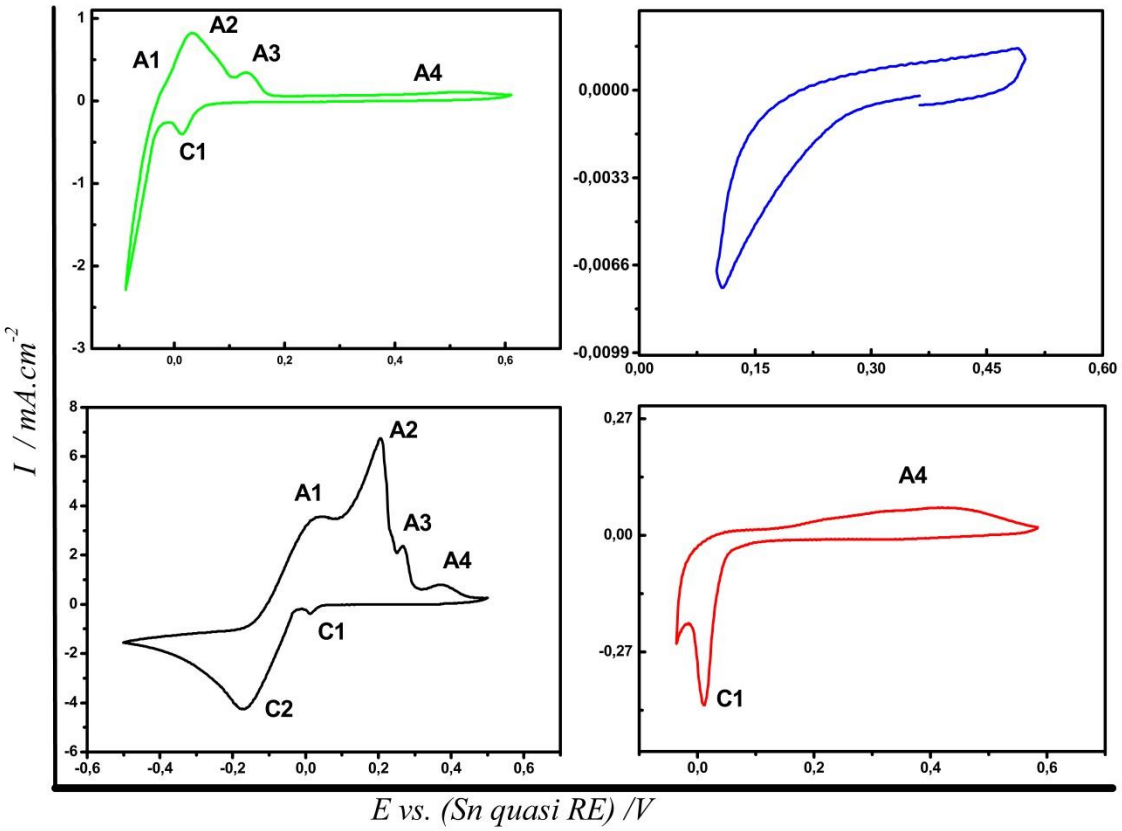

Fig. 4.1.3. *Cyclic voltammograms of Sn deposition on gold substrates in 0.1 M $SnCl_2$/[EMIm]DCA at different switching potentials, 25 °C and scan rate of 10 mV s^{-1}*

The top view of the sample after removing of the template by chemical dissolution in dichloromethane is shown in figure 4.1.5c where vertical Sn nanowires have bunched together. A higher magnification SEM micrograph presented in Fig. 4.1.5d shows the good adhesion of the nanowires to the supporting Sn layer. However the porous structure of the electrodeposited Sn supporting layer makes it quite brittle and sensitive to a certain damage.

Due to this complication, a thicker supporting layer of copper was alternatively deposited on the Cu sputtered membrane side from 1M CuCl/[EMIm]DCA.

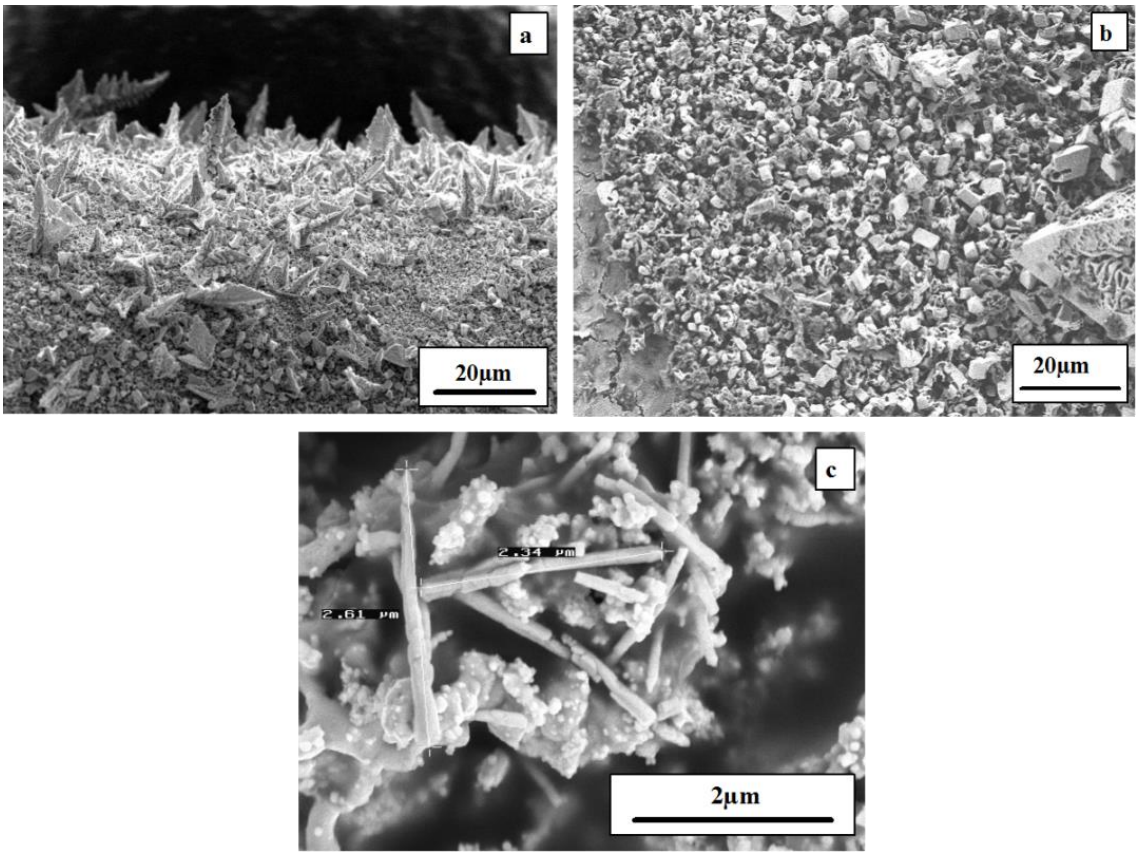

Fig. 4.1.4. *SEM micrographs of bulk Sn deposition in 0.1 M $SnCl_2$/[EMIm]DCA.* ***(a)*** *Constant potential deposition on Au-sputtered membrane at -0.2 V for 1 h.* ***(b)*** *Pulsed potentiostatic deposition at -0.3 V for 2 h (1 s on and 4 s off).* ***(c)*** *After removing the template*

As copper is used as anode current collector in Li ion batteries [203], the direct deposition of Sn nanowires on an electrodeposited Cu supporting layer might overcome the capacity fading that usually results from the bad connection between an anode material and the current collector.

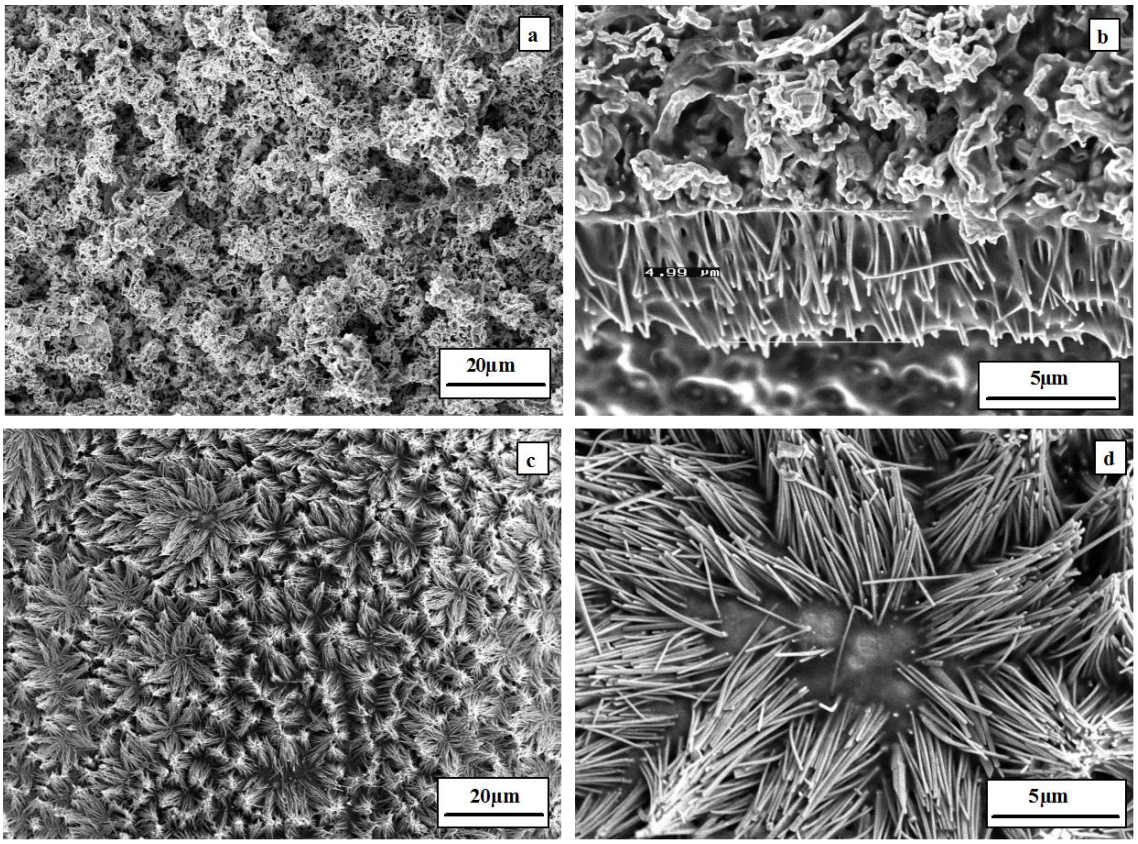

Fig. 4.1.5. *SEM micrographs of a Sn deposit in 0.1M $SnCl_2$/[$Py_{1,4}$]DCA by pulsed galvanostatic deposition at -2 mA for 2 h (1 s on and 4 s off). (a) Top view of bulk Sn obtained on the sputtered side. (b) Grown nanowires through the template. (c, d) Top view of Sn nanowires.*

For this purpose, the electrochemical deposition process was done in two steps; in the first step Sn was deposited from 0.1 M $SnCl_2$/[EMIm]DCA at -0.5 V for 30 min., through the non-sputtered side of the template while the sputtered side was completely isolated from the deposition electrolyte by Teflon tape. Thus, Sn nanowires grow through the membrane. In the second step the template was carefully removed from the ionic liquid as described above, rinsed with high purity isopropanol to remove the electrolyte residues, dried, and finally the side with the nanowires was isolated using Teflon tape so that only the Cu sputtered surface was in contact with the solution.

The thickness of such a deposited Cu layer can be controlled by several parameters including the concentration of the copper salt, the applied potential and the time of deposition. Figure 4.1.6 shows the cross section of the Cu layer that was potentiostatically deposited on a Cu sputtered membrane at -0.7V for 2 hours. As seen, the thickness of the deposited Cu layer is more than 20 µm with a dense and compact structure that makes it a suitable supporting layer for free standing Sn nanowires.

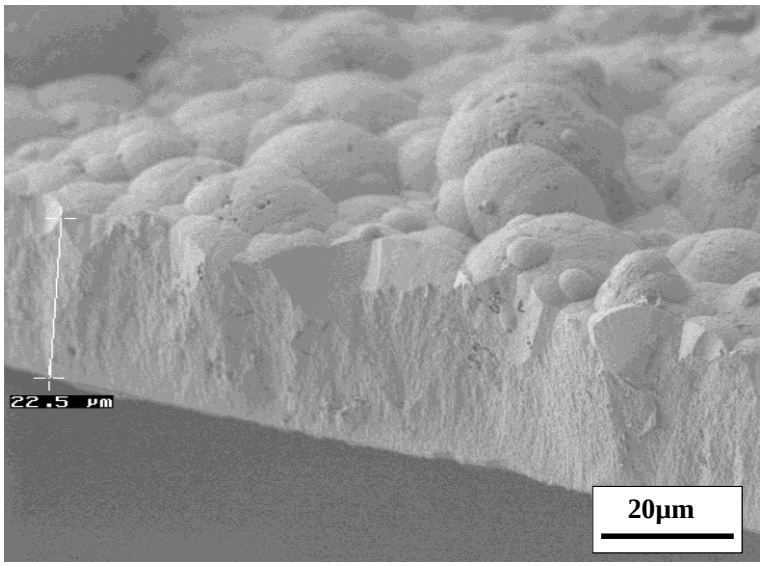

Figu.4.1.6. *Cross section of a Cu layer deposited potentiostatically at -0.7 V for 2 h from 1 M CuCl/[EMIm]DCA on a Cu-sputtered template*

The top view SEM micrograph of the vertically aligned Sn nanowires that were deposited at -0.5V for 30 min from 0.1M $SnCl_2$/[EMIm]DCA is depicted in figure 4.1.7. The nanowires are - more or less - vertically aligned on the Cu layer and bunched together. The length of the individual Sn nanowires ranges from 5 to 8 µm and is affected by the time of deposition, with the expected diameter from 90 to 120 nm.

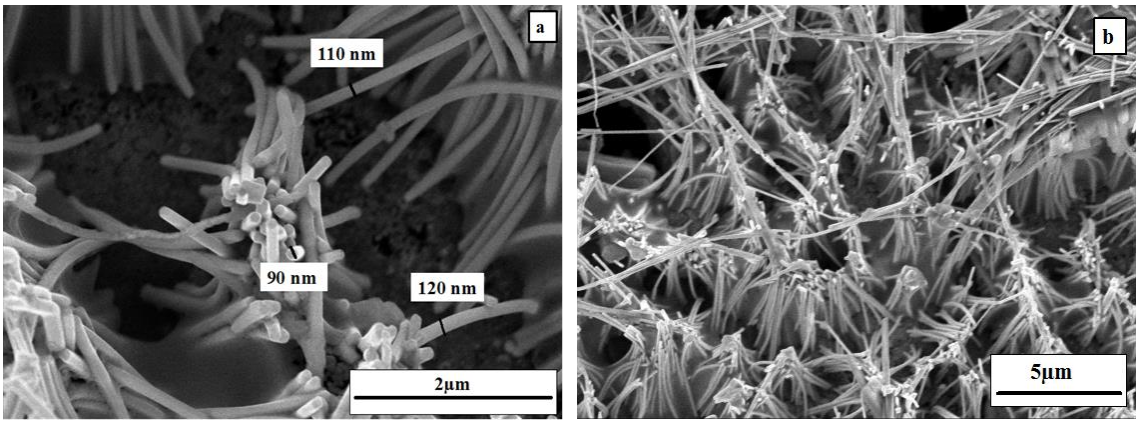

Fig.4.1.7. *SEM micrographs of Sn nanowires at different magnifications obtained potentiostatically in 0.1 M $SnCl_2$/[EMIm]DCA at a potential of -0.5 V versus Sn for 30 min on Cu sputtered membrane.*

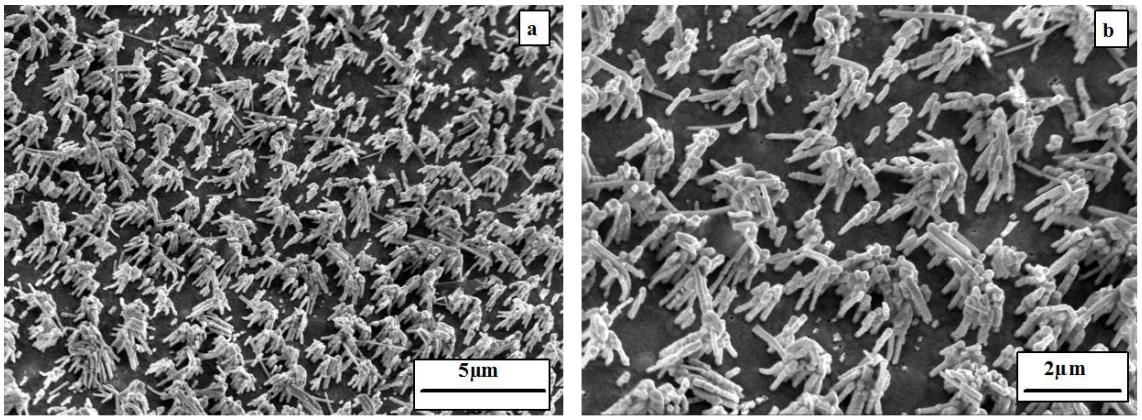

Fig. 4.1.8. *SEM micrographs of the Sn nanowires at different magnifications that were electrodeposited potentiostatically from 0.1 M $SnCl_2$/[EMIm]DCA at -0.5 V for 10 min on an electrodeposited Cu layer*

Figure 4.1.8 shows the SEM micrograph of the Sn nanowires electrodeposited from 0.1M $SnCl_2$/[EMIm]DCA at -0.5V for 10 min on an electrodeposited Cu layer.

As can be seen, free standing nanowire arrays are obtained on an electrochemically deposited Cu supporting layer, showing that such structures on electrodeposited Cu are feasible and of potential interest for the application as anodes in Li ion batteries.

4.2 Effect of the ionic liquid anion on the deposition morphology [204]

This part of the present thesis deals with the influence of the ionic liquid anion on the morphology of the tin deposits through a comparative study on the electrodeposition of tin from two different Ionic Liquids.

The electrodeposition of tin from two ionic liquids (ILs) containing the 1-butyl-1-methylpyrrolidinium cation ($[Py_{1,4}]^+$) and the trifluoromethylsulfonate (TfO^-) or dicyanamide (DCA^-) anion is investigated by cyclic voltammetry, scanning electron microscopy (SEM), infrared (IR) spectroscopy and X-ray diffraction. Cyclic voltammetry is employed to evaluate the electrochemical behavior of $SnCl_2$ in the two ILs, and IR spectroscopy is used to study the difference in the complexation of $SnCl_2$ in the two ILs. The electrodeposition of tin is also studied in 1-ethyl-3-methylimidazolium dicyanamide ([EMIm]DCA) for the purpose of comparison.

Gold and copper electrodes were employed to investigate the electrochemical behavior of $SnCl_2$ and the morphology of the tin deposits.

The morphology of the electrodeposited tin from the different ILs is investigated by SEM, which shows that the morphology of the tin deposits changes upon changing the IL. Agglomerated tin deposits are obtained on gold and copper from $[Py_{1,4}]$TfO. Tin dendrites were obtained both from $[Py_{1,4}]$DCA and [EMIm]DCA as will be shown in the SEM micrographs.

A comparison of two cyclic voltammograms on gold from 0.05 M $SnCl_2$/$[Py_{1,4}]$TfO and 0.05 M $SnCl_2$/$[Py_{1,4}]$DCA is shown in figure 4.2.1. The electrode potential was scanned initially from the open circuit potential in the negative direction at a scan rate of 10 mVs^{-1}.

The cyclic voltammogram of 0.05 M $SnCl_2$/$[Py_{1,4}]$TfO on gold exhibits four reduction peaks/waves in the forward scan and four oxidation processes in the backward scan. The reduction peak at C4 is attributed to the bulk deposition of tin. The reduction process at C1 might be an adsorption process of the ionic liquid on gold. The reduction processes C2 and C3 are

discussed below. In contrast, the CV of 0.05 M $SnCl_2$/[$Py_{1,4}$]DCA on gold shows three reduction peaks in the forward scan. The reduction process at C3 is due to the bulk deposition of tin on gold. Four oxidation peaks (A1, A2, A3, and A4) were clearly observed in the backward scan of the CV on gold for both ionic liquids. The peaks at A4 and A3 are correlated with the stripping of the electrodeposited tin. The other two peaks at A2 and A1 seem to be associated with C2 and C1, respectively.

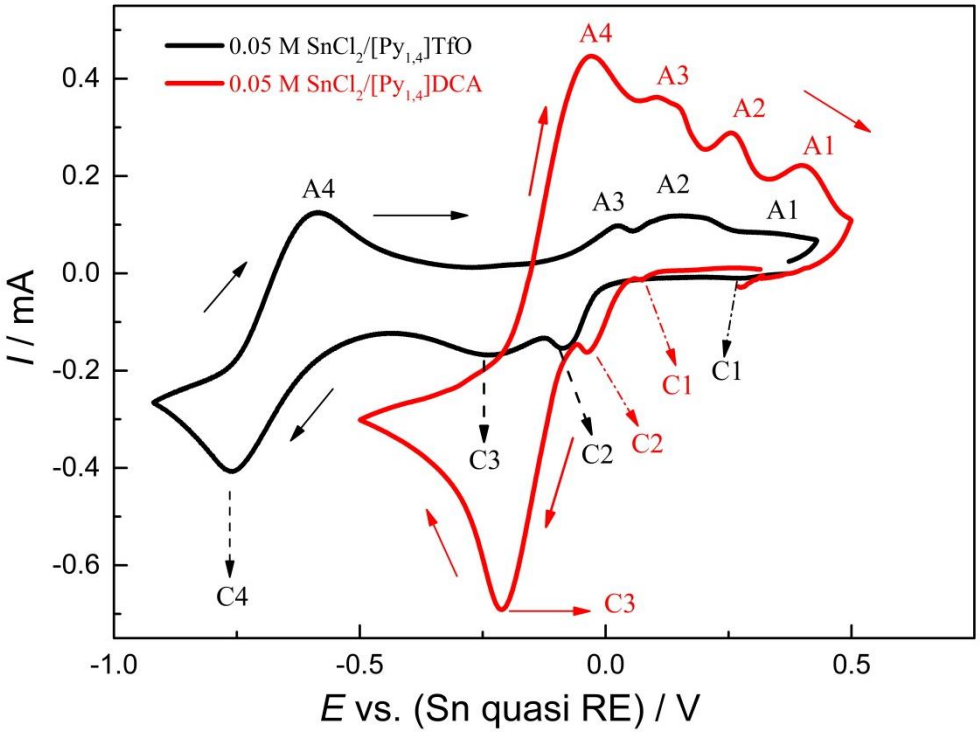

Fig. 4.2.1. *CVs of 0.05 M $SnCl_2$ in [$Py_{1,4}$]TfO (black) (between the vertex potentials -0.85 and +0.5 V) and [$Py_{1,4}$]DCA (red) (between the vertex potentials -0.5 and +0.5 V) on microcrystalline gold electrodes at room temperature. Scan rate:10 mVs^{-1}.*

In order to get a deeper insight into the complicated electrochemical behavior of $SnCl_2$ in [$Py_{1,4}$]TfO on gold, CVs were recorded at two different switching potentials and the corresponding voltammograms are compared in figure 4.2.2. It was observed that only one reduction peak (C2) and its corresponding counterparts A1 (seen as a shoulder) and A2 are obtained when the scan is switched at -0.1 V. Two reduction peaks (C2 & C3) and their

corresponding oxidation peaks A1, A2, A3 and $A3^{I}$, respectively, were observed when the scan was switched at -0.4 V. It is evident from figure 4.2.2 that the oxidation peaks at A3 and A4 in figure 4.2.1 can thus be related to the reduction peaks at C3 and C4, respectively.

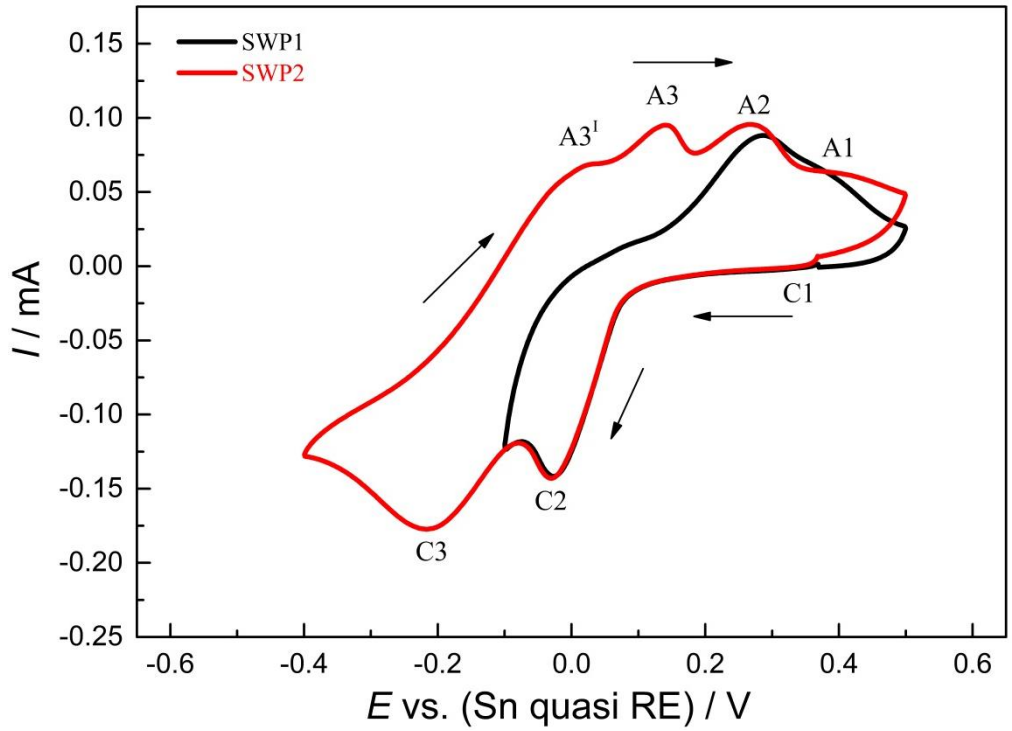

Fig. 4.2.2. *CVs of 0.05 M $SnCl_2$ in $[Py_{1,4}]TfO$ on gold at two different switching potentials (SWPs) at room temperature. Scan rate: 10 mVs^{-1}.*

To understand the complicated reduction processes of $SnCl_2$ in $[Py_{1,4}]$DCA better, CVs were recorded at various switching potentials, too. Figure 4.2.3 shows the CVs at three different anodic/cathodic switching potentials. When the applied switching potentials were chosen between - 0.1 V and + 0.65 V, three reduction peaks (C1, C2, and C3) and also three oxidation peaks A1, A2, and A3 were observed. Upon decreasing the range of the applied switching potentials to - 0.03V and + 0.6V, two reduction peaks (C1 and C2) were clearly seen and the anodic peaks A2 and A3 disappeared, with only one single wide oxidation process at A1. Upon further decreasing the range of the applied switching potentials to + 0.1 V and + 0.5 V, only one

slight reduction process (C1) and no clear anodic process were recorded. This indicates that the anodic peaks A2 and A3 are related to the deposition of tin at C3.

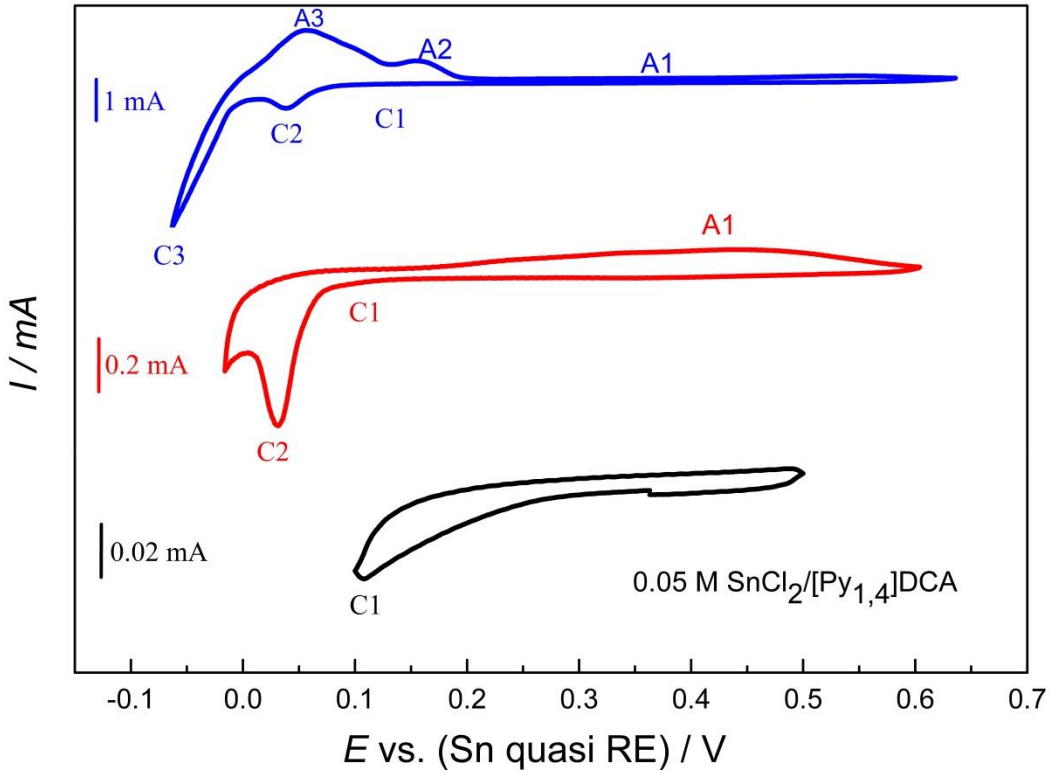

Fig. 4.2.3. *CVs of 0.05 M $SnCl_2$ in $[Py_{1,4}]DCA$ on gold at various switching potentials at room temperature. Scan rate: 10 mVs^{-1}.*

To analyse further the behavior of $SnCl_2$/$[Py_{1,4}]TfO$, potentiostatic electrolysis with 0.1 M $SnCl_2$ in $[Py_{1,4}]TfO$ was carried out at C2 and at C3 for 1 hour on gold at RT. Neither any macroscopic deposit nor a visual colour change on the gold surface was observed after electrolyzing the solutions at C2. Therefore, this reduction process is presumably due to an underpotential deposition process (upd). However, electrolysis at C3 yielded a silver grey mirror-like finish on the gold surface from both of the solutions. The samples were thoroughly washed and analysed by XRD. The XRD analysis reveals the formation of AuSn alloys and the corresponding diffractograms are shown in figure 4.2.4.

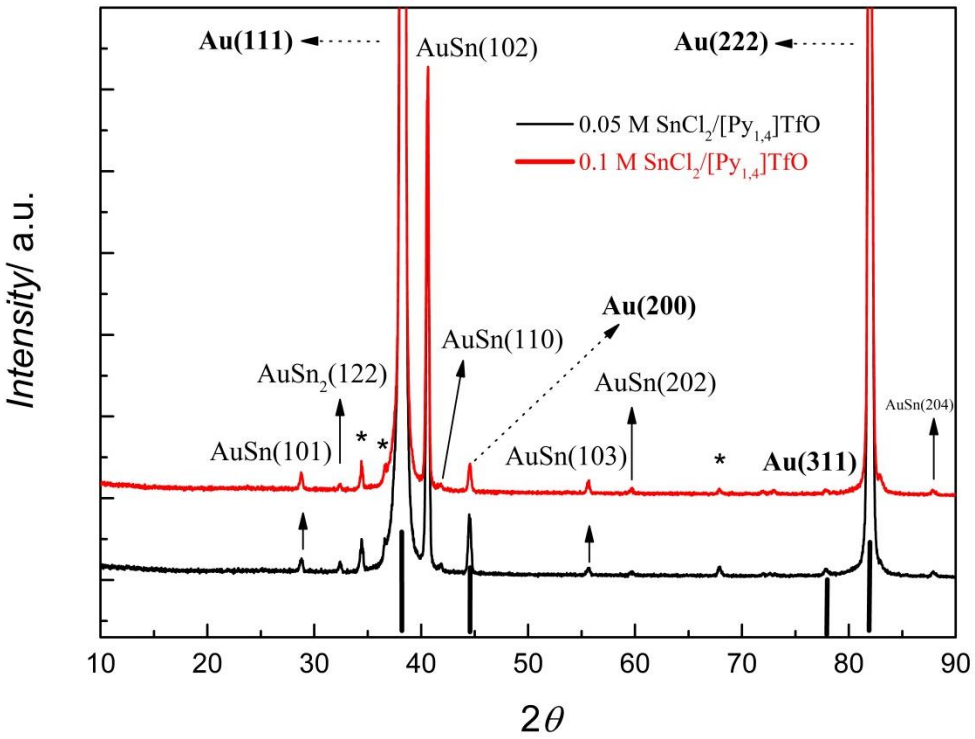

Fig. 4.2.4. *XRD of gold/tin after electrolysis at -0.2 V from $SnCl_2$/[$Py_{1,4}$]TfO at room temperature. The bold vertical lines and stars indicate diffraction patterns due to the gold substrate.*

A clear peak is observed at 40.6° that corresponds to AuSn(102), as well as other representative peaks of AuSn (JCPDS No. 08-0463) are observed in both of the diffractograms. Furthermore, quite a low intensity peak is observed at ~ 32.4° that belongs to the $AuSn_2$(122) plane (JCPDS No. 28-0440). Thus, from the cyclic voltammetry and electrolysis results, the reduction peaks (C2 and C3) are indeed related to surface reduction processes and alloying.

In order to obtain information on the morphology of the tin deposits, a controlled-potential electrolysis was carried out on gold from 0.05 M $SnCl_2$/[$Py_{1,4}$]TfO and from 0.05 M $SnCl_2$/[$Py_{1,4}$]DCA at -0.7 V and at -0.1 V, respectively, for one hour at RT. The samples were washed in dichloromethane followed by acetone and dried inside of the glove-box to avoid oxidation of the deposits. The corresponding SEM images are shown in figures 4.2.5a and 4.2.5b. It can be seen in figure 4.2.5a that a tin deposit with particles is obtained from 0.05 M

$SnCl_2$/[$Py_{1,4}$]TfO on gold whereas rather spiral tin dendrites were achieved from $SnCl_2$/[$Py_{1,4}$]DCA.

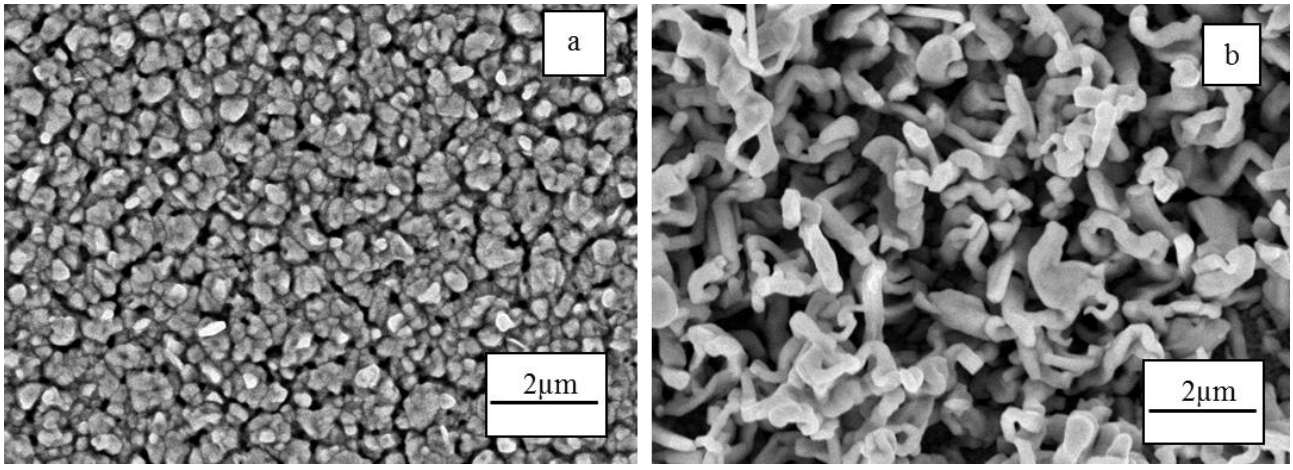

Fig. 4.2.5. *Microstructure of the tin deposits obtained from 0.05 M $SnCl_2$ in (a) [$Py_{1,4}$]TfO and (b) [$Py_{1,4}$]DCA on gold at room temperature.*

These results suggest that, at the very least, the anion has an influence on the deposition which can be due to different $SnCl_2$ complexes or to different interfacial processes. Thus, to better understand, the behavior of $SnCl_2$ in ILs was investigated using IR spectroscopy.

Figure 4.2.6a represents the mid-IR spectra of $SnCl_2$/[$Py_{1,4}$]TfO with reference to the neat ionic liquid. The spectrum of the pure [$Py_{1,4}$]TfO (black line, Figure 4.2.6a) shows peaks of $[Py_{1,4}]^+$ in the range between 2700 and 3100 cm^{-1} and TfO^- species in the range between 500 and 1500 cm^{-1} [205]. Upon addition of $SnCl_2$ to the ionic liquid, a slight decrease in the peak intensities at 516, 572, 635, 1028, 1223 and 1254 cm^{-1} was observed. No additional peaks are observed in the mid-IR region. In the far-IR region, the peaks around 350, 320 and 209 cm^{-1} correspond to the vibration modes of the TfO^- anion. Upon addition of $SnCl_2$ (Figure 4.2.6b), two new peaks at 265 and 296 cm^{-1} were observed in the far-IR spectrum, and all TfO^- peaks decreased in intensity.

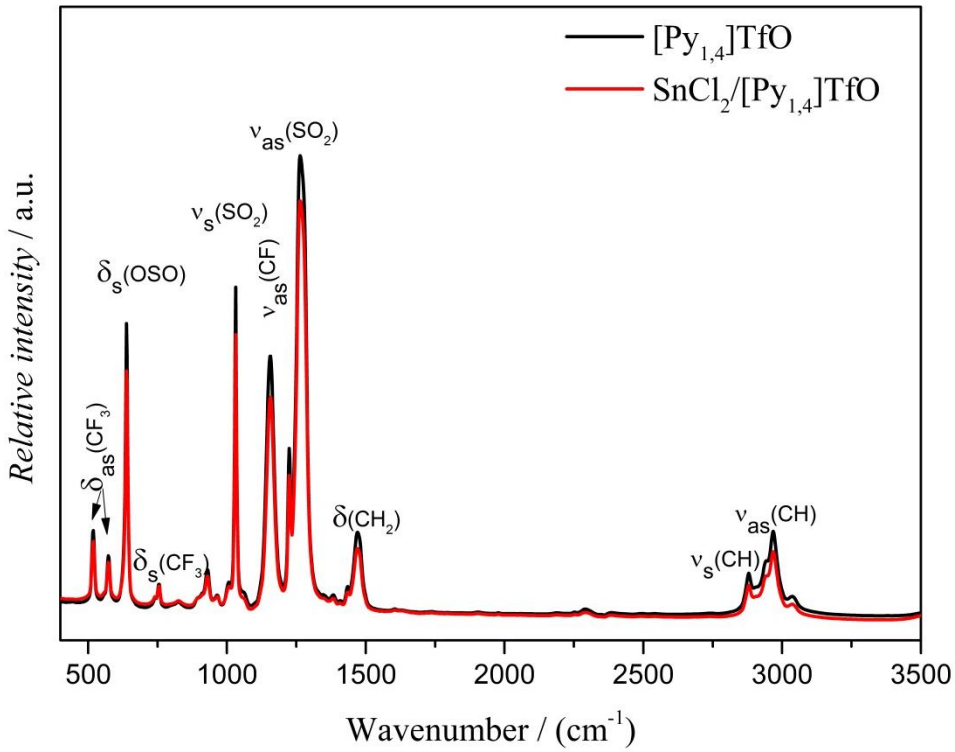

Fig. 4.2.6a. *mid-IR spectra of $SnCl_2$/[$Py_{1,4}$]TfO and neat [$Py_{1,4}$]TfO*
δ = group angle deformation, ν= bond stretch, s =totally symmetric and as= asymmetric

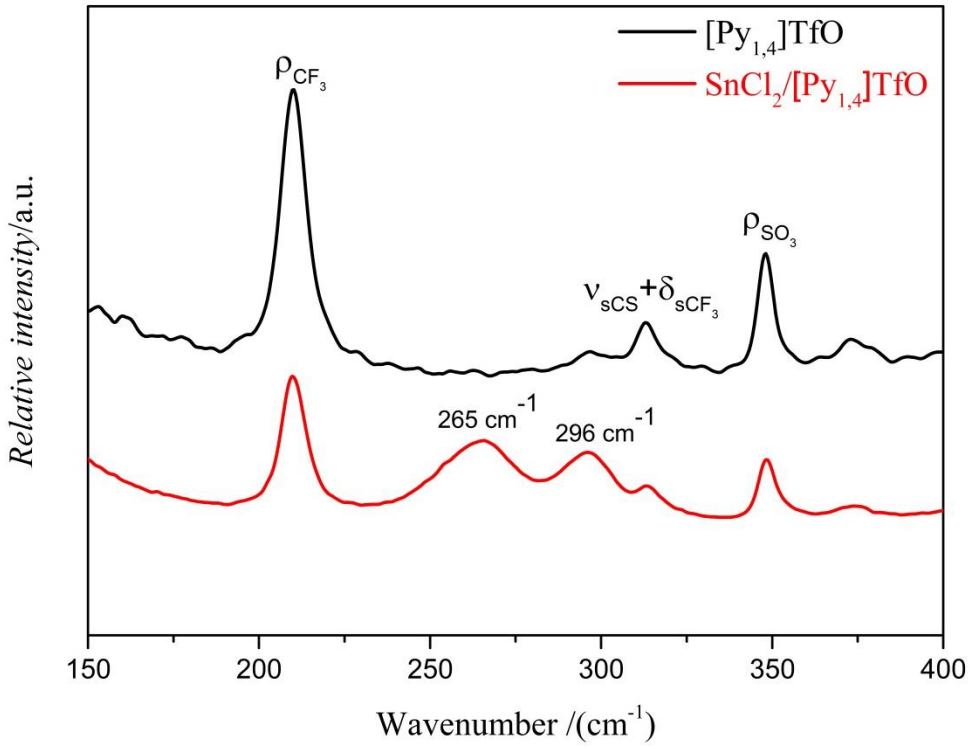

Fig. 4.2.6b. *far-IR spectra of $SnCl_2$/[$Py_{1,4}$]TfO and neat [$Py_{1,4}$]TfO*
δ = group angle deformation, ρ= group, rock, ν= bond stretch and s =totally symmetric

The Sn-Cl stretching occurs approximately between 330 and 354 cm^{-1}. It has been shown that there is a negative shift in the Sn-Cl band stretching frequencies upon complexation [206]. Therefore, the two new peaks at 265 and 296 cm^{-1} might correspond to a complex formation between the $SnCl_2$ and $[CF_3SO_3]^-$ and $[Py_{1,4}]^+$ species [205]. A similar type of decrease in intensity and formation of additional peaks in the mid-IR region was also observed in the $TaCl_5$/$[Py_{1,4}]$TfO system [207].

Figure 4.2.7a compares the mid-IR spectra of $[Py_{1,4}]$DCA and $SnCl_2$/$[Py_{1,4}]$DCA. Prominent IR peaks of both $[Py_{1,4}]^+$ and DCA anion are observed for the pure ionic liquid. The dicyanamide ion peaks were assigned on the basis of lead dicyanamide reported in literature [208]. After addition of $SnCl_2$ to the ionic liquid, no changes in the spectra especially between 2000 and 2300 cm^{-1} are observed which suggests that tin(II) dicyanamide has not formed. However, in the far-IR spectra two new peaks at 254 and 291 cm^{-1} are evident (Figure 4.2.7b). As the Sn-Cl stretching arises between 330 and 350 cm^{-1}, the shift to lower wavenumbers can be assigned to the complex species formed between $SnCl_2$ and $[Py_{1,4}]$DCA. By comparing figure 4.2.7b with figure 4.2.6b, it is evident that there is a shift in the peak positions for the Sn-Cl complex species, indicating the formation of different complex species in the DCA^- and TfO^- ionic liquids. A comprehensive analysis of the IR spectra is, however, beyond the scope of the present thesis.

Therefore, from IR spectroscopy, it can be concluded that the complex species of $SnCl_2$ formed are different in the two different ILs containing the same cation. These $SnCl_2$ species might influence the kinetics of the deposition and thus partially contribute to suppress the rate of tin deposition in the case of $SnCl_2$/$[Py_{1,4}]$TfO to obtain dendrite free tin deposits. Furthermore, the interfacial behavior of both liquids must be different and could also be an influencing factor for the deposition of Sn. It is an open question at this point, what the exact species are in the bulk and at the interface and how the Sn deposition is influenced by the species.

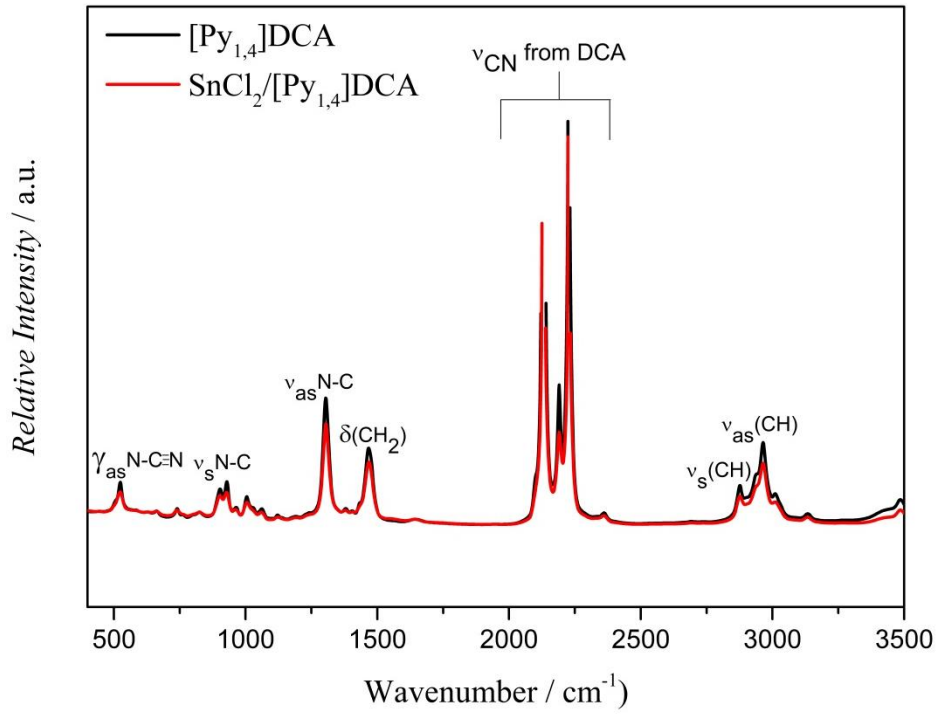

Fig. 4.2.7a. *Mid-IR spectra $SnCl_2$/[$Py_{1,4}$]DCA (red) and neat [$Py_{1,4}$]DCA (black)*
δ = group angle deformation, γ= out of –plane vibration, ν= bond stretch and s =totally symmetric, as= asymmetric

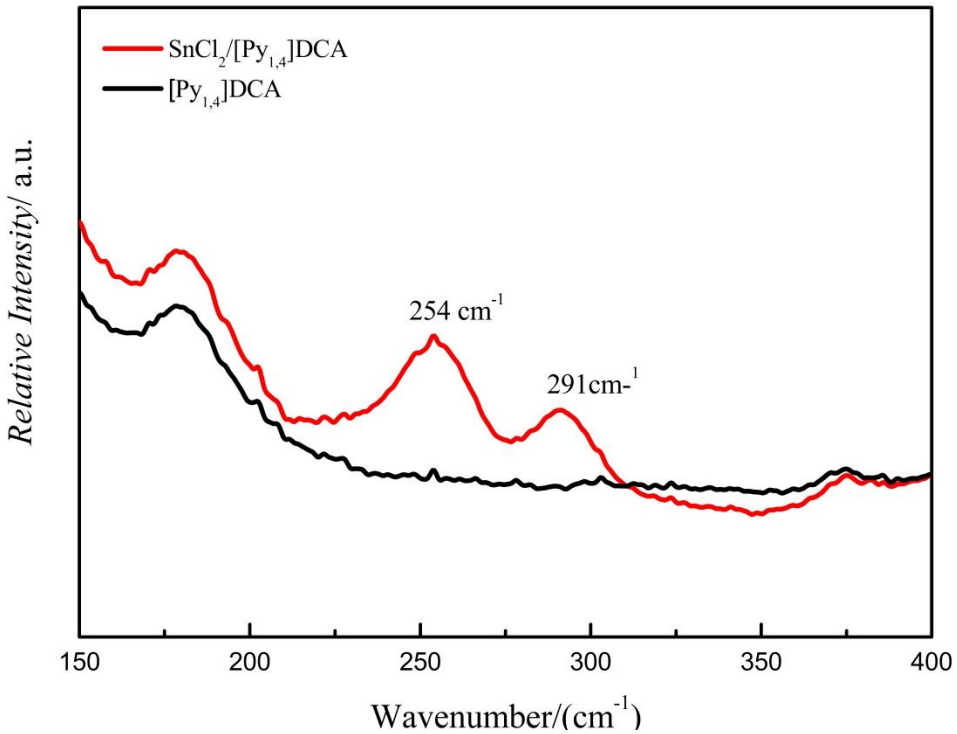

Fig. 4.2.7b. *Far-IR spectra of $SnCl_2$/[$Py_{1,4}$]DCA (red) and neat [$Py_{1,4}$]DCA (black)*

Since tin films on copper are possibly suitable candidates as an anode host material in Li-ion batteries, it is interesting to study tin deposition on copper from the employed ionic liquids, too. Thus, electrochemical experiments on copper from the mentioned ionic liquids were carried out. A comparison of two cyclic voltammograms of 0.05 M $SnCl_2$/$[Py_{1,4}]$TfO and 0.05 M $SnCl_2$/$[Py_{1,4}]$DCA on copper is given in Figure 4.2.8.

The voltammograms were recorded by sweeping the electrode potential in the negative direction from the OCP at a scan rate of 10 mVs^{-1}. Here, three reduction processes C1 to C3 were observed in the forward scan on copper from 0.05 M $SnCl_2$/$[Py_{1,4}]$TfO and one reduction peak C1 in 0.05 M $SnCl_2$/$[Py_{1,4}]$DCA, respectively. In both CVs several oxidation processes were observed. The processes at C3 and C1 are due to the bulk deposition of tin from $[Py_{1,4}]$TfO and $[Py_{1,4}]$DCA, respectively. The reduction waves at C1 and C2 in the case of $SnCl_2$/$[Py_{1,4}]$TfO might be due to under potential deposition (upd) of tin and alloying of tin with copper, respectively. According to literature data, various copper-tin alloys can exist such as Cu_6Sn, Cu_3Sn, and Cu_4Sn. The anodic peaks A3 and A2 in the CV of $SnCl_2$/$[Py_{1,4}]$TfO must be due to the stripping of Sn and the shoulder at A1 seems to be associated with the reduction process C1.

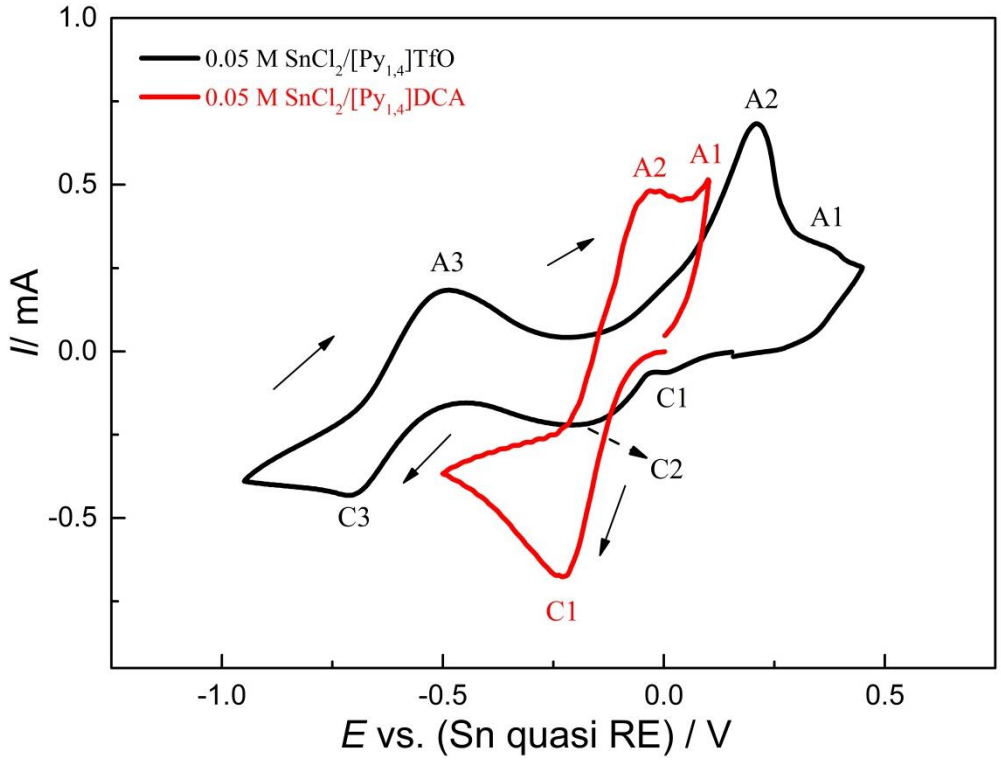

Fig. 4.2.8. *CVs of 0.05 M $SnCl_2$/[$Py_{1,4}$]TfO and 0.05 M $SnCl_2$/[$Py_{1,4}$]DCA on copper at room temperature. Scan rate: 10 mVs^{-1}.*

Constant-potential electrolysis was subsequently carried out on copper from 0.05 M $SnCl_2$/[$Py_{1,4}$]TfO and 0.05 M $SnCl_2$/[$Py_{1,4}$]DCA at -0.75 V and at -0.25 V for one hour at RT, respectively. The obtained deposits were washed in dichloromethane followed by acetone and dried inside the glove box to prevent oxidation of the deposits. The corresponding SEM images are shown in figures 4.2.9a and 4.2.9b. Similar to the deposition results on gold, tin crystals were obtained from 0.05 M $SnCl_2$/[$Py_{1,4}$]TfO (Figure 4.2.9a). However, rather a dendritic deposit was obtained from $SnCl_2$/[$Py_{1,4}$]DCA (Figure 4.2.9b) as well as rods, as can be seen in the inset of figure 4.2.9b.

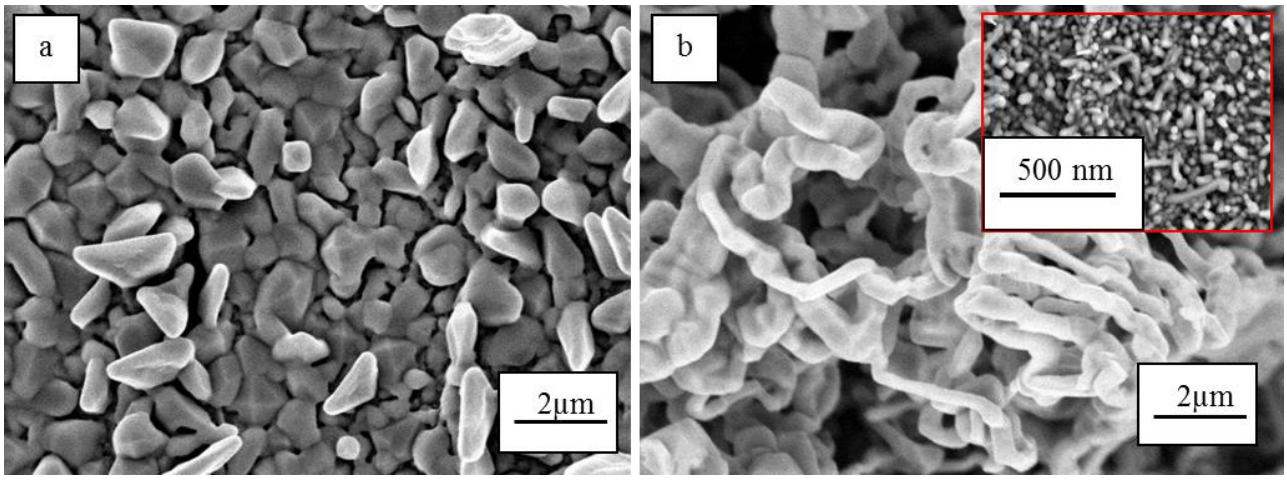

Fig. 4.2.9. *Microstructure of tin electrodeposits obtained on copper from a) [$Py_{1,4}$]TfO and b) [$Py_{1,4}$]DCA.*

For the sake of comparison, electrochemical studies were also carried out for 0.05 M $SnCl_2$/[EMIm]DCA on gold and copper under similar experimental conditions as described above. Two cyclic voltammograms on gold and on copper from 0.05M $SnCl_2$ in [EMIm]DCA are shown in figure 4.2.10. The voltammograms were obtained by scanning the electrode potential first in the negative direction from OCP at 10 mVs^{-1} scan rate.

Two reduction processes C1 and C2 were observed in the forward scan on gold from $SnCl_2$ in [EMIm]DCA. In the backward scan of CV, four oxidation processes A1 to A4 were observed. The electrochemical behavior of $SnCl_2$ in [EMIm]DCA is quite similar to that of [$Py_{1,4}$]DCA except an increase in the current, likely due to the lower viscosity of [EMIm]DCA compared to the higher viscosity of [$Py_{1,4}$]DCA. The bulk deposition of tin was observed at C2, and the reduction process C1 seems to be due to the adsorption of the ionic liquid on the working electrode or to a surface alloying/upd of tin with gold. Furthermore, the electrochemical behavior of $SnCl_2$ in [EMIm]DCA on copper is quite similar to that of $SnCl_2$ in [$Py_{1,4}$]DCA. The reduction peak at C1 is attributed to the bulk deposition of tin on copper.

In this case vibrational spectroscopy of [EMIm]DCA and $SnCl_2$/[EMIm]DCA were also performed for comparison purposes. The mid-IR spectra of [EMIm]DCA and $SnCl_2$/[EMIm]DCA are shown in figure 4.2.11a.

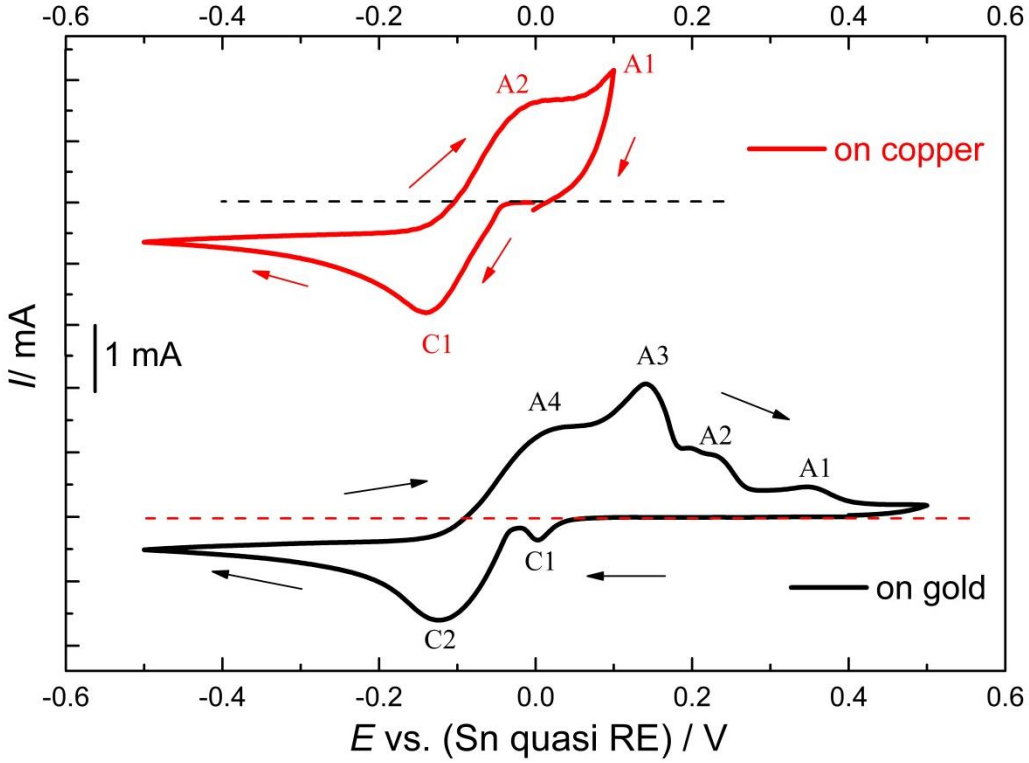

Fig. 4.2.10. *CVs of 0.05 M $SnCl_2$ in [EMIm]DCA on gold (black) and on copper (red) at room temperature. Scan rate: 10 mVs^{-1}.*

The pure ionic liquid shows prominent vibration modes of EMIm and DCA. After addition of $SnCl_2$ to the ionic liquid, a decrease of intensity is evident. Furthermore, a shift in the γCH_3 peak can be observed. In the far-IR spectra (Figure 4.2.11b), two medium intensity peaks were seen at 246 and 287 cm^{-1} in $SnCl_2$/[EMIm]DCA, indicating a formation of Sn-Cl complex species with the ionic liquid. Furthermore, the peak positions of $SnCl_2$ complex species have shifted to lower wavenumbers upon varying the cation of the ionic liquid, i.e. 246 and 287 cm^{-1} for $SnCl_2$/[EMIm]DCA (Figure 4.2.11b), and 254 and 291 cm^{-1} for $SnCl_2$/[$Py_{1,4}$]DCA (Figure 4.2.7b).

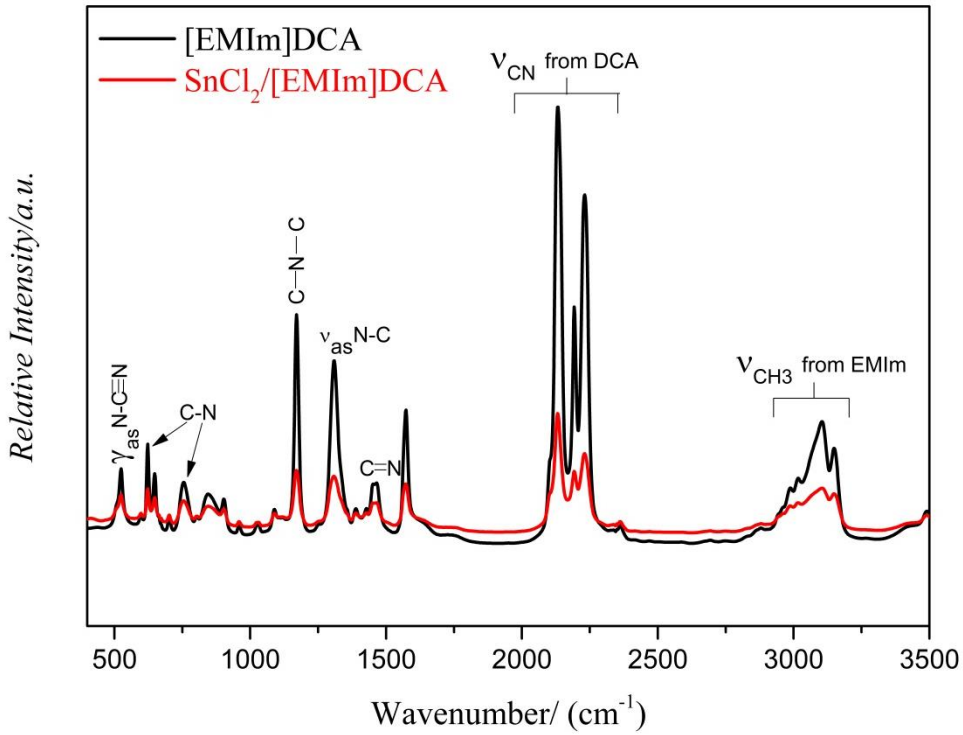

Figure 4.2.11a. *mid-IR spectra of $SnCl_2$/[EMIm]DCA (red) and neat [EMIm]DCA (black). γ= out of –plane vibration, ν= bond stretch and as= asymmetric*

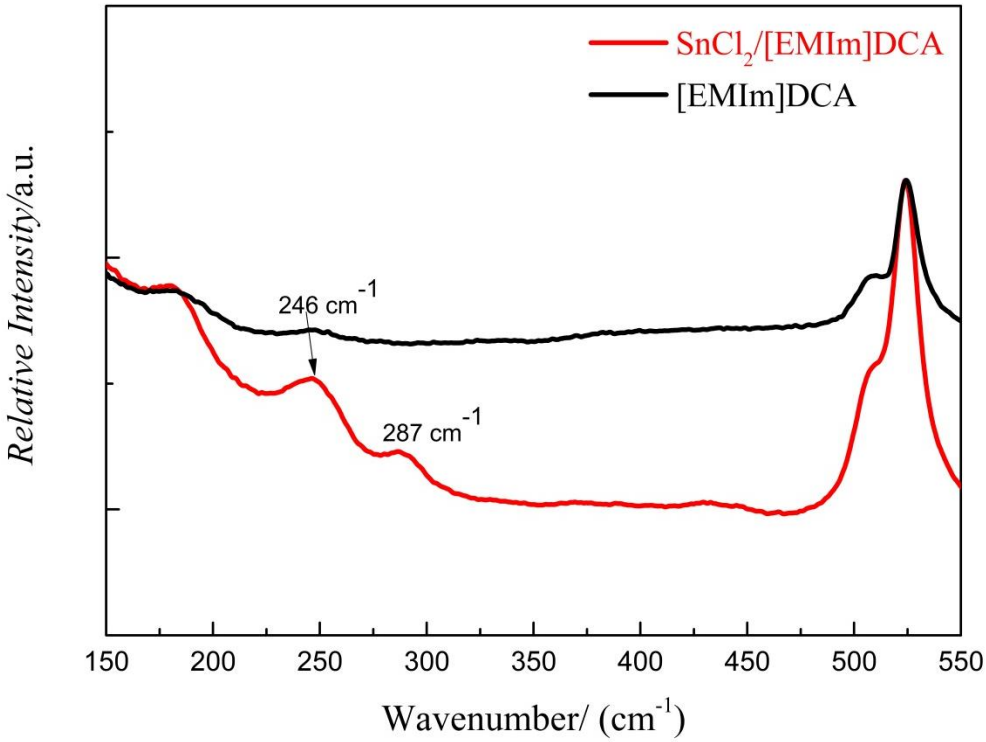

Figure 4.2.11b. *Far-IR spectra of $SnCl_2$/[EMIm]DCA (red) and neat [EMIm]DCA (black).*

This shift in the peaks appears to be due to the difference of cation species of the DCA ionic liquids. Thus, from the IR studies in figures 4.2.6, 4.2.7 and 4.2.11, it is evident that both cation and anion influence the complex formed between $SnCl_2$ and the ionic liquid.

Controlled-potential electrolysis was carried out to deposit tin either on gold (at -0.25 V) or on copper (at -0.25 V) from [EMIm]DCA. The washed deposits were analyzed using SEM. Figures 4.2.12a and 4.2.12b show the SEM images of tin that was obtained on gold and on copper from [EMIm]DCA, respectively. The deposits on both of the substrates are similar to each other and to the deposit obtained from $SnCl_2$/$[Py_{1,4}]$DCA.

The X-ray diffractograms of the tin deposits on copper and on gold from potentiostatic electrolysis are depicted in figure 4.2.13a and figure 4.2.13b from the three ionic liquids at RT, respectively. The tin deposits on gold from DCA liquids exhibit the characteristic diffraction peaks of tetragonal tin (JCPDS No: 04-0673). Furthermore, peaks are observed, which correspond to gold-tin alloys (AuSn, JCPDS No. 08-0463). In the case of tin on gold obtained from $[Py_{1,4}]$TfO the deposit exhibits the characteristic peaks of tetragonal tin.

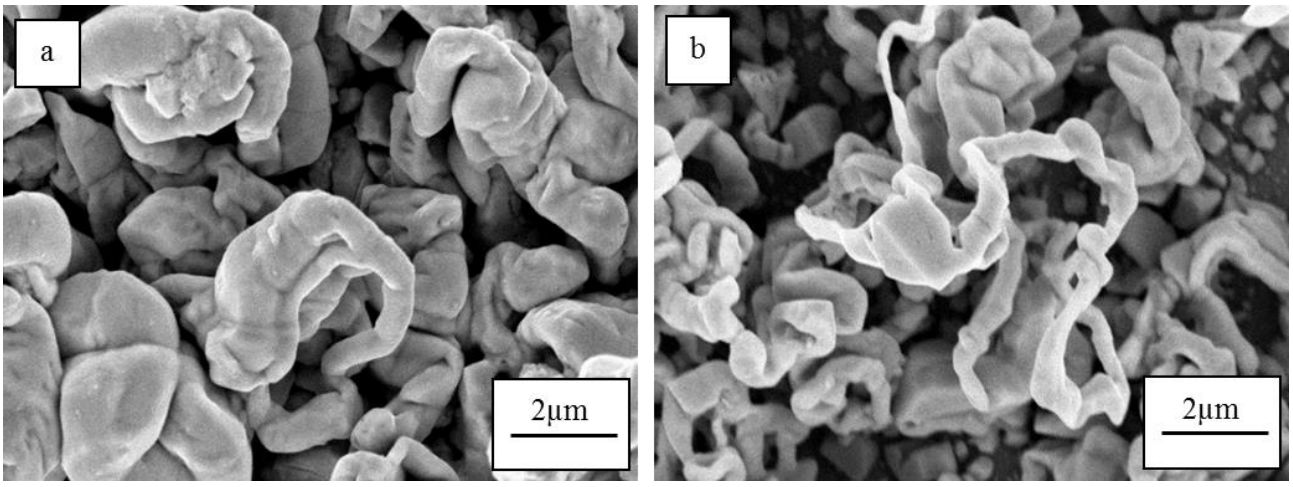

Fig. 4.2.12. *Microstructure of tin electrodeposits obtained from [EMIm]DCA on (a) gold and on (b)copper.*

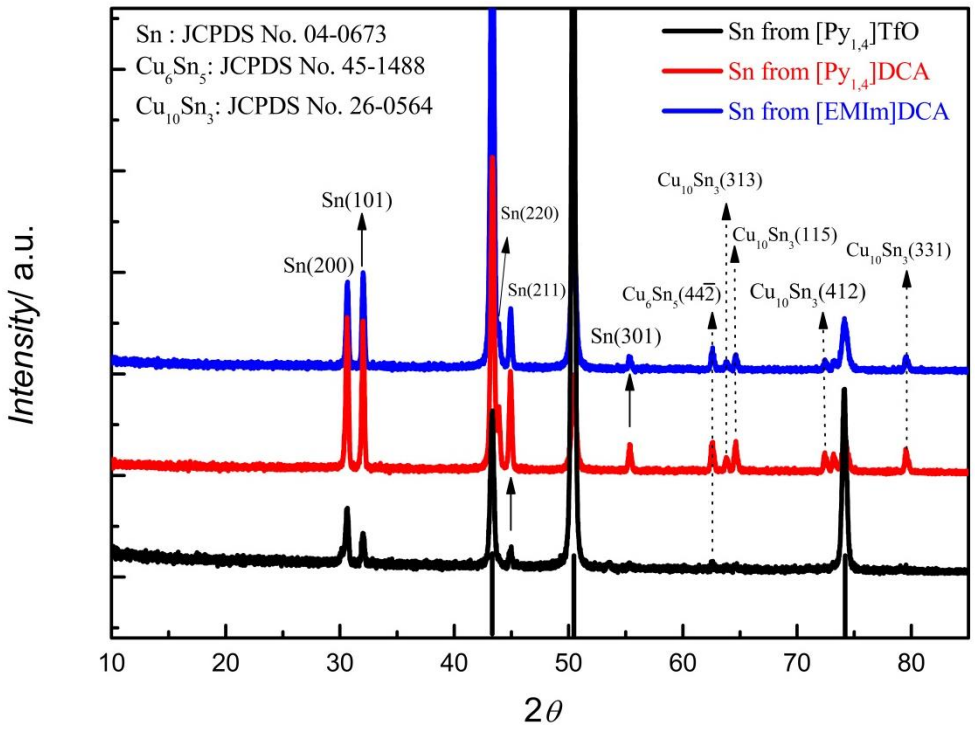

Figure 4.2.13a *XRD of the tin deposits obtained on copper from [$Py_{1,4}$]TfO,[$Py_{1,4}$]DCA and [EMIm]DCA. The bold vertical lines indicate the diffraction peaks of copper*

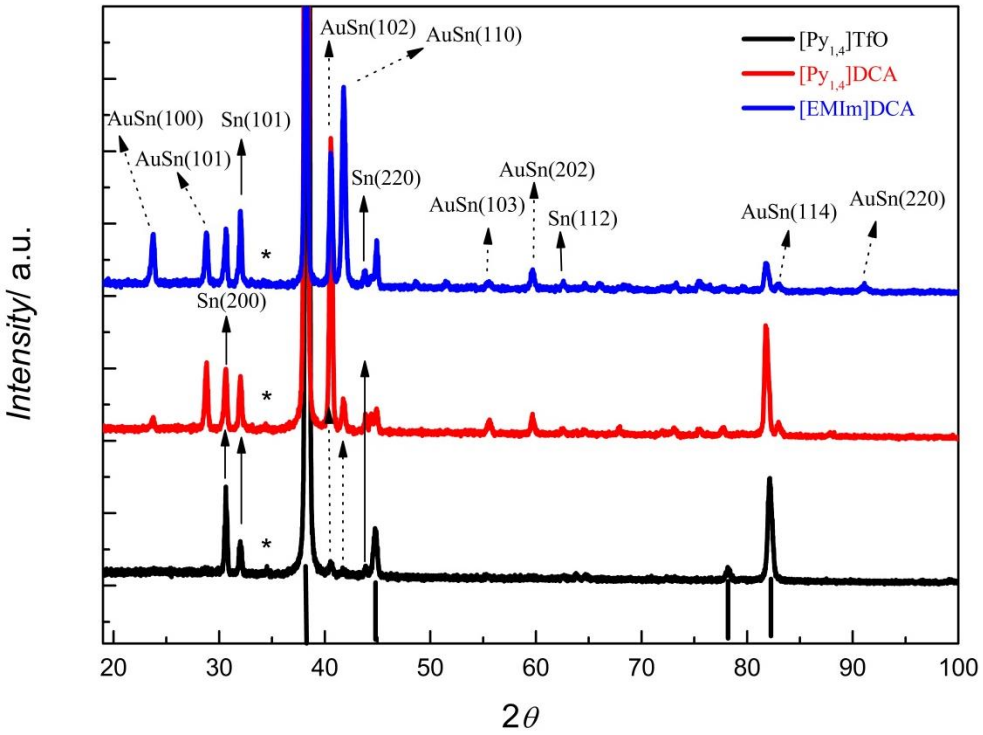

Figure 4.2.13b *XRD of the tin deposits obtained on gold from [$Py_{1,4}$]TfO, [$Py_{1,4}$]DCA and [EMIm]DCA. The bold vertical lines and stars represent the diffraction peaks of gold.*

A surprising result is that the alloying seems to be suppressed in the case of TfO^-, in comparison to ILs with DCA^-. The deposits obtained on copper from $[Py_{1,4}]$DCA and [EMIm]DCA show the characteristic diffraction peaks of tetragonal tin (JCPDS No. 04-0673) along with diffraction peaks of copper-tin alloys (Cu_6Sn_5 and $Cu_{10}Sn_3$). However, the diffractogram of tin on copper from $[Py_{1,4}]$TfO also exhibits mostly the characteristic peaks of tin as in the case of tin deposit on gold from the same liquid. In direct comparison $[Py_{1,4}]$TfO seems to suppress alloying of Sn with copper.

4.3 Electrodeposition of ZnSn [209]

Tin based alloys such as Zn-Sn, for example, can provide better corrosion protection than zinc alone or tin alone. Moreover, they can be regarded as promising anode host materials for lithium ion batteries. Traditionally, Zn-Sn deposits can be obtained from aqueous and organic electrolytes. Nevertheless, due to environmental concerns and hydrogen evolution of aqueous electrolytes, Ionic liquids have also been used as electrolytes. Sun et al. reported the deposition of Cu-Zn and Zn-Sn alloys from $ZnCl_2$/1-ethyl-3-methylimidazolium chloride ionic liquids and of tin from 1-ethyl-3-methylimidazolium dicyanamide [91,181]. Abbott et al. reported the electrodeposition of Zn-Sn from urea and ethylene glycol/choline chloride based deep eutectic solvents [93]. Recently, Pereira et al. studied the electrodeposition of Zn-Sn from deep eutectic solvents containing Ethylenediaminetetraacetic acid (EDTA), (Hydroxyethyl)ethylenediaminetriacetic acid (HEDTA), and *N*-(2-hydroxyethyl)ethylenediamine-*N*,*N'*,*N'*-triacetic acid trisodium salt (Idranal VII) and described their effects on the voltammetric behavior of zinc and tin and on the resultant morphology [210].
In this part of the present thesis the electrodeposition of ZnSn films and of free standing nanowire arrays from the ionic liquid $[Py_{1,4}]$TfO is reported.

The deposits obtained by electrodeposition on gold substrates were characterized by SEM-EDX and XRD. The effect of the deposition potential on the composition, phase structure and morphology of the deposits was also examined. Furthermore, free-standing Zn-Sn nanowires with different diameters and lengths were synthesized by template-assisted electrodeposition using polycarbonate membranes as templates.

4.3.1 Electrodeposition of Zn, Sn and Zn-Sn films

Fig. 4.3.1 shows the cyclic voltammograms of 0.05 M $Zn(TfO)_2$/$[Py_{1,4}]TfO$ (Fig. 4.3.1a), 0.05 M $Sn(TfO)_2$/$[Py_{1,4}]TfO$ (Fig. 4.3.1b) and 0.05 M $Sn(TfO)_2$ + 0.05 M $Zn(TfO)_2$ in $[Py_{1,4}]TfO$ (Fig. 4.3.1.1c) on gold, respectively. In Fig. 4.3.1a, four reduction peaks were observed on the cathodic branch of the cyclic voltammogram. The peak c1 can be attributed to underpotential deposition of Zn. The peaks (c2 and c3) and their anodic counterparts (a2 and a3) can be correlated to the formation and stripping of Au-Zn alloys, respectively, while the peaks c4 and a4 are due to the bulk deposition and stripping of Zn, respectively.

In order to confirm this assumption, a potential of -1.5 V vs. Pt was applied for 3h. The SEM and XRD characterization of that deposit is shown in Fig. 4.3.2. The SEM image shows the formation of a thin layer with some hexagonal particles on the surface, but no bulk deposits were found. The XRD results reveal that only $AuZn_3$ alloy (JCPDS File No.50-1336) was formed and no diffraction peak belonging to Zn can be found (Fig. 4.3.2b). The electrochemical behavior of 0.05 M $Sn(TfO)_2$/$[Py_{1,4}]TfO$ is shown in Fig. 4.3.1b. The reduction peaks c1 and c2 are due to the deposition of Au-Sn alloy and of bulk Sn, respectively. The anodic peaks a2 and a2* recorded on the reverse scan are attributed to the stripping of Sn and a1 is related to stripping of the Au-Sn alloy. While in the case of 0.05 M $Sn(TfO)_2$ + 0.05 M $Zn(TfO)_2$ in $[Py_{1,4}]TfO$ (Fig. 4.3.1c) the peaks c1 and c2 are due to the deposition of the Au-Sn alloy and of bulk Sn, respectively, the

peak c3 can be related to the codeposition of Zn/Sn. In the anodic regime, the peaks a3 and a3* are related to the stripping of Zn/Sn. The anodic peaks a2 and a1 are attributed to the stripping of Sn and of the Au-Sn alloy. This explanation is further supported by the SEM and XRD results as will be shown below.

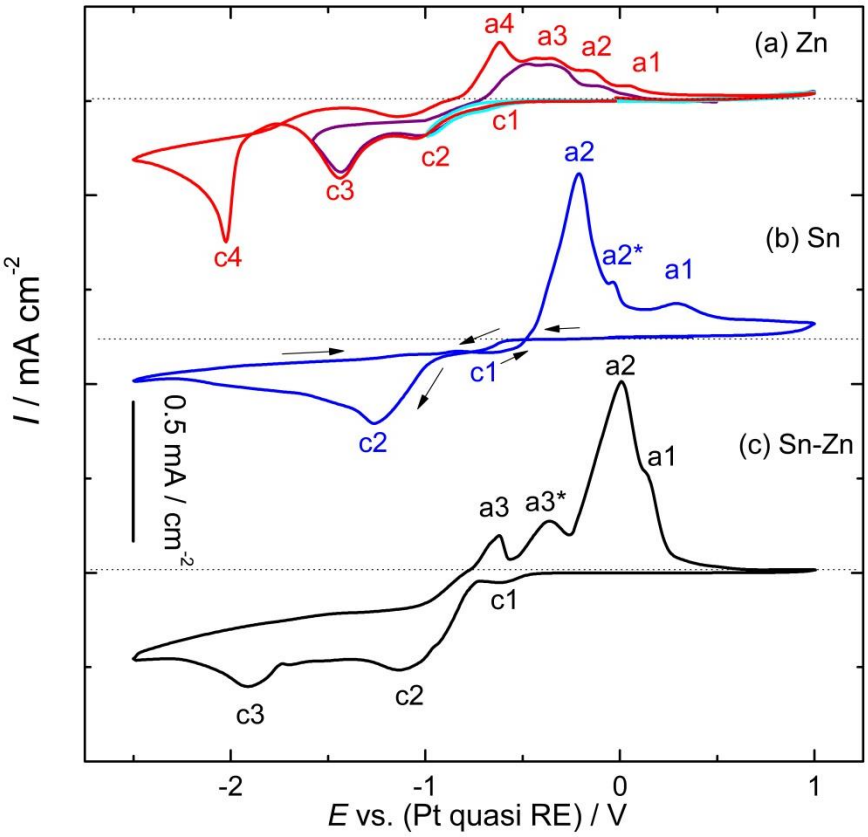

Fig. 4.3.1. *Cyclic voltammograms of (a) 0.05 M $Zn(TfO)_2$, (b) 0.05 M $Sn(TfO)_2$ and (c) 0.05 M $Zn(TfO)_2$+0.05 M $Sn(TfO)_2$ in $[Py_{1,4}]TfO$ recorded on gold at room temperature. Scan rate: 10 mV s^{-1}.*

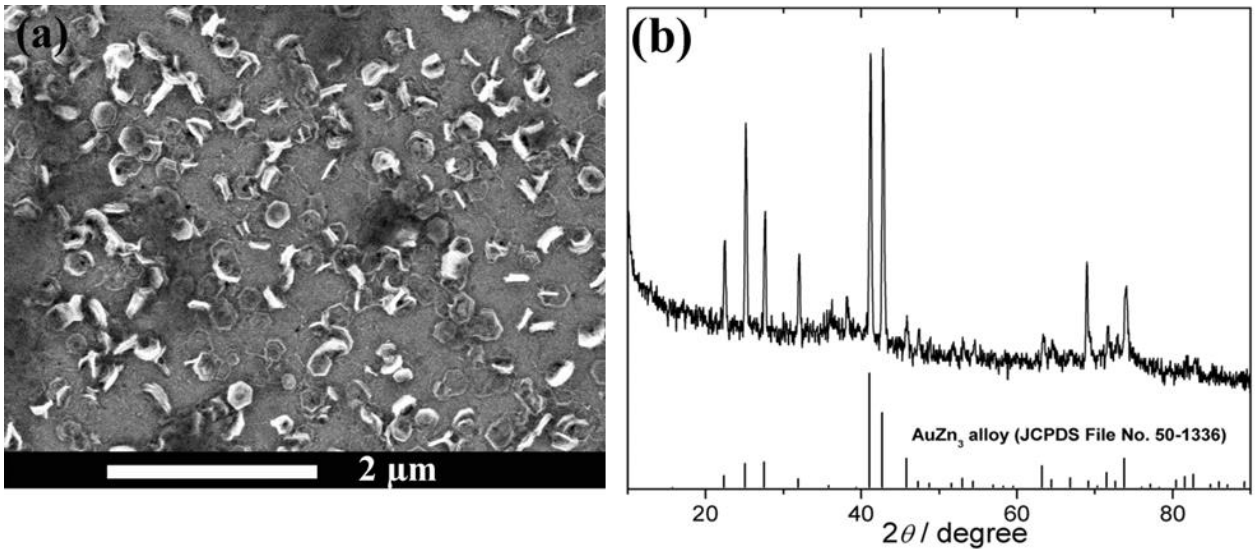

Fig. 4.3.2. *The SEM (a) and XRD (b) characterization of the Zn deposits obtained by potentiostatic electrodeposition at -1.5 V vs. Pt for 3 h from 0.05 M $Zn(TfO)_2$/$[Py_{1,4}]TfO$*

The Zn, Sn and Zn-Sn films obtained at different potentials were investigated by SEM and the results are shown in Fig. 4.3.3. Visually, the Zn deposits are dark black and the Sn deposits appear silverish, well adhering to the gold substrate. The Zn-Sn deposits appear rather gray. The Zn deposit obtained from 0.05 M $Zn(TfO)_2$/$[Py_{1,4}]TfO$ is nanocrystalline, whereas a microcrystalline Zn deposit was obtained from [EMIm]TfO [209]. The difference in grain size can be explained with a different surface adsorption of the cations ($[Py_{1,4}]^+$ and $[EMIm]^+$) on the substrate [190].

In Fig. 4.3.3b, the Sn deposit shows grains of ~300-400 nm in size. Fig. 4.3.3c-e shows, on the same scale, SEM micrographs of Zn-Sn on gold substrates made potentiostatically at potentials of -2.0, -2.25, and -2.5 V (vs. Pt), respectively, for 2 h. The Zn-Sn codeposit in Fig. 4.3.3c appears to be a mixture of Zn and Sn particles. The morphologies tend to be mossy or spongy upon further decreasing the deposition potential (Fig. 4.3.3d and e).

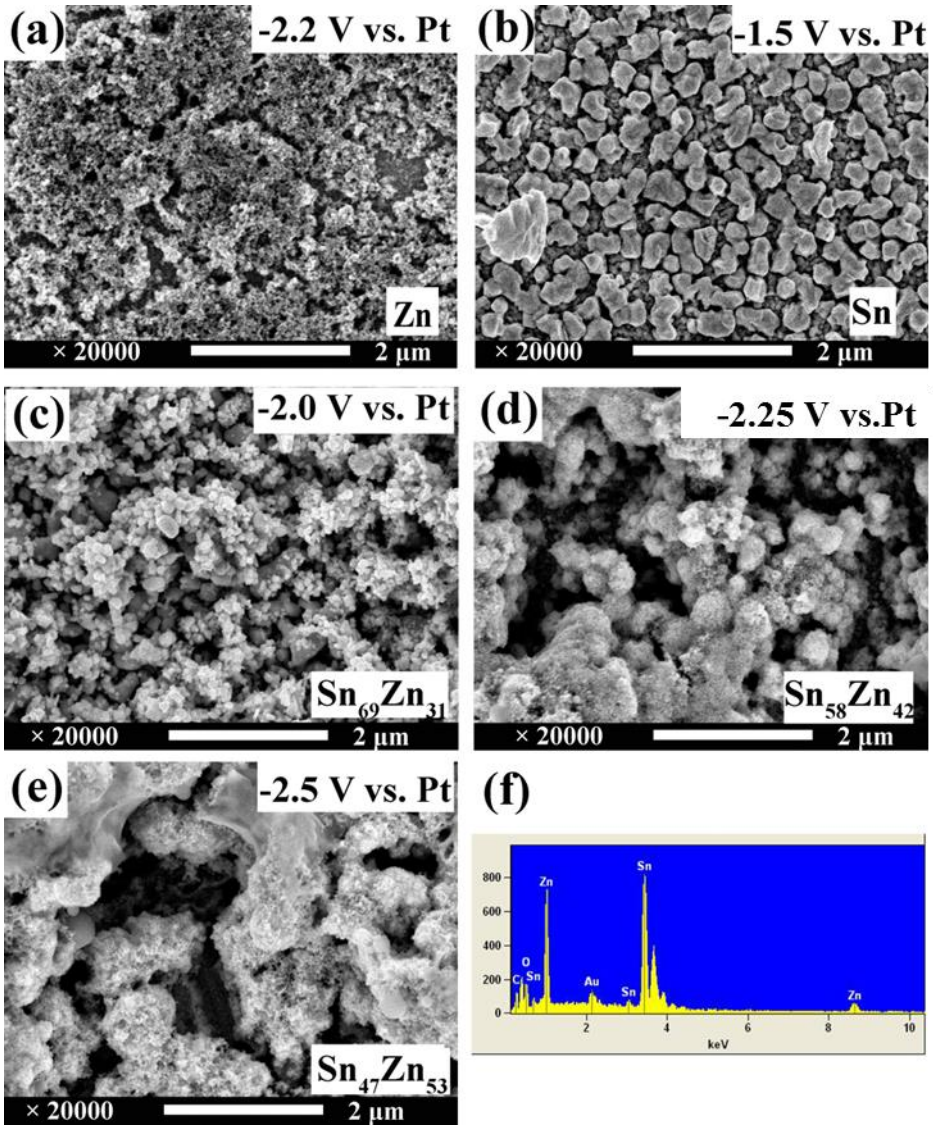

Fig. 4.3.3. *SEM images of Zn, Sn and Zn-Sn films obtained by potentiostatic electrodeposition at different potentials and EDX analysis of Zn-Sn films obtained at a potential of -2.0 V vs. Pt.*

Fig. 4.3.4 shows the XRD patterns of Zn, Sn and Zn-Sn films (the morphologies are shown in Fig. 4.3.3a, b and c) on gold substrates, respectively. Several distinct diffraction peaks at 2θ = 30.6^{o}, 32^{o}, 43.8^{o} and 44.8^{o} are obtained which agree well with the (200), (101), (2 2 0) and (211) diffraction patterns of cubic Sn (JCPDS No. 04-0673) (Fig. 4.3.4a, top).

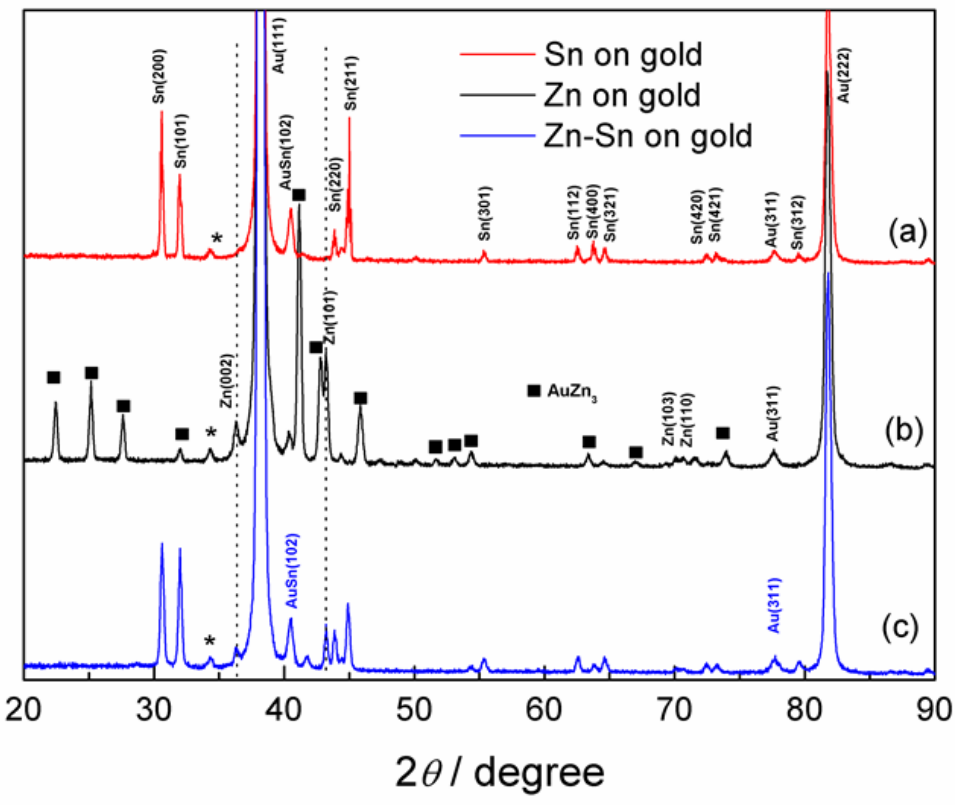

Fig. 4.3.4. *XRD patterns of the electrodeposited Zn (black), Sn (red), and Zn-Sn (blue) films (the morphologies of the films are shown in Fig. 4.3.3a, 4.3.3b and 4.3.3c), respectively.*

The characteristic diffraction peaks of Zn (JCPDS File No. 04-0831) and of $AuZn_3$ (JCPDS File No.50-1336) (as shown in Fig. 4.3.4b, middle) are shown for comparison. Fig. 4.3.4c, bottom, shows the XRD pattern of Zn-Sn films on gold, which shows both the diffraction peaks of Zn and of Sn without other diffraction peaks. The diffraction peak at $2\theta = 34.2^{o}$ marked as a star in the patterns is from gold. The results suggest that the Zn/Sn deposit is a simple mixture of tetragonal tin and of hexagonal close-packed zinc. This is consistent with the bulk phase diagram of Zn-Sn binary systems where tin and zinc do not form a metallic compound.

4.3.2 Electrosynthesis of biphasic Zn-Sn nanowires

Free standing Zn-Sn nanowires are potential candidates as an anode material in Li-ion batteries due to their high surface area and their good electron conductivity. Therefore, it was attempted to synthesize vertically aligned arrays of Zn-Sn nanowires by the help of PC membranes from $Sn(TfO)_2$+$Zn(TfO)_2$ in $[Py_{1,4}]TfO$. First, the nanowires were prepared from 0.05 M $Sn(TfO)_2$ + 0.05 M $Zn(TfO)_2$/$[Py_{1,4}]TfO$ with the membranes having pore sizes of 100 nm. SEM micrographs of such Zn-Sn nanowires obtained potentiostatically at -2.25 V vs. Pt for 10 h on a Au-sputtered membrane are shown in Fig. 4.3.5a and b. The top view of the nanowires (Fig. 4.3.5a) shows that they have a length of about 5 µm and a diameter of about 100 nm. A higher magnification view of the nanowires is shown in Fig. 4.3.5b. The nanowires rather seem to consist of Zn and Sn particles. The XRD pattern, as indicated in Fig. 4.3.5f, shows the presence of both Zn and Sn in the nanowires. Compared with the homogenous free standing Cu-Zn nanowires where α–Cu(Zn) alloys are formed, the mechanical strength of the Zn-Sn nanowires is weaker and they are rather brittle, thus, the nanowires are not free standing. By increasing the pore size of the membrane to 200 nm, free standing nanowires can be obtained at -2.25 V vs. Pt for 4 h. Fig. 4.3.5c shows a low magnification SEM image of the free standing nanowires. With a higher magnification, Fig. 4.3.5d, rather free standing nanowires with a length of about 2 µm are evident.

Fig. 4.3.6 shows free standing nanowires made by electrodeposition from 0.1 M $Sn(TfO)_2$ + 0.1 M $Zn(TfO)_2$ in $[Py_{1,4}]TfO$ with a pore size of 200 nm at a potential of -2.3 V vs. Pt for 1 h.

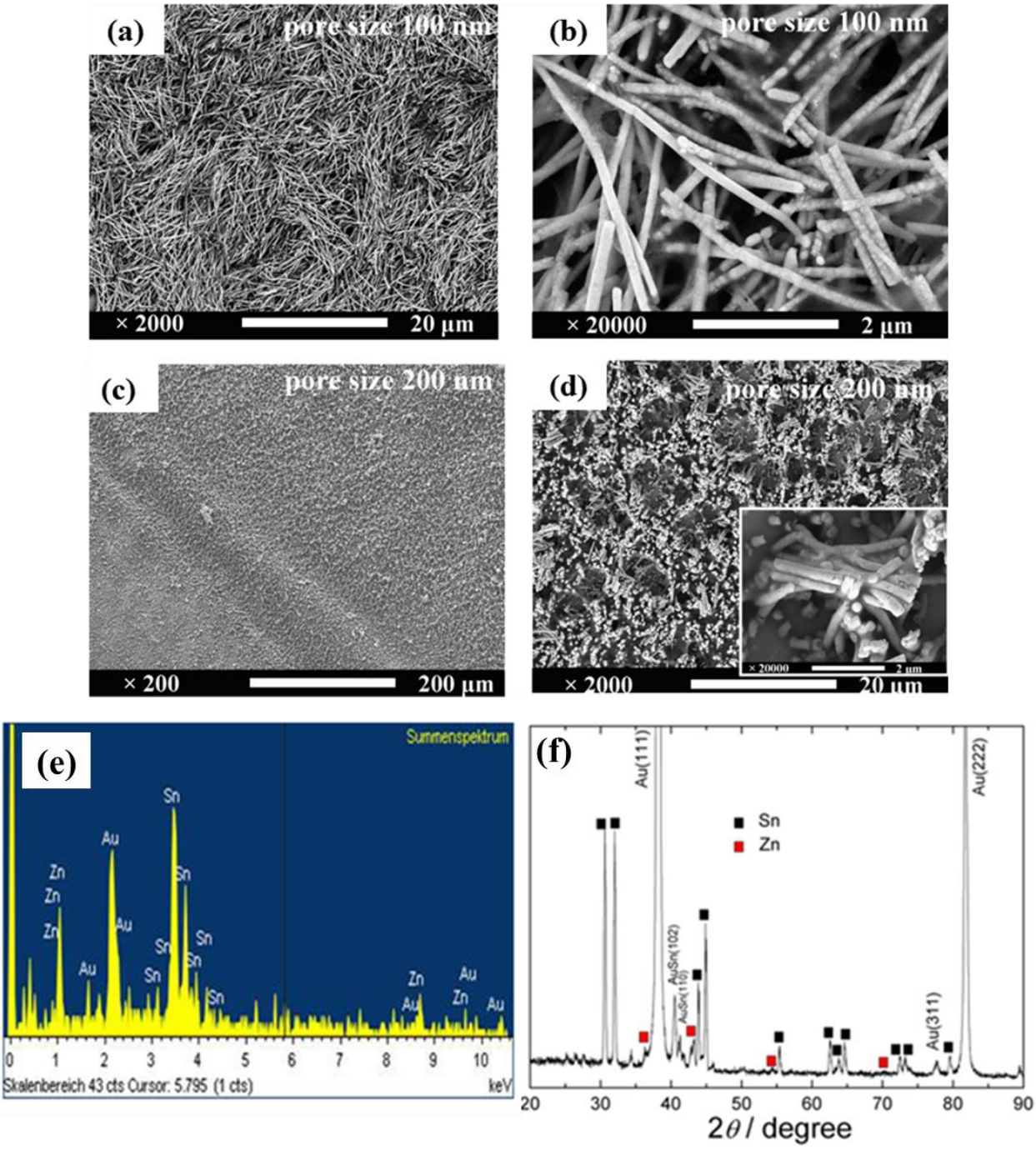

Fig. 4.3.5. *Zn-Sn nanowires obtained by deposition at -2.25 V vs. Pt from 0.05 M $Zn(TfO)_2$ + 0.05 M $Sn(TfO)_2$ in $[Py_{1,4}]TfO$ on sputtered gold with a membrane pore size of 100 nm (a and b) and of 200 nm (c and d). EDX analysis of the nanowires (e) and XRD pattern of the nanowires (f).*

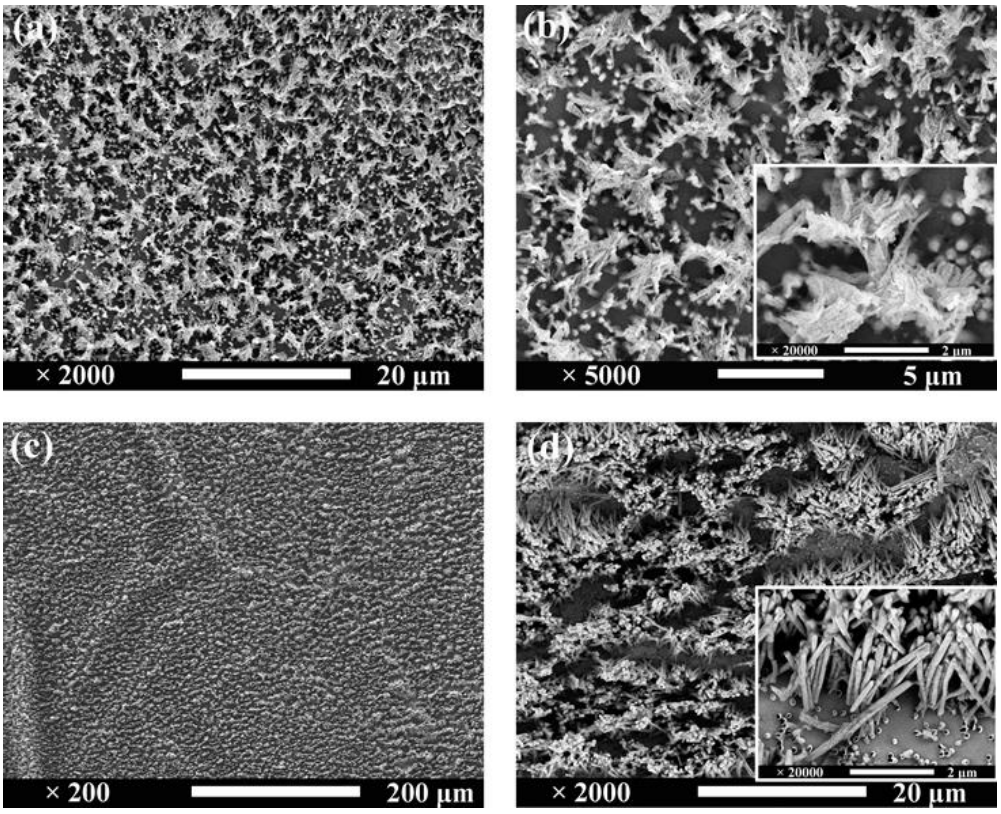

Fig. 4.3.6. *SEM images of Zn-Sn nanowires obtained by deposition at -2.3 V vs. Pt from 0.1 M $Zn(TfO)_2$ + 0.1 M $Sn(TfO)_2$ in $[Py_{1,4}]TfO$ on sputtered gold with a membrane pore size of 200 nm for 1 h (a and b) and deposition for 3 h (c and d).*

Free standing nanowires with lengths of about 1-2 micrometers can be obtained (Fig. 4.3.6a and b). Some of the nanowires are bunched together and others are vertically aligned. By increasing the deposition time to 3 h, the length of the wires can reach more than 4 µm and the nanowires are then free standing (Fig. 4.3.6c and d). The nanowire arrays are dense and well adhering to the gold surface. Such structures are very interesting as an anode material in Li-ion batteries or maybe also for Zn-based batteries in the future.

4.4 Electrodeposition of CuSn [211-214]

Due to their strong structural integrity Cu-Sn intermetallic compounds have been proposed as alternative anode materials for lithium ion batteries [211,212], moreover these compounds are relatively cheap and environmentally friendly. Therefore, in this part of the study macroporous and nanowire CuSn deposits were electrodeposited from the ionic liquid [EMIm]DCA by a template assisted processes.

For obtaining macroporous structures, polystyrene (PS) spheres were used as templates over gold substrates, and CuSn films were electrodeposited within the interstitial voids of the template. In the case of nanowires, polycarbonate membranes, which are on one side sputtered with copper, were used as templates. The small area electrochemical cell (Fig. 3.2) is used in this study and platinum wire and ring were used as quasi reference and counter electrodes, respectively.

4.4.1 Macroporous CuSn

The PS spheres have been self-assembled into three-dimensional close-packed arrays on the gold surface. Fig. 4.4.1 shows the cyclic voltammograms of 0.05 M $SnCl_2$, 0.25 M CuCl and 0.05 M $SnCl_2$ + 0.25 M CuCl in [EMIm]DCA recorded on gold, respectively. The electrode potential was ramped down from the initial potential (open circuit potential) towards the negative regime at -1.5V in the forward scan and then up to the positive direction at +0.5V in the backward scan with a scan rate of 10 mV s^{-1}. The voltammogram of 0.05 M $SnCl_2$ in [EMIm]DCA is shown in figure 4.4.1a where two reduction peaks (C1 and C2) are found and four oxidation peaks (A1-A4) are shown in the anodic direction.

The reduction process (C1) might be correlated to surface alloying processes or to underpotential deposition. The second peak (C2) is due to the bulk deposition of Sn.

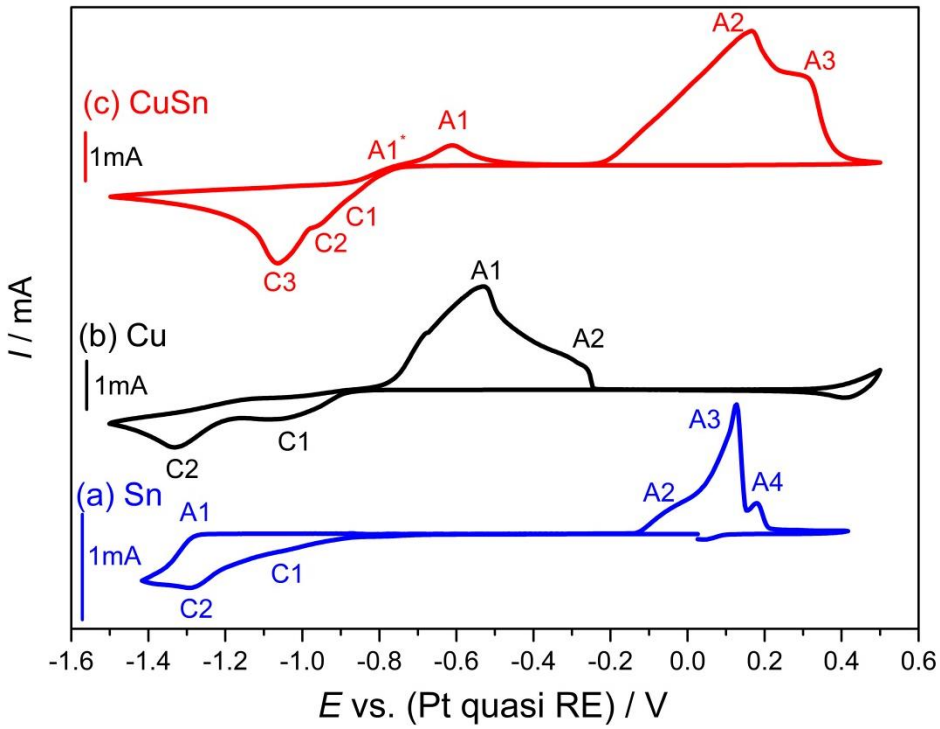

Fig. 4.4.1. *Cyclic voltammograms of (a) 0.05 M $SnCl_2$, (b) 0.25 M CuCl and (c) 0.05 M $SnCl_2$ + 0.25 M CuCl in [EMIm]DCA recorded on PS- covered gold with scan rate 10 mV s^{-1}.*

The anodic peaks A1 and A2 are correlated with the stripping of the electrodeposited tin, and the other peaks A3 and A4 might be due to dealloying processes. A detailed study on a similar system has been discussed before (electrodeposition of tin nanowires) which revealed that the anodic peaks A1, A2, and A3 are related to the oxidation of deposited Sn and that the peak A4 must be due to dealloying/stripping of Sn considering that C1 is due to the alloying of Sn with Au or due to an underpotential deposition process.

Fig. 4.4.1b reveals the electrochemical behavior of 0.25 M CuCl in [EMIm]DCA. In the cathodic range two reduction peaks (C1 and C2) are observed. The first cathodic process at (C1) is attributed to the underpotential deposition of Cu or Au-Cu alloys, since the system starts with Cu(I) and there is no reduction step from Cu(II) to Cu(I). The second reduction process (C2) is attributed to the bulk deposition of Cu. Correspondingly, in the anodic range two main oxidation

peaks (A1 and A2) are observed which can be assigned to the stripping of the deposited Cu and Au-Cu dealloying, respectively.

The CV of 0.05 M $SnCl_2$ + 0.25 M CuCl in [EMIm]DCA is shown in figure 4.4.1c which exhibits three reduction peaks (C1-C3) and three oxidation peaks (A1-A3). The peak C1 is corresponding to the Au-Cu alloying while C2 is corresponding to the bulk electrodeposition of Cu and the peak C3 is corresponding to the codeposition of Cu-Sn. In the anodic regime, the peaks $A1^*$ and A1 are related to the stripping of Cu-Sn deposits and the anodic peaks A2 and A3 are related to the stripping of Cu and Au-Cu alloy, respectively.

After immersion of the electrode in the employed ionic liquid electrolyte for about 15 min, the PS template became almost transparent which indicates the complete infiltration of the liquid into the voids of the PS spheres. By running the potentiostatic deposition the nucleation occurs over all the active area and a uniform Cu-Sn film is formed. There are many factors which can affect the homogeneity of the macroprous structure such as electrolyte concentration, deposition potential and also the time of deposition [213]. Thus the deposition parameters should be perfectly controlled in order to get the optimum conditions for a well-ordered macroporous structure. Obtaining highly ordered macroporous structure through electrodeposition techniques is a difficult process where the alloying of the deposited element with the substrate makes it difficult to get an ordered macroporous structure.

Figure 4.4.2 shows SEM images of the macroporous CuSn (after removal of the PS spheres with THF) obtained at a constant potential of -1.0V for 10 minutes at room temperature. Fig. 4.4.2a shows a well-covered CuSn porous surface with interconnected pores. A uniform periodicity underneath this top layer is clearly seen at higher magnification, (Fig. 4.4.2b). However the CuSn macroporous film also shows some disordered areas which might be due to defects in the PS template and/or due to uneven current densities inside the electrochemical cell.

Increasing the applied potential does -surprisingly- not lead to three dimensional macroporous structures. The polystyrene spheres can be pushed away forming less ordered honeycomb like structures (Figure 4.4.3a). Moreover, dendrites can be formed even at rather short deposition time (Fig 4.4.3).

Therefore, the potential was kept at -1.0V and with increasing the time of deposition (15 min) three dimensional macroporous structures could be obtained. Fig 4.4.4 shows the SEM micrographs of well-ordered three dimensional CuSn films obtained potentiostatically at -1.0V vs platinum quasi reference electrode for 15 minutes. An ordered multi layered macroporous structure can be clearly seen, indicated by several layers seen in figure 4.4.4 b.

It's important to mention that it can happen that some parts of the deposits are not 3DOM, possibly the result of inhomogeneous current density.

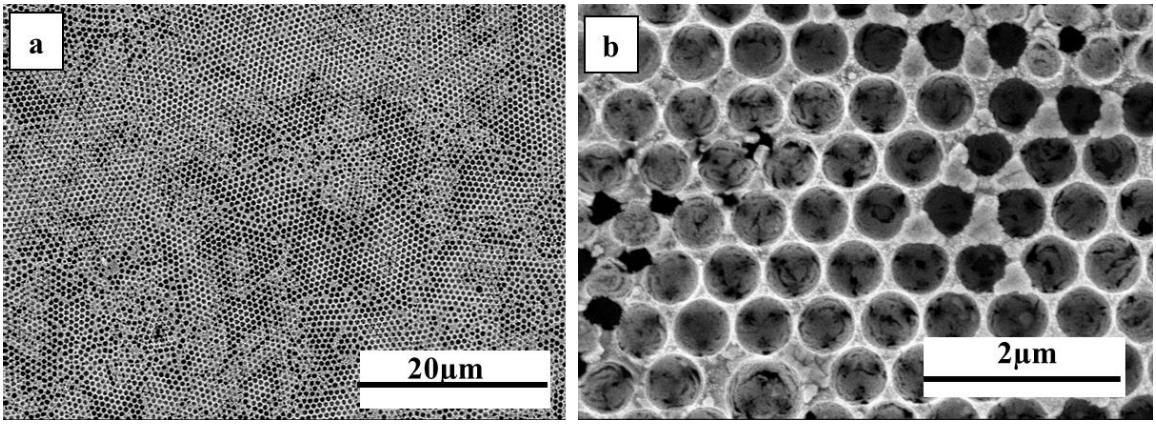

Fig. 4.4.2. *SEM images of a uniform periodicity macroporous CuSn films at (a) lower magnification and (b) higher magnification obtained from 0.05 M $SnCl_2$ + 0.25 M CuCl in [EMIm]DCA.*

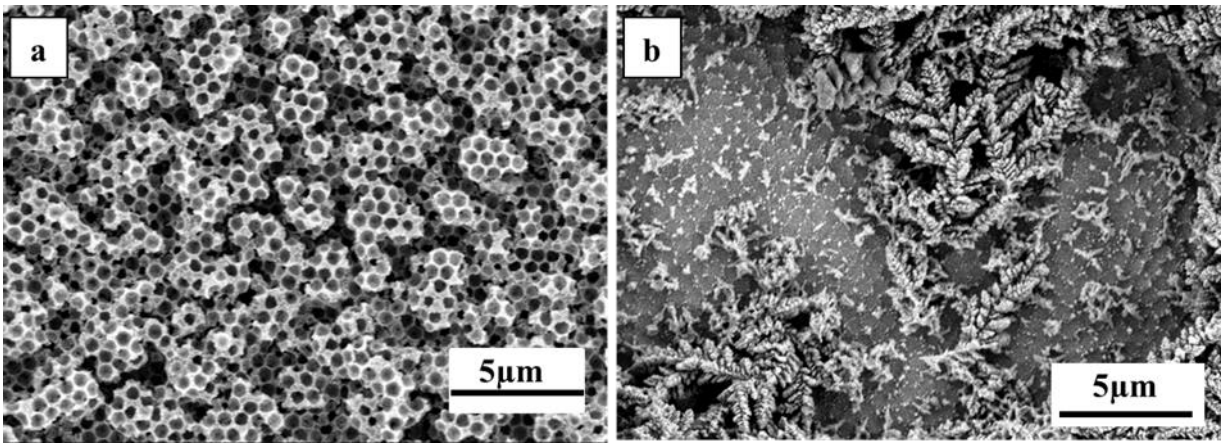

Fig. 4.4.3. *SEM images of (a) CuSn less ordered honeycomb structure obtained at -1.2V for 5 minutes. (b) dendrites of CuSn obtained at -1.2V for 10 minutes; from 0.05 M $SnCl_2$ + 0.25 M CuCl in [EMIm]DCA.*

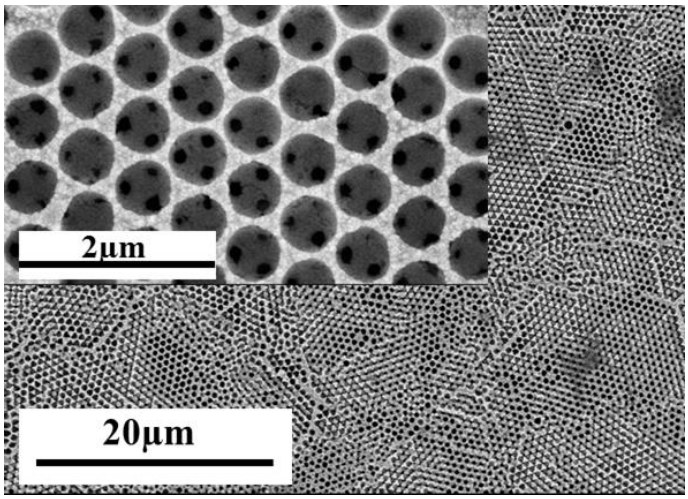

Fig. 4.4.4. *SEM micrographs of a three dimensional macroporous CuSn structure obtained from 0.05 M $SnCl_2$ + 0.25 M CuCl in [EMIm]DCA.*

4.4.2 CuSn nanowires

Vertically aligned Cu-Sn alloy nanowires were electrochemically synthesized from a solution of 0.05 M $SnCl_2$ + 0.25 M CuCl in [EMIm]DCA through potentiostatic deposition into gold sputtered polycarbonate membranes. Fig. 4.4.5a shows the SEM micrograph of the free standing CuSn alloy nanowires at lower magnification where the deposition was performed at -1.0 V for 30 minutes. The higher magnification of SEM images shows that the average diameter of the fabricated nanowires is about 100 nm which is consistant with the pore diameter of the polycarbonate membrane (Fig. 4.4.5b). As has been shown in chapter 3.4, the electrodeposited tin nanowires are bunched together even when the lengths of the wires are rather short. However, a cross sectional view of the CuSn nanowires (Fig. 4.4.5c) reveals that the wires are free standing even with lengths up to 7μm. The length of the nanowires can be controlled by changing the time of deposition.

Fig 4.4.5d. shows the EDX analysis of the electrodeposited alloy where the weight percent of Cu is almost twice the one of tin, a consequence of to the higher concentration of the Cu salt in the deposition bath. This higher concentration of Cu in the alloy gives better mechanical stability to the nanowires.

Oxygen in the EDX is due to some oxidation under air. Carbon is from the ionic liquid, gold from the sputtered layer on the membrane.

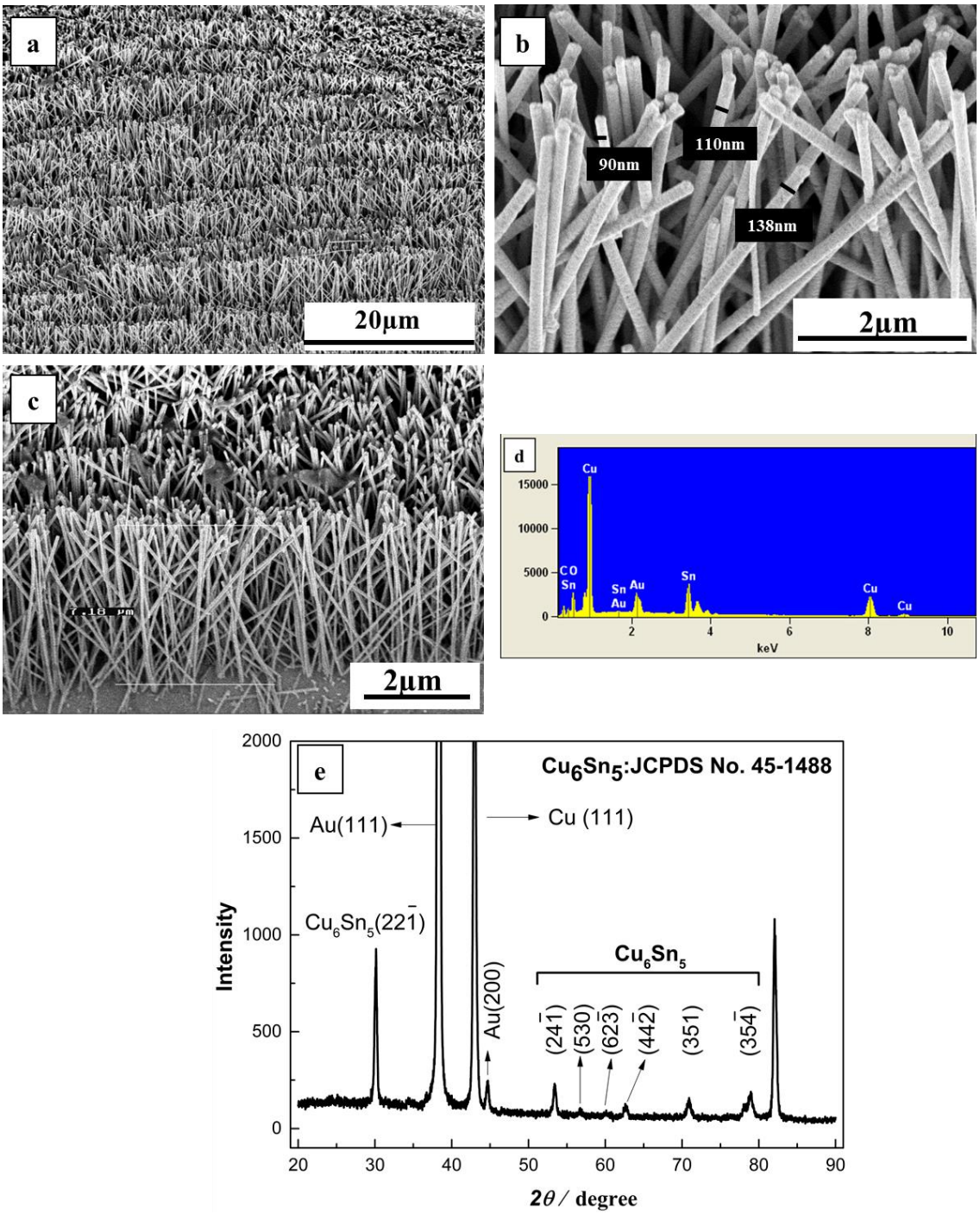

Fig. 4.4.5. *CuSn nanowires deposited from 0.05 M $SnCl_2$ + 0.25 M CuCl in [EMIm]DCA over a gold sputtered membrane at -1.0 V vs Pt for 30 minutes. (a) top view at low magnification. (b) high magnification of the nanowires with diameters of about 100 nm. (c) cross section view showing free standing arrays with wire length of up to7µm. (d) EDX of the nanowires (e) XRD pattern of CuSn alloy.*

The Cu-Sn phase diagram (see appendix) indicates that Cu and Sn can form many intermetallic compounds, such as β ζ δ γ ε and ή Cu_xSn [214]. The XRD pattern of the obtained CuSn alloy is shown in Fig 4.4.5e. The two strong peaks at around 38.3° and 43° correspond to the Au(111) and Cu(111) respectively, originating from Au substrate and from Cu. The XRD patterns show different diffraction peaks for Cu_6Sn_5.The peaks at 30.1°, 53.4° are assigned to the $(22\bar{1})$, $(24\bar{1})$, reflection of Cu_6Sn_5 (JCPDS card no. 45-1488), respectively. Two other weak peaks at 56.7° and 60° are also assigned to the Cu_6Sn_5 phase. The reflection peaks at 62.6°, 70.8° and 79.0° are assigned to $(44\bar{2})$, (351) and $(35\bar{4})$ reflections of Cu_6Sn_5, respectively.

4.5 Electrodeposition of SiSn nanowires [38, 127, 128, 130, 215-226]

Nanostructured semiconductors are very important materials for many applications due to their variable properties. The optical and electronic properties of such materials make them interesting for electrical and photonic devices. The technically most important semiconductor is Si which is found in many applications such as computer chips, photovoltaic devices optical devices and many other ones [215,216]. However, Si is a very reactive element, thus it's easily oxidized to from SiO_2 when it is exposed to air. One method to get pure Si is the electrodeposition from water- and air stable ionic liquids, which has been reported in several articles [38,127,128,217–220].

As microcrystalline silicon is an indirect semiconductor, compound semiconductors [221] and quantum dot silicon structures have been in the focus of interest [222]. α-Sn has no band gap, thus at sufficient high concentrations of Sn a direct gap of Sn/Si compounds can be achieved. The incorporation of even small amounts of Sn creates a strain in the silicon lattice which changes its electronic and optical properties [223].

In 2013 Hussain et al. reported the first metal-oxide-semiconductor field-effect transistor using SiSn as a channel material [224] and they proved that SiSn can be used in different applications where the use of SiSn instead of Si alone is more advantageous. MOSFET's are a good example for using SiSn for a technically important application [224].

According to Hume-Rothery rules for solid state solubility, silicon and tin match in three of four parameters as they have the same valance, have similar electronegativity and α-Sn can be inserted into the cubic diamond structure of silicon. Due to size misfit the solid state solubility of tin in silicon is limited [225].

In this part of the present thesis the elctrodeposition of SiSn films and of SiSn nanowires from $[Py_{1,4}]TfO$ is presented and the as-deposited alloy is characterized with different methods. $SnCl_2$

and $SiCl_4$ are used in equimolar concentrations in $[Py_{1,4}]TfO$. Cyclic voltammetry was used to investigate the electrochemical behavior of these electrolytes. The obtained deposits on gold substrates were characterized by SEM/EDX and XRD. The formed hairy-like nanowires are of potential interest in different applications such as batteries, electronic and optical devices

The cyclic voltammograms (CVs) of 0.1M $SiCl_4$, 0.1M $SnCl_2$ and a mixture of 0.1 M $SiCl_4$ + 0.1 M $SnCl_2$ in $[Py_{1,4}]TfO$ on gold substrates are shown in figure 4.5.1.

The electrode potential was scanned initially from (OCP) to -3.0 V in the negative direction and then up to +1.0 V in the reverse scan at a scan rate of 10 mV s^{-1}. The voltammogram of 0.1 M $SiCl_4$ in $[Py_{1,4}]TfO$ is shown in Fig. 4.5.1a and it shows four reduction processes in the cathodic regime. There is no visible deposition at C_1 and C_2, thus these two reduction processes are due to the adsorption of the ionic liquid to the gold substrate and to the gold reconstruction, but also a reduction process of $SiCl_4$ to Si_2Cl_6, Si_3Cl_8 and higher ones might occur [130]. The reduction peak C_3 is attributed to the bulk deposition of silicon, at C_4 the decomposition of the ionic liquid starts.

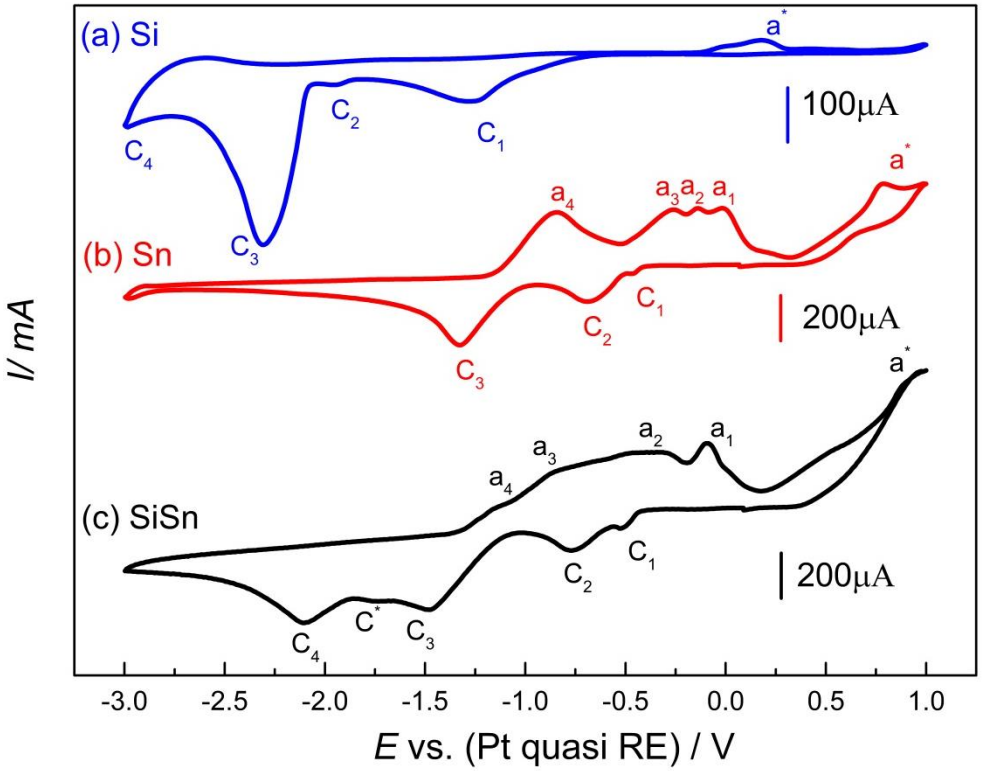

Fig. 4.5.1. *Cyclic voltammograms of (a) 0.1 M $SiCl_4$, (b) 0.1 M $SnCl_2$ and (c) 0.1 M $SnCl_2$ + 0.1 M $SiCl_4$ in $[Py_{1,4}]TfO$ on gold substrates. Scan rate: 10 mV s^{-1}.*

There is no clear oxidation peak for Si and the anodic shoulder a* at the anodic limit can be due to the formation of chlorine from $SiCl_4$, the oxidation of the gold substrate and to the oxidation of the products made at C_1.

The voltammogram of 0.1 M $SnCl_2$ in $[Py_{1,4}]TfO$ is shown in Fig. 4.5.1b where four reduction processes appeared in the forward scan and five oxidation peaks appear in the backward scan. The bulk deposition of tin occurs at C_4 and the first reduction peak C_1 might be attributed to the adsorption process of the ionic liquid onto the electrode substrate. C_2 and C_3 might be underpotential deposition processes or alloying of Sn with gold. In a previous study the oxidation peaks a_4 and a_3 were shown to be corresponding to the stripping of electrodeposited Sn, they are related to the reduction peaks C_4 and C_3, respectively, where the CVs were done at different

switching potentials. The deposition at C_2 for 1 hour gives no deposit while the deposition at C_3 yields a silver-grey mirror like finish on the gold substrate which indicates that the reduction process at C_2 is only related to the underpotential deposition of tin and C_3 might be alloying of Sn with gold [204]. The other oxidation peaks a_1 and a_2 seem to be associated with the reduction at C_1 and C_2, respectively. The CV of 0.1 M $SnCl_2$ + 0.1 M $SiCl_4$ in $[Py_{1,4}]TfO$ (Fig.4.5.1c) exhibits four-five reduction processes in the forward scan and five oxidation peaks in the backward scan. The first two reduction peaks C_1 and C_2 are related to the underpotential deposition of Sn and the formation of Au-Sn alloy, respectively. The bulk Sn deposition occurs at C_3 while the Si/Sn codeposit starts at C^* and the peak C_4 can be correlated with the deposition of Si. In the backward scan, the peaks a_4 and a_3 are related to the stripping of Si/Sn and bulk deposited Sn, respectively. The peaks a_1 and a_2 are related to the reduction processes C_1 and C_2 and they express the stripping of Au-Sn alloys. The anodic peak a^* is like the ones shown for the tin and silicon CVs possibly related to the oxidation of the gold substrate. A clear allocation is, however, difficult.

The obtained films of Si, Sn and SiSn at different applied potentials (peak potential) on gold substrates for 1 hour were investigated by SEM as shown in Fig. 4.5.2, 4.5.3 and 4.5.4 respectively. Tin deposition was carried out using controlled-potential electrolysis of 0.1 M $SnCl_2$/$[Py_{1,4}]TfO$ on gold at -1.3V versus platinum quasi reference electrode for 1 hour. Dense and uniform silvery tin deposits were obtained.

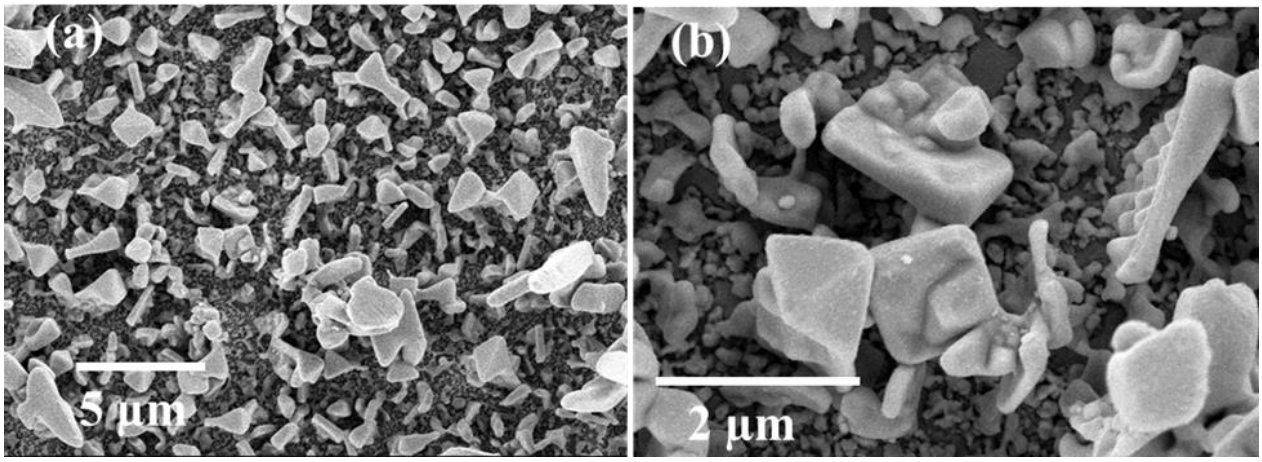

Fig. 4.5.2. *Microstructure of the tin deposits at different magnifications obtained potentiostatically from 0.1 M $SnCl_2$ in $[Py_{1,4}]TfO$ at a potential of -1.3 V versus platinum for 1 hour.*

The morphology of the Sn deposits is shown in figure 4.5.2 at different magnifications, indicating that the deposits consist of microcrystalline particles. Silicon deposits were made by current-controlled electrolysis of 0.1 M $SiCl_4$/$[Py_{1,4}]TfO$ on gold at -20 µA for 6 hours (due to the lower concentration of Si). The obtained deposit was a thin film which has a greyish appearance (figure 4.5.3).

For SiSn the electrodeposition was carried out from 0.1 M $SnCl_2$ + 0.1 M $SiCl_4$ in $[Py_{1,4}]TfO$ by controlled potential deposition on gold at -2V for 1 hour. The obtained deposits were dense and uniform with dark black appearance and the morphology of the electrodeposited SiSn on pure gold is shown in figure 4.5.4. It's clear that the deposit consists of tiny nanoparticles, (figure 4.5.4 b). The EDX results show that the deposits contain about 15 atom % of Si (figure 4.5.4 c).

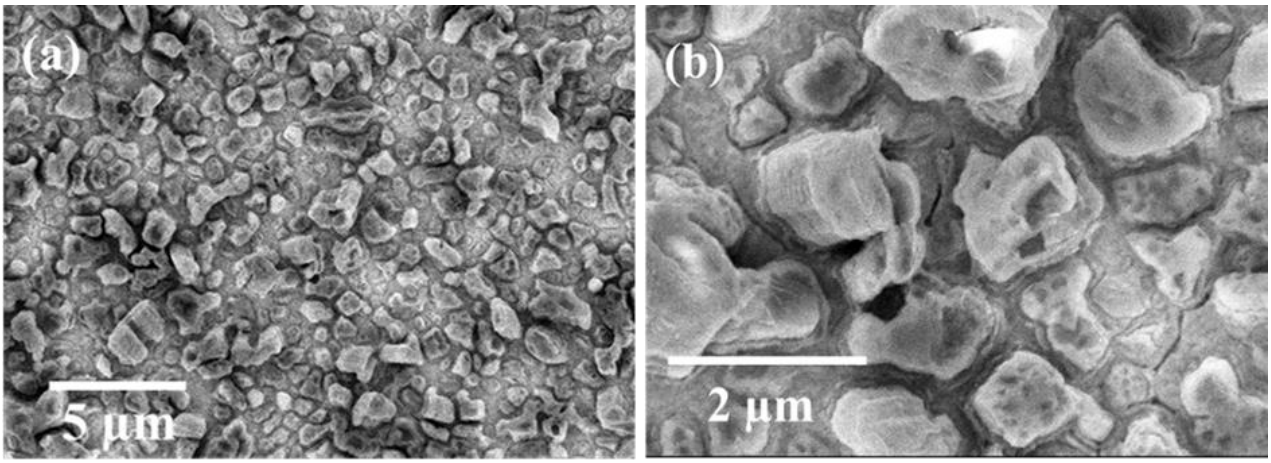

Fig. 4.5.3. *Microstructure of the silicon deposits at different magnifications obtained galvanostatically from 0.1 M $SiCl_4$ in $[Py_{1,4}]TfO$ at -20 µA versus platinum for 1 hour.*

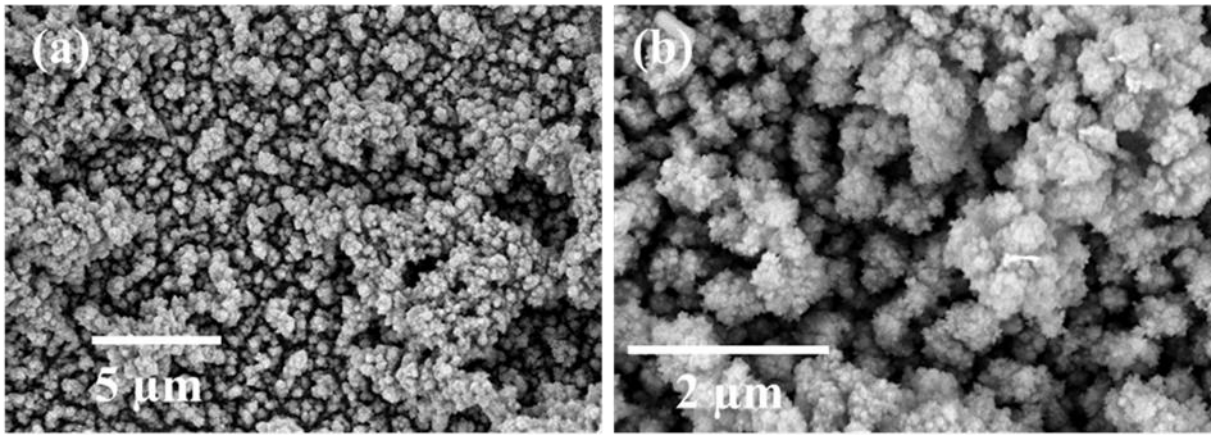

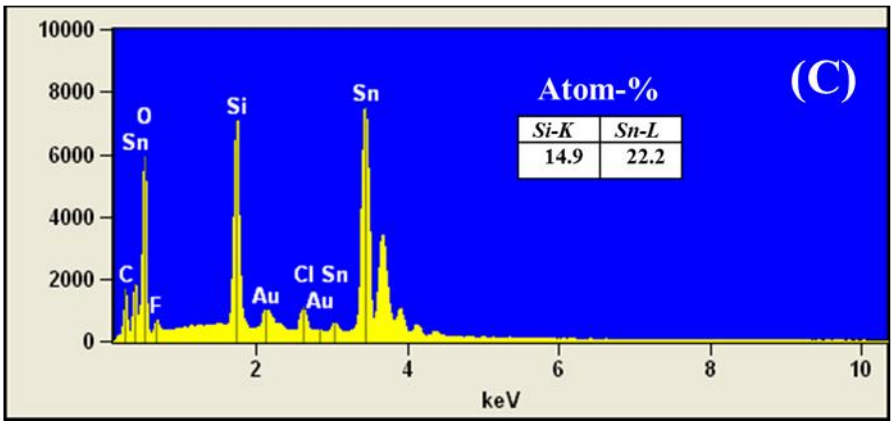

Fig. 4.5.4. *Microstructure of the silicon-tin deposits at different magnifications obtained potentiostatically from 0.1 M $SnCl_2$ +0.1 M $SiCl_4$ in $[Py_{1,4}]TfO$ at a potential of -2 V versus platinum for 1 hour (a) scale bar 5µm, (b) scale bar 2µm and (c) EDX analysis of SiSn deposit.*

Hair-like structured SiSn nanowires were obtained when the electrolysis process was carried out at -2V for 1h after running cyclic voltammetry first (Fig. 4.5.5a). This can be explained by the fact that during the forward scan in cyclic voltammetry Sn is deposited firstly at low potential, thus it forms a thin film on gold. Then Si starts to be deposited at a more negative potential. During the backward scan in the anodic regime the deposited Sn film will be oxidized somehow activating gold giving a template. This might help the formation of hair-like nanowires. SiSn nanowires bunches are formed (figure 4.5.5b) which are quite similar to those obtained using polycarbonate templates [226]. The EDX results show that the deposits contain about 10 atom % of Si (Fig. 4.5.5c).

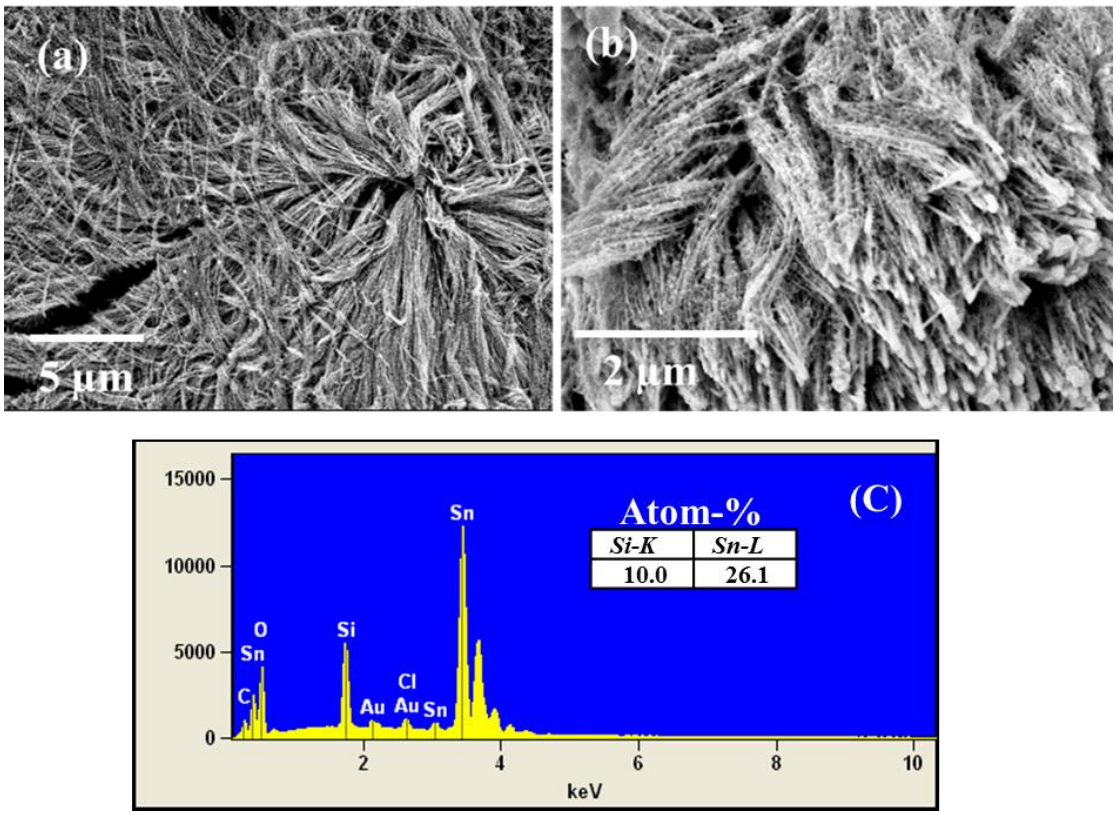

Fig. 4.5.5. *Microstructure of the silicon-tin deposits at different magnifications obtained potentiostatically from 0.1 M $SnCl_2$ +0.1 M $SiCl_4$ in $[Py_{1,4}]TfO$ at a potential of -2 V versus platinum for 1 hour after running CV (a) scale bar 5µm, (b) scale bar 2µm and (c) EDX analysis of SiSn deposit.*

The deposition at more negative potential of -2.7 V led to nanowires which seem to be free standing in contrast to those obtained at a lower potential. Fig. 4.5.6a shows the top view of the obtained nanowires where they are bunched together. At a higher magnification the wires appear clearly as free standing ones with an average diameter of about 100 nm and a length of ~ 5 µm (Fig. 4.5.6 b, c and d). It is important to mention that these nanowires were obtained without a template. Because of time limitations the reasons for this interesting growth could not be investigated in more detail.

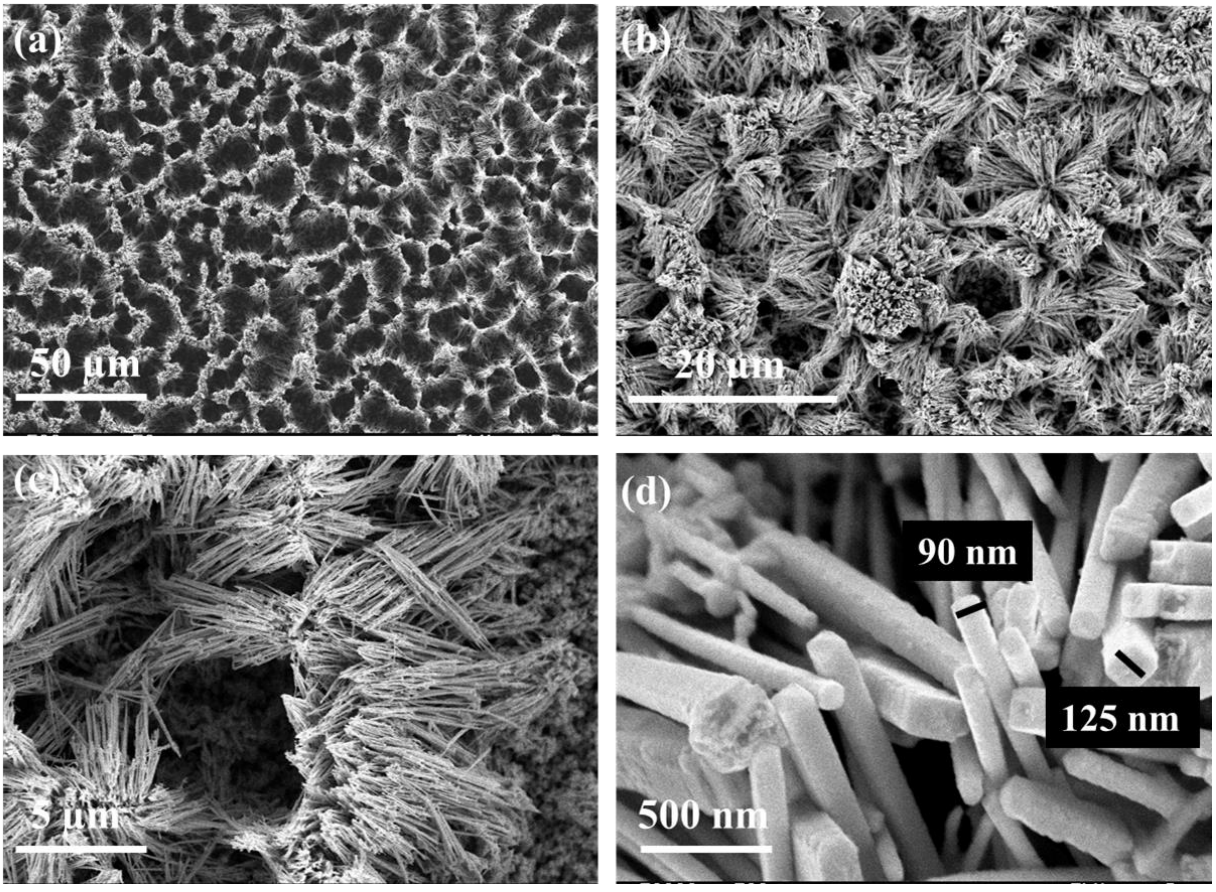

Fig. 4.5.6. *Microstructure of the silicon-tin deposits at different magnifications obtained potentiostatically from 0.1 M $SnCl_2$ + 0.1 M $SiCl_4$ in $[Py_{1,4}]TfO$ at a potential of -2.7 V versus platinum for 1 hour after running CV (a) scale bar 50µm, (b) scale bar 20µm and (c) scale bar 5µm and (d) scale bar 500 nm.*

5. Summary

In the present thesis the electrodeposition of nanowires, thin films and macroporous tin and tin based alloys was investigated in the ionic liquids [EMIm]DCA, $[Py_{1,4}]$DCA and $[Py_{1,4}]$TfO. The effect of the ionic liquid anion on the morphology of the obtained deposits was also studied. Template assisted and template free electrodeposition processes were used to fabricate tin, copper-tin and silicon-tin nanowires. Polystyrene templates were used for the synthesis of copper-tin macroporous alloys.

5.1 Electrodeposition of Sn nanowires

A simple template-assisted method is presented to produce Sn nanowire arrays from ionic liquids. The electrodeposition process includes both the deposition of Sn nanowires and thick deposits of either Sn or Cu as supporting layers for nanowire films. The results show that Sn films from the employed ionic liquids are not suitable to support the freestanding nanowires due to dendrite formation. However, a compact layer of an electrodeposited Cu film is a suitable supporting electrode. After dissolution of the membrane in dichloromethane, well-ordered Sn nanowires on Cu were obtained. Such Sn nanowire films on a supporting Cu layer are expected to be promising anode host materials for Li-ion batteries. The growing of Sn nanowire films on electrodeposited Cu current collectors might overcome the capacity fading resulting from the bad connection between the anode material and the current collector.

5.2 Influence of the anion on the morphology of the tin deposits

Electrodeposition of tin was studied from two ILs with the same $[Py_{1,4}]^+$ cation and two different anions, TfO^- and DCA^-. Four reduction processes were observed in the CV of $SnCl_2$/$[Py_{1,4}]$TfO on gold, and three cathodic processes were evident in the CV of $SnCl_2$/$[Py_{1,4}]$TfO on copper. However, three reduction processes were observed in the CV of $SnCl_2$/$[Py_{1,4}]$DCA on gold, and a

single reduction process was seen in the CV of $SnCl_2$/$[Py_{1,4}]$DCA on copper. The electrochemical behavior of $SnCl_2$ in [EMIm]DCA on gold and copper was also investigated for comparison purposes. Electrolysis of $SnCl_2$/$[Py_{1,4}]$TfO at -0.2 V for 1 h on gold yielded only a gold-tin alloy. Bulk deposition of tin on gold and on copper was observed at about -0.75, -0.25 and -0.1 V from $[Py_{1,4}]$TfO, $[Py_{1,4}]$DCA and [EMIm]DCA, respectively. A change in the morphology of the tin deposits was observed upon changing the anion of the ILs from TfO^- to DCA^-. Dendrite-free tin deposits were obtained from $[Py_{1,4}]$TfO, whereas tin dendrimers were obtained from both $[Py_{1,4}]$DCA and [EMIm]DCA. Apart from presumably different interfacial layers, different complexation of $SnCl_2$ species in the three different ILs occurs. IR spectra indicated that different complexes are formed in the different ILs. The XRD analysis of the deposits obtained on gold and copper from the three ILs indicated the existence of tetragonal tin. Alloy formation of tin with gold or copper seems to be suppressed by $[Py_{1,4}]$TfO in comparison to ILs with the DCA ion.

This study reveals that dendrite-free tin deposits can be obtained from $[Py_{1,4}]$TfO and that both anion and cation play a role in the deposition process.

5.3 Electrodeposition of ZnSn thin films and nanowires

The electrochemical deposition of Zn-Sn films and nanowires from ionic liquids was successful. Zn, Sn, and Zn-Sn biphasic films were electrodeposited from $[Py_{1,4}]$TfO. SEM showed that Zn deposit obtained from 0.05 M $Zn(TfO)_2$/$[Py_{1,4}]$TfO are nanocrystalline, whereas a microcrystalline Zn deposit was obtained from [EMIm]TfO, as also shown in literature. The difference in grain size can be explained by a different surface adsorption of the cations ($[Py_{1,4}]^+$

and $[EMIm]^+$) on the substrate. The Sn deposit shows grains of approximately 300–400 nm in size. The morphology of Zn-Sn deposits depends on the deposition potential.

Nanocrystalline Zn deposits can be obtained from $[Py_{1,4}]TfO$. The Zn–Sn co-deposit appears to be a mixture of Zn and Sn particles. The results of XRD analysis show diffraction peaks of both Sn and Zn in the films. Zn–Sn nanowires with a diameter of 100 nm are rather brittle, whereas free-standing nanowires can be made with a pore size of 200 nm. The length of the wires can be controlled by the deposition time.

5.4 Electrodeposition of CuSn

Polystyrene spheres were self-assembled into three-dimensional close-packed arrays on the gold surface to act as a template for the synthesis of macroporous structures. A uniform periodicity of macroporous CuSn was obtained at -1V for 10 minutes from 0.05 M $SnCl_2$ + 0.25 M CuCl in [EMIm]DCA.

Increasing the time of deposition (15 min.) at the same potential leads to three dimensional CuSn deposits. The template assisted process was used to produce CuSn nanowires with an average diameter of 100 nm and a length of 7μm. The wires are free standing and are less bunched together as the obtained Sn nanowires. The higher concentration of Cu in the alloy gives more mechanical stability to the nanowires.

5.5 Electrodeposion of SiSn nanowires

A template free process was used to make SiSn nanowires from an ionic liquid solution containing 0.1 M $SnCl_2$ + 0.1M $SiCl_4$ in $[Py_{1,4}]TfO$. Sn, Si and SiSn deposits were obtained from $[Py_{1,4}]TfO$. The electrodeposition of tin gives thin films consisting of microcrystals. Greyish white Silicon deposits were obtained galvanostatically at -20 μA from 0.1M $SiCl_4$/$[Py_{1,4}]TfO$.

Thin films consisting of tiny SiSn particles were obtained by direct potentiostatic electrodeposition at -2V for 1 hour. When the electrodeposition process is done after runing cyclic voltammetry, hair-like SiSn nanowires were obtained, that can be free standing nanowires.

6. Appendix [199,214]

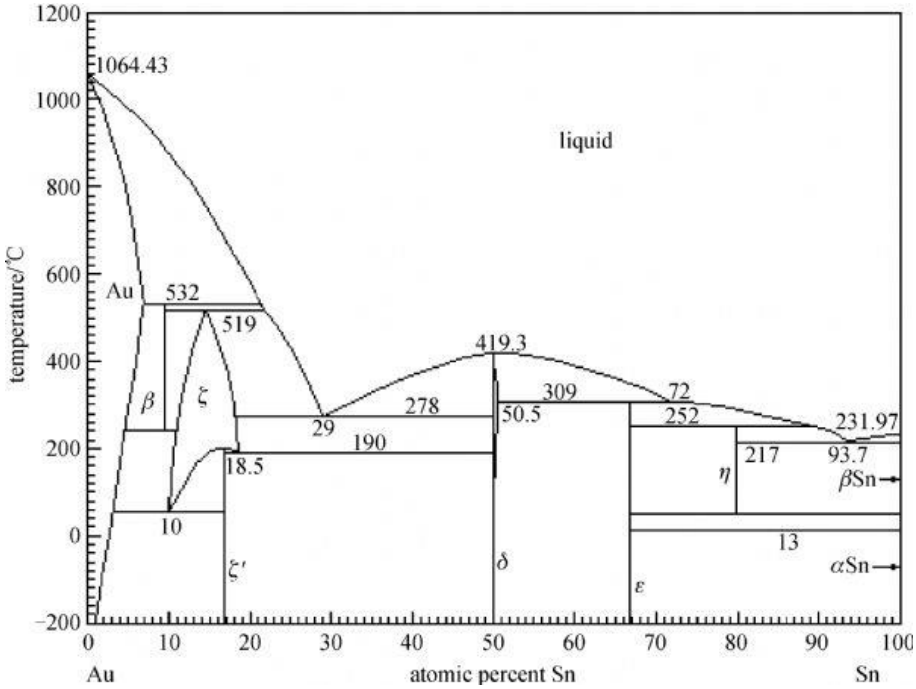

Au-Sn phase diagram [199]

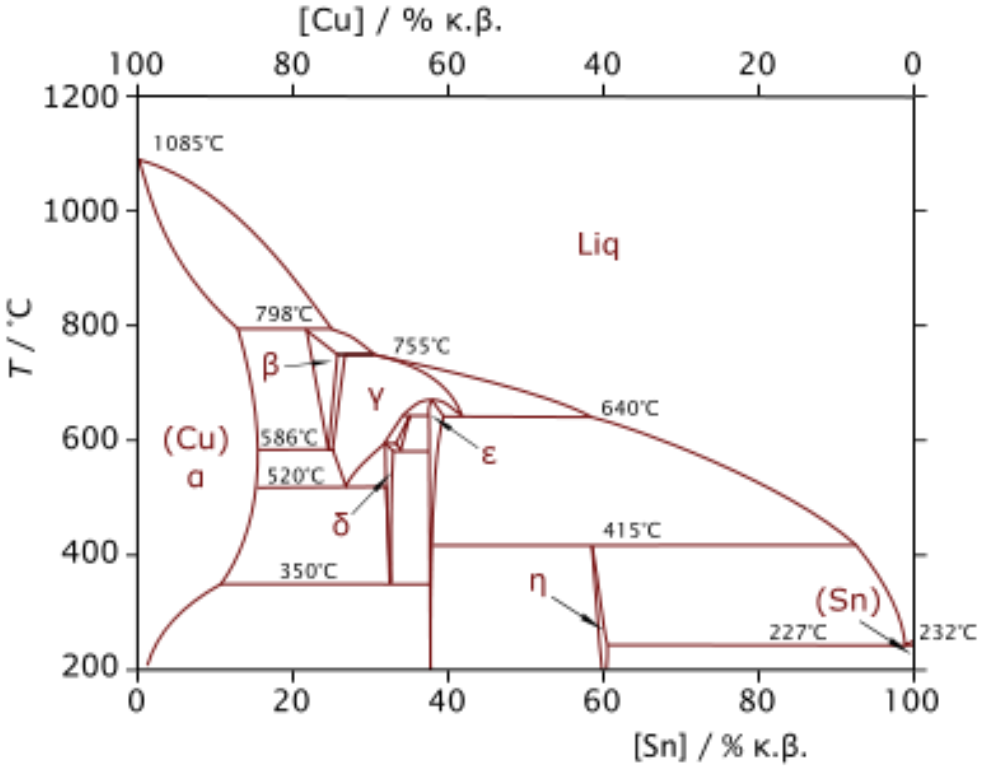

CuSn phase diagram. [214]

7. Outlook

The present work shows the electrodeposition of tin and/or of some tin alloys from ionic liquids in the form of free standing nanowires, thin films and macroporous structures. The employed ionic liquids are 1-ethyl-3-methylimidazolium dicyanamide ([EMIm]DCA), 1-butyl-1-methylpyrrolidinium dicyanamide ($[Py_{1,4}]$DCA) and 1-butyl-1-methylpyrrolidinium trifluoromethylsulfonate ($[Py_{1,4}]$TfO).

The results obtained here might give rise to further studies

- Electrodeposition of other Sn based alloys such as AlSn, InSn, NbSn which already have many important applications. The electrodeposition process could be performed using different ionic liquids that are more electrochemically stable such as tris(pentafluoroethyl)trifluorophosphate ($[Py_{1,4}]$FAP) or with hydrophobic character such as 1-butyl-1-methylpyrrolidinium bis(trifluoromethylsulfonyl)amide ($[Py_{1,4}]$TFSA), as a few examples.
- The effect of temperature on the structure of the deposits is an important factor that can influence the morphology and crystallinity of the obtained films, therefore the study of electrodeposition of tin and tin based material at elevated temperature is one important future task.
- Additives have a strong effect on the electrodeposition process, thus it would be important to study the effect of different additives on the electrodeposition of tin and tin based materials.

8. References

[1] F. Endres, D. MacFarlane, A. Abbott, Electrodeposition from ionic liquids, Wiley-VCH, Weinheim, **2008**, 4-208.

[2] K.R. Seddon, Molten salt chemistry and technology 5 ; proceedings of the 5th International Symposium on Molten Salt Chemistry and Technology, Dresden, Germany, August 1997. In: Wendt, H. (ed.): MS5. Molten salt forum, **1998**, p. 53.

[3] D. Pletcher, F. Walsh, Industrial electrochemistry, 2nd ed., Blackie Academic & Professional, London, New York, **1993**.

[4] Z. Yinghuai, K. Tang, N. S., Chapt. 13, Applications of Ionic Liquids in Lignin Chemistry, in: J.-i. Kadokawa (Ed.), Ionic Liquids - New Aspects for the Future, InTech, **2013**, pp. 319–321.

[5] A. Winkel, P. Reddy, R. Wilhelm, Synthesis, 2008 (**2008)** 999–1016.

[6] P. Walden, Bulletin of the Russian Academy of Sciences (**1914)** 405–422.

[7] F.H. Hurley, T.P. WIer, Electrochem. Soc., 98 (**1951)** 207.

[8] R.J. Gale, B. Gilbert, R.A. Osteryoung, Inorg. Chem., 17 (**1978)** 2728–2729.

[9] J. Robinson, R.A. Osteryoung, Am. Chem. Soc., 101 (**1979)** 323–327.

[10] J.S. Wilkes, J.A. Levisky, R.A. Wilson, C.L. Hussey, Inorg. Chem., 21 (**1982)** 1263–1264.

[11] T.B. Scheffler, C.L. Hussey, K.R. Seddon, C.M. Kear, P.D. Armitage, Inorg. Chem., 22 (**1983)** 2099–2100.

[12] D. Appleby, C.L. Hussey, K.R. Seddon, J.E. Turp, Nature, 323 (**1986)** 614–616.

[13] C.L. Hussey, Adv. Molten Salt Chem, 5 (**1983)** 185–229.

[14] H.A. Øye, M. Jagtoyen, T. Oksefjell, J.S. Wilkes, Materials Science Forum, 73-75 (**1991)** 183–190.

[15] P. Koronaios, D. King, R.A. Osteryoung, Inorg. Chem., 37 (**1998)** 2028–2032.

[16] S.E. Fry, N.J. Pienta, Am. Chem. Soc., 107 (**1985)** 6399–6400.

[17] J.A. Boon, J.A. Levisky, J.L. Pflug, J.S. Wilkes, Org. Chem., 51 (**1986)** 480–483.

[18] R. Hagiwara, Y. Ito, Fluorine Chem., 105 (**2000)** 221–227.

[19] J.S. Wilkes, M.J. Zaworotko, Chem. Soc., Chem. Commun. (**1992)** 965.

[20] F. Endres, PCCP, 3 (**2001)** 3165–3174.

[21] P. Bonhôte, A.-P. Dias, N. Papageorgiou, K. Kalyanasundaram, M. Grätzel, Inorg. Chem., 35 (**1996)** 1168–1178.

[22] J. Fuller, R.T. Carlin, Proceedings of the Eleventh International Symposium on Molten Salts. In: Trulove, P., Delong, H. C., Stafford, G. R., Deki, S. (eds.). Proceedings of Electrochemical Society, **1998**, p. 227.

[23] D.R. MacFarlane, P. Meakin, J. Sun, N. Amini, M. Forsyth, Phys. Chem. B, 103 (**1999)** 4164–4170.

[24] P. Wasserscheid, T. Welton, Ionic Liquids in Synthesis, Wiley-VCH Verlag GmbH & Co. KGaA, Weinheim, Germany, **2007**.

[25] K. Marsh, J. Boxall, R. Lichtenthaler, Fluid Phase Equilibria, 219 (**2004)** 93–98.

[26] F. Endres, S. Zein El Abedin, PCCP, 8 (**2006)** 2101–2116.

[27] Souza, Michèle O. de, Journal of the Brazilian Chemical Society, 25 (**2014)** 2140–2150.

[28] K.R. Seddon, Kinet. Catal, 37 (**1996)** 693–697.

[29] M.J. Earle, K.R. Seddon, Pure Appl. Chem., 72 (**2000)** 1391–1398.

[30] P. Wasserscheid, W. Keim, Angew. Chem. Int. Ed., 39 (**2000)** 3772–3789.

[31] T. Welton, Chem. Rev., 99 (**1999)** 2071–2084.

[32] M.E. Valkenburg, R.L. Vaughn, M. Williams, J.S. Wilkes (Eds.), Fifteenth Symposium on Thermophysical Properties, Boulder, Colorado, USA, **2003**.
[33] M.E. Valkenburg, R.L. Vaughn, M. Williams, J.S. Wilkes, Thermochimica Acta, 425 (**2005)** 181–188.
[34] H. Davis, Jr., James, Chem. Lett., 33 (**2004)** 1072–1077.
[35] P. Wasserscheid and T. Welton (Ed.), Ionic Liquids in Synthesis, Wiley-VCH, Weinheim, **2003**.
[36] M. Freemantle, An Introduction to ionic liquids, RSC Pub., Cambridge, UK, **2010**, 34-38.
[37] M. Galiński, A. Lewandowski, I. Stępniak, Electrochimica Acta, 51 (**2006)** 5567–5580.
[38] N. Borissenko, S. Zein El Abedin, F. Endres, Phys. Chem. B, 110 (**2006)** 6250–6256.
[39] T.J. Melton, Electrochem. Soc., 137 (**1990)** 3865.
[40] S.V. Dzyuba, R.A. Bartsch, ChemPhysChem, 3 (**2002)** 161–166.
[41] K.R. Seddon, A. Stark, M.-J. Torres, Pure Appl. Chem., 72 (**2000)**.
[42] L.L. Lazarus, C.T. Riche, N. Malmstadt, R.L. Brutchey, Langmuir, 28 (**2012)** 15987–15993.
[43] J. Stoimenovski, D.R. MacFarlane, K. Bica, R.D. Rogers, Pharmaceutical Research, 27 (**2010)** 521–526.
[44] F. Postleb, D. Stefanik, H. Seifert, R. Giernoth, Z. Naturforsch. B, 68b (**2013)** 1123–1128.
[45] D.A. Fort, R.P. Swatloski, P. Moyna, R.D. Rogers, G. Moyna, Chem. Commun. (Cambridge, England) (**2006)** 714–716.
[46] A.A. Lapkin, P.K. Plucinski, M. Cutler, Nat Prod., 69 (**2006)** 1653–1664.
[47] T. Waldmann, H.-H. Huang, H.E. Hoster, O. Höfft, F. Endres, R.J. Behm, ChemPhysChem, 12 (**2011)** 2565–2567.
[48] Y. Chauvin, B. Gilbert, I. Guibard, Chem. Soc., Chem. Commun. (**1990)** 1715.
[49] R.T. Carlin, J.S. Wilkes, Mol. Cat., 63 (**1990)** 125–129.
[50] Y. Chauvin, L. Mussmann, H. Olivier, Angew. Chem. Int. Ed., 34 (**1996)** 2698–2700.
[51] P.A. Suarez, J.E. Dullius, S. Einloft, R.F. De Souza, J. Dupont, Polyhedron, 15 (**1996)** 1217–1219.
[52] P.J. Dyson, T.J. Geldbach, Metal catalysed reactions in ionic liquids, Springer, Dordrecht, **2005**.
[53] C. Daguenet, P.J. Dyson, Organometallics, 23 (**2004)** 6080–6083.
[54] P. Giridhar, K.A. Venkatesan, T.G. Srinivasan, P.V. Rao, Electrochimica Acta, 52 (**2007)** 3006–3012.
[55] M. Jayakumar, K.A. Venkatesan, T.G. Srinivasan, Electrochimica Acta, 52 (**2007)** 7121–7127.
[56] M. Jayakumar, K.A. Venkatesan, T.G. Srinivasan, Vasudeva Rao, P. R., Appl. Electrochem., 39 (**2009)** 1955–1962.
[57] C.J. Rao, K.A. Venkatesan, K. Nagarajan, T.G. Srinivasan, Radiochimica Acta, 96 (**2008)**.
[58] C. Jagadeeswara Rao, K.A. Venkatesan, K. Nagarajan, T.G. Srinivasan, Vasudeva Rao, P. R., Nucl. Mater., 408 (**2011)** 25–29.
[59] C. Jagadeeswara Rao, K.A. Venkatesan, K. Nagarajan, T.G. Srinivasan, Vasudeva Rao, P. R., Electrochimica Acta, 54 (**2009)** 4718–4725.
[60] A.J. Carmichael, K.R. Seddon, Phys. Org. Chem., 13 (**2000)** 591–595.
[61] C.M. Gordon, A.J. McLean, Chem. Commun. (**2000)** 1395–1396.
[62] M. Alvaro, E. Carbonell, B. Ferrer, H. Garcia, J.R. Herance, Photochemistry and photobiology, 82 (**2006)** 185–190.
[63] M. Matsunaga, Electrochemistry, 70 (**2002)** 126.

[64] R. Hagiwara, Electrochemistry, 70 (**2002)** 130.
[65] A. Noda, M. Watanabe, Electrochemistry, 70 (**2002)** 140–144.
[66] N. Koura, Y. Suzuki, F. Matsumoto, Electrochemistry, 70 (**2002)** 203.
[67] R.D. Rogers, K.R. Seddon, S. Volkov, Green industrial applications of ionic liquids, Kluwer Academic Publishers, Dordrecht, Boston, **2002**.
[68] H. Ohno, Electrochemical aspects of ionic liquids, Wiley-Interscience, Hoboken, N.J., **2005**.
[69] J.F. Liu, G.B. Jiang, J.Å. Jönsson, Trends Anal. Chem., 24 (**2005)** 20–27.
[70] Di Wei, A. Ivaska, Anal.Chim. Acta, 607 (**2008)** 126–135.
[71] P. He, H. Liu, Z. Li, Y. Liu, X. Xu, J. Li, Langmuir, 20 (**2004)** 10260–10267.
[72] S. Zein El Abedin, N. Borissenko, F. Endres, Electrochem. Commun., 6 (**2004)** 422–426.
[73] J. Robinson, Electrochem. Soc., 127 (**1980)** 122.
[74] B.J. Welch, R.A. Osteryoung, Electroanal. Chem., 118 (**1981)** 455–466.
[75] P.K. Lai, M. Skyllas-Kazacos, Electroanal. Chem., 248 (**1988)** 431–440.
[76] Q. Liao, Electrochem. Soc., 144 (**1997)** 936.
[77] A.P. Abbott, C.A. Eardley, N.R. Farley, G.A. Griffith, A. Pratt, Appl. Electrochem., 31 (**2001)** 1345–1350.
[78] F. Endres, M. Bukowski, R. Hempelmann, H. Natter, Angew. Chem. Inter. Ed., 42 (**2003)** 3428–3430.
[79] M. Lipsztajn, R.A. Osteryoung, Inorg. Chem., 24 (**1985)** 716–719.
[80] B.J. Piersma, Electrochem. Soc., 143 (**1996)** 908.
[81] G.E. Gray, Electrochem. Soc., 142 (**1995)** 3636.
[82] K. Kim, C. Lang, R. Moulton, P.A. Kohl, Electrochem. Soc., 151 (**2004)** A1168.
[83] J.S.-Y. Liu, Electrochem. Soc., 144 (**1997)** 140.
[84] M.K. Carpenter, M.W. Verbrugge, Mater. Res., 9 (**1994)** 2584–2591.
[85] P.-Y. Chen, Electrochem. Soc., 146 (**1999)** 3290.
[86] W.R. Pitner, Electrochem. Soc., 144 (**1997)** 3095.
[87] D.A. Habboush, R.A. Osteryoung, Inorg. Chem., 23 (**1984)** 1726–1734.
[88] M. Lipsztajn, R.A. Osteryoung, Inorg. Chem., 24 (**1985)** 3492–3494.
[89] E.G.-S. Jeng, Electrochem. Soc., 144 (**1997)** 2369.
[90] Y.-F. Lin, I.-W. Sun, Electrochimica Acta, 44 (**1999)** 2771–2777.
[91] P.-Y. Chen, M.-C. Lin, I.-W. Sun, Electrochem. Soc., 147 (**2000)** 3350.
[92] P.-Y. Chen, I.-W. Sun, Electrochimica Acta, 46 (**2001)** 1169–1177.
[93] A.P. Abbott, G. Capper, K.J. McKenzie, K.S. Ryder, Electroanal. Chem., 599 (**2007)** 288–294.
[94] P.-Y. Chen, I.-W. Sun, Electrochimica Acta, 45 (**1999)** 441–450.
[95] K. Murase, K. Nitta, T. Hirato, Y. Awakura, Appl. Electrochem., 31 (**2001)** 1089–1094.
[96] S. Zein El Abedin, A.Y. Saad, H.K. Farag, N. Borisenko, Q.X. Liu, F. Endres, Electrochimica Acta, 52 (**2007)** 2746–2754.
[97] P.-Y. Chen, I.-W. Sun, Electrochimica Acta, 45 (**2000)** 3163–3170.
[98] J.-F. Huang, I.-W. Sun, Electrochem. Soc., 149 (**2002)** E348.
[99] A.P. Abbott, G. Capper, D.L. Davies, R.K. Rasheed, Chemistry (Weinheim, Germany), 10 (**2004)** 3769–3774.

[100] A.P. Abbott, G. Capper, D.L. Davies, R.K. Rasheed, J. Archer, C. John, Trans. Inst. Met. Finish., 82 (**2004)** 14–17.
[101] C.-C. Tai, F.-Y. Su, I.-W. Sun, Electrochimica Acta, 50 (**2005)** 5504–5509.
[102] F.-Y. Su, J.-F. Huang, I.-W. Sun, Electrochem. Soc., 151 (**2004)** C811.
[103] S.-I. Hsiu, C.-C. Tai, I.-W. Sun, Electrochimica Acta, 51 (**2006)** 2607–2613.
[104] M. Yang, I. Sun, Appl. Electrochem., 33 (**2003)** 1077–1084.
[105] M.-H. Yang, M.-C. Yang, I.-W. Sun, Electrochem. Soc., 150 (**2003)** C544.
[106] X.-H. Xu, Electrochem. Soc., 139 (**1992)** 1295.
[107] F. Endres, W. Freyland, Phys. Chem. B, 102 (**1998)** 10229–10233.
[108] C.A. Zell, F. Endres, W. Freyland, PCCP, 1 (**1999)** 697–704.
[109] Y. Katayama, S. Dan, T. Miura, T. Kishi, Electrochem. Soc., 148 (**2001)** C102.
[110] P. He, H. Liu, Z. Li, J. Li, Electrochem. Soc., 152 (**2005)** E146.
[111] S. Zein El Abedin, E.M. Moustafa, R. Hempelmann, H. Natter, F. Endres, Electrochem. Commun., 7 (**2005)** 1111–1116.
[112] S. Zein El Abedin, E.M. Moustafa, R. Hempelmann, H. Natter, F. Endres, ChemPhysChem, 7 (**2006)** 1535–1543.
[113] Y. NuLi, J. Yang, P. Wang, Appl. Surf. Sci., 252 (**2006)** 8086–8090.
[114] P. Wang, Y. NuLi, J. Yang, Z. Feng, Surf. Coat. Technol., 201 (**2006)** 3783–3787.
[115] Z. Feng, Y. NuLi, J. Wang, J. Yang, Electrochem. Soc., 153 (**2006)** C689.
[116] Y. NuLi, J. Yang, R. Wu, Electrochem. Commun., 7 (**2005)** 1105–1110.
[117] G.T. Cheek, W.E. O'Grady, S. Zein El Abedin, E.M. Moustafa, F. Endres, Electrochem. Soc., 155 (**2008)** D91.
[118] Y. Katayama, T. Morita, M. Yamagata, T. Miura, Electrochemistry, 71 (**2003)** 1033.
[119] P.C. Howlett, D.R. MacFarlane, A.F. Hollenkamp, Electrochem. Solid-State Lett., 7 (**2004)** A97.
[120] S. Zein El Abedin, U. Welz-Biermann, F. Endres, Electrochem. Commun., 7 (**2005)** 941–946.
[121] I. Mukhopadhyay, C.L. Aravinda, D. Borissov, W. Freyland, Electrochimica Acta, 50 (**2005)** 1275–1281.
[122] P.C. Howlett, E.I. Izgorodina, M. Forsyth, D.R. MacFarlane, Z. Phys. Chem., 220 (**2006)** 1483–1498.
[123] F. Endres, S. Zein El Abedin, A.Y. Saad, E.M. Moustafa, N. Borissenko, W.E. Price, G.G. Wallace, D.R. MacFarlane, P.J. Newman, A. Bund, PCCP, 10 (**2008)** 2189–2199.
[124] F. Endres, Electrochem. Solid-State Lett., 5 (**2002)** C38.
[125] F. Endres, S. Zein El Abedin, PCCP, 4 (**2002)** 1649–1657.
[126] F. Endres, S. Zein El Abedin, Chem. Commun. (**2002)** 892–893.
[127] S. Zein El Abedin, N. Borissenko, F. Endres, Electrochem. Commun., 6 (**2004)** 510–514.
[128] J. Mallet, M. Molinari, F. Martineau, F. Delavoie, P. Fricoteaux, M. Troyon, Nano Letters, 8 (**2008)** 3468–3474.
[129] J. Mallet, F. Martineau, K. Namur, M. Molinari, PCCP, 15 (**2013)** 16446–16449.
[130] G. Pulletikurthi, A. Lahiri, T. Carstens, N. Borisenko, S. Zein El Abedin, F. Endres, Solid State Electrochem., 17 (**2013)** 2823–2832.
[131] S.-I. Hsiu, I.-W. Sun, Appl. Electrochem., 34 (**2004)** 1057–1063.
[132] A. Lahiri, G. Pulletikurthi, S. Zein El Abedin, F. Endres, Solid State Electrochem. (**2014)**.

[133] A.M. Fenelon, C.B. Breslin, Electrochem. Soc., 152 (**2005)** D6.
[134] D.L. Boxall, R.A. Osteryoung, Electrochem. Soc., 151 (**2004)** E41.
[135] K. Sekiguchi, M. Atobe, T. Fuchigami, Electrochem. Commun., 4 (**2002)** 881–885.
[136] K. Wagner, J.M. Pringle, S.B. Hall, M. Forsyth, D.R. MacFarlane, D.L. Officer, Synthetic Metals, 153 (**2005)** 257–260.
[137] E. Naudin, H.A. Ho, S. Branchaud, L. Breau, D. Bélanger, Phys. Chem. B, 106 (**2002)** 10585–10593.
[138] T. Carstens, S. Zein El Abedin, F. Endres, ChemPhysChem, 9 (**2008)** 439–444.
[139] J. Emsley, Nature's building blocks: An A-Z guide to the elements, Oxford University Press, Oxford, New York, **2011**, 554.
[140] A.F. Holleman, N. Wiberg, E. Wiberg, "Tin". Lehrbuch der Chemie, 91st ed., Veit, Leipzig, **1985**, 793-800.
[141] A.M. Molodets, S.S. Nabatov, High Temp, 38 (**2000)** 715–721.
[142] M.L. Casella, G.J. Siri, G.F. Santori, O.A. Ferretti, M.M. Ramírez-Corredores, Langmuir, 16 (**2000)** 5639–5643.
[143] T.H. Geballe, Phys. Today, 46 (**1993)** 52.
[144] A. Godeke, Supercond. Sci. Technol., 19 (**2006)** R68.
[145] M. Winter, J.O. Besenhard, Electrochimica Acta, 45 (**1999)** 31–50.
[146] R.A. Huggins, Power Sources, 81-82 (**1999)** 13–19.
[147] A. Finke, P. Poizot, C. Guéry, J.-M. Tarascon, Electrochem. Soc., 152 (**2005)** A2364.
[148] I. Amadei, S. Panero, B. Scrosati, G. Cocco, L. Schiffini, Power Sources, 143 (**2005)** 227–230.
[149] I.S. Kim, G.E. Blomgren, P.N. Kumta, Electrochem. Solid-State Lett., 7 (**2004)** A44.
[150] O. Mao, Electrochem. Soc., 146 (**1999)** 405.
[151] S.D. Beattie, J.R. Dahn, Electrochem. Soc., 150 (**2003)** A894.
[152] H. Mukaibo, T. Sumi, T. Yokoshima, T. Momma, T. Osaka, Electrochem. Solid-State Lett., 6 (**2003)** A218.
[153] J. Hassoun, S. Panero, B. Scrosati, Power Sources, 160 (**2006)** 1336–1341.
[154] F. Bauch, F.F. Oplinger, in: A.G. Gray (Ed.), Modern Electroplating, wiley, New York, **1953**, pp. 387–409.
[155] J.W. Cuthberton, in: E.S. Hedges (Ed.), Tin and its alloys, Edward Arnold, London, Chapt. V, **1960**, p. 99.
[156] F. A. Lowenheim, in Electroplating (Ed.:F. A. Lowenheim), McGraw-Hill, New York, **1978**, pp. 307–320.
[157] J.I. Duffy, in Electroplating Technology: Recent Developments (Ed.: J. I. Duffy), Noyes Data Corporation, Park Ridge, New Jersey, **1981**, pp. 92–120.
[158] J.W. Price, Tin and tin-alloy plating, Electrochemical Publications, Ayr, Scotland, **1983**, pp. 5.
[159] Y. Zhang, J. A. Abys, in Modern Electroplating, 4th ed. (Eds.: M. Schlesinger, M. Paunovic), Wiley-Interscience, New York, **2000**, pp. 139.
[160] C. Low, F.C. Walsh, Electrochimica Acta, 53 (**2008)** 5280–5286.
[161] C. Santato, C.M. López, K.-S. Choi, Electrochem. Commun., 9 (**2007)** 1519–1524.
[162] F. Endres, ChemPhysChem, 3 (**2002)** 144–154.
[163] A.P. Abbott, K.J. McKenzie, PCCP, 8 (**2006)** 4265–4279.
[164] M. Armand, F. Endres, D.R. MacFarlane, H. Ohno, B. Scrosati, Nat. Mater, 8 (**2009)** 621–629.

[165] A. Betts, US patent, 712277, **1902**.
[166] H.L. Hollis, US patent, 916155, **1909**.
[167] M. Schloetter, British patent, 329308, **1929**.
[168] M. Schloetter, British patent, 443429, **1936**.
[169] A.H. Alexander, J.R. Stack, Trans. Am. Inst. Mining and Met. Eng., 70 (**1924)** 404.
[170] F.C. Mathers, US patent, 1397222, **1921**.
[171] C.A. Dischee, F.C. Mathers, Electrochem. Soc., 102 (**1955)** 387.
[172] H. Nawafune, Lead-free soldering in electronics: Science, technology and environmental impact, Chapter 4, ed. by K. Suganuma, Marcel Dekker; Momenta, New York, London, **2004**, pp. 91.
[173] K. Whitlaw, J. Crosby, M. Toben, Circuit World, 32 (**2006)** 23–30.
[174] A. He, Q. Liu, D.G. Ivey, Mater Sci: Mater Electron, 19 (**2008)** 553–562.
[175] F. Lowenheim, Modern Electroplating, 3rd ed., (John Wiley and Sons, New York), **1974**.
[176] Tin Research Institute. Instruction for Electrodepositing Tin, 5th ed., 1979. in T.M.C. Nogueira, Ph.D. Thesis, Universidade Federal de São Carlos, Brazil, **(1996)**.
[177] S. Hirsch, Metal Finishing, 93 (**1995)** 298–313.
[178] J.P. Nityanandan, H.V. Udupa, Metal Finishing (**1973)** 44.
[179] T.T. Campbell, R. Abel, Codepositlon of Tin-Nickel Plate From Organic and Mixed Aqueous-Organic Solvents:, Washington, D.C. U.S. Dept. of the Interior, Bureau of Mines Rept. of Investigations, 5482, **1959**, pp. 11.
[180] X.-H. Xu, Electrochem. Soc., 140 (**1993)** 618.
[181] J.-F. Huang, I.-W. Sun, Electrochem. Soc., 150 (**2003)** E299.
[182] G. Ling, N. Koura, Electrochemistry, 65 (**1997)** 149–153.
[183] N. Tachikawa, N. Serizawa, Y. Katayama, T. Miura, Electrochimica Acta, 53 (**2008)** 6530–6534.
[184] M. Morimitsu, Y. Nakahara, Y. Iwaki, M. Matsunaga, Min. Metall., B Metall., 39 (**2003)** 59–67.
[185] M. Morimitsu, Y. Nakahara, M. Matsunaga, Electrochemistry, 73 (**2005)** 754–757.
[186] M.-J. Deng, T.-I. Leong, I.-W. Sun, P.-Y. Chen, J.-K. Chang, W.-T. Tsai, Electrochem. Solid-State Lett., 11 (**2008)** D85.
[187] F. Endres, O. Höfft, N. Borisenko, L.H. Gasparotto, A. Prowald, R. Al-Salman, T. Carstens, R. Atkin, A. Bund, S. Zein El Abedin, PCCP, 12 (**2010)** 1724–1732.
[188] N.M. Rocher, E.I. Izgorodina, T. Rüther, M. Forsyth, D.R. MacFarlane, T. Rodopoulos, M.D. Horne, A.M. Bond, Chemistry (Weinheim, Germany), 15 (**2009)** 3435–3447.
[189] E.M. Moustafa, S. Zein El Abedin, A. Shkurankov, E. Zschippang, A.Y. Saad, A. Bund, F. Endres, Phys. Chem. B, 111 (**2007)** 4693–4704.
[190] R. Atkin, S. Zein El Abedin, R. Hayes, L.H.S. Gasparotto,, N. Borisenko, F. Endres, Phys. Chem. C, 113 (**2009)** 13266–13272.
[191] Q.X. Liu, S. Zein El Abedin, F. Endres, Electrochem. Soc., 155 (**2008)** D357.
[192] S. Zein El Abedin, P. Giridhar, P. Schwab, F. Endres, Electrochem. Commun., 12 (**2010)** 1084–1086.
[193] P. Giridhar, S. Zein El Abedin, F. Endres, Solid State Electrochem., 16 (**2012)** 3487–3497.
[194] M. Wu, N.R. Brooks, S. Schaltin, K. Binnemans, J. Fransaer, PCCP, 15 (**2013)** 4955–4964.
[195] R. Al-Salman, M. Al Zoubi, F. Endres, Mol. Liq., 160 (**2011)** 114–118.

[196] A.J. Bard, L.R. Faulkner, Electrochemical methods: Fundamentals and applications, 2nd ed., John Wiley and Sons, New York, **2001**, 114–115.
[197] P. Scherrer, Göttinger, Nachrichten Gesell, 2 (**1918)** 98.
[198] Elbasiony, A. M. R., S. Zein El Abedin, F. Endres, Solid State Electrochem., 18 (**2014)** 951–957.
[199] H. Okamoto, T.B. Massalski, Phase diagrams of binary gold alloys, ASM International, Metals Park, Ohio, **1987**, 278–289.
[200] W.A. Harrison, Electronic structure and the properties of solids, Freeman, San Francisco CA, **1980**, 1–586.
[201] G.S. Matijasevic, C.C. Lee, C.Y. Wang, Thin Solid Films, 223 (**1993)** 276–287.
[202] S. Zein El Abedin, F. Endres, ChemPhysChem, 13 (**2012)** 250–255.
[203] Y.-L. Kim, Y.-K. Sun, S.-M. Lee, Electrochimica Acta, 53 (**2008)** 4500–4504.
[204] P. Giridhar, A.M. Elbasiony, S. Zein El Abedin, F. Endres, ChemElectroChem, 1 (**2014)** 1549–1556.
[205] D.H. Johnston, D.F. Shriver, Inorg. Chem., 32 (**1993)** 1045–1047.
[206] D. Tevault, K. Nakamoto, Inorg. Chem., 15 (**1976)** 1282–1287.
[207] O.B. Babushkina, S. Ekres, G.E. Nauer, Z. Naturforsch, A, 63a (**2008)** 73–80.
[208] B. Jürgens, H.A. Höppe, W. Schnick, Solid State Sciences, 4 (**2002)** 821–825.
[209] Z. Liu, A.M. Elbasiony, S. Zein El Abedin, F. Endres, ChemElectroChem, 2 (**2014)** 389–395.
[210] N.M. Pereira, S. Salomé, C.M. Pereira, A. Fernando Silva, Appl. Electrochem., 42 (**2012)** 561–571.
[211] M. Thackeray, J. Vaughey, C. Johnson, A. Kropf, R. Benedek, L. Fransson, K. Edstrom, Power Sources, 113 (**2003)** 124–130.
[212] R. Benedek, M.M. Thackeray, Power Sources, 110 (**2002)** 406–411.
[213] S. Zein El Abedin, A. Prowald, F. Endres, Electrochem. Commun., 18 (**2012)** 70–73.
[214] T.B. Massalski, Binary alloy phase diagrams, American Soc. for Metals, Metals Park, Ohio, **1986**, PP. 964.
[215] R.T. Collins, P.M. Fauchet, M.A. Tischler, Phys. Today, 50 (**1997)** 24.
[216] M.L. Mastronardi, E.J. Henderson, D.P. Puzzo, G.A. Ozin, Adv. Mater., 24 (**2012)** 5890–5898.
[217] Y. Katayama, M. Yokomizo, T. Miura, T. Kishi, Electrochemistry, 69 (**2001)** 834–836.
[218] R. Al-Salman, S. Zein El Abedin, F. Endres, PCCP, 10 (**2008)** 4650–4657.
[219] F. Bebensee, N. Borissenko, M. Frerichs, O. Höfft, W. Maus-Friedrichs, S. Zein El Abedin, F. Endres, Z. Phys. Chem., 222 (**2008)** 671–686.
[220] R. Al-Salman, J. Mallet, M. Molinari, P. Fricoteaux, F. Martineau, M. Troyon, S. Zein El Abedin, F. Endres, PCCP, 10 (**2008)** 6233–6237.
[221] A.W. Fang, H. Park, O. Cohen, R. Jones, M.J. Paniccia, J.E. Bowers, Opt. Express, 14 (**2006)** 9203.
[222] M. Zacharias, J. Heitmann, R. Scholz, U. Kahler, M. Schmidt, J. Bläsing, Appl. Phys. Lett., 80 (**2002)** 661.
[223] E. Simoen, C. Claeys (Eds.), "Tin Doping Effects in Silicon": Electrochem. Soc. Proc., **2000**, 17: 223.
[224] A.M. Hussain, H.M. Fahad, N. Singh, K.R. Rader, G.A.T. Sevilla, U. Schwingenschlögl, M.M. Hussain, Exploring SiSn as channel material for LSTP device applications, in: Device Research Conference (DRC), 2013 71st Annual, vol., no., pp. 93-94, 23-26 June 2013.
[225] Y. Akasaka, K. Horie, G. Nakamura, K. Tsukamoto, Y. Yukimoto, Appl. Phys., 13 (**1974)** 1533–1540.
[226] S. Zein El Abedin, A. Garsuch, F. Endres, Aust. J. Chem., 65 (**2012)** 1529.

9. CV and publications

PERSONAL DATA:

Name: Amr Mohamed Wahba Elbasiony
Nationality: Egyptian
Date of Birth: 24/9/1984
Marital Status: Single
Permanent address: National Research Centre 33 El Bohouth, Ad Doqi, Giza, Cairo
Current address: Osteröder Straße 49, D 38678 Clausthal-Zellerfeld, Germany.**TEL: +49** 17691101506
E-Mail: chem_orgnic2000@yahoo.com

ACADEMIC QUALIFICATIONS:

- M.Sc. "Corrosion Resistance Improvement of Titanium and 316L Stainless Steel in Simulated Body Fluid" Mansoura University 2009.
- Preliminary M.Sc. Courses In Physical, Inorganic And Analytical Chemistry, Mansoura University, May 2006.
- B.Sc., Chemistry, Mansoura University, May 2005, very good, (77.2 %)
- Training (1 year) in glass and ceramic department & CECICO - Aveiro University-Portugal "sol-gel coatings for Aluminum and Magnesium alloys"

Area of research

- Materials Science
- Nanotechnology
- Electrochemistry

Research experiences

- Assistant researcher at National Research Centre- Egypt - Advanced materials and Nanotechnology lab. 2006 – 2011
- Junior researcher in the frame of two RTD projects "Detection of micro-distribution of chemical species in solution near the active metals and "Nanostructured sol-gel pre-treatments for aluminum alloys used in aeronautics" at Ceramic and Glass Engineering department - University of Aveiro-Portugal 2011-2012
- PhD candidate at Clausthal University of Technology - Germany 2012- present

Publications within the framework of this thesis:

1- Electrochemical synthesis of freestanding tin nanowires from ionic liquids
***A. M. R. Elbasiony**, S. Zein El Abedin, F. Endres, J. Solid State Electrochem. (2014) 18:951–957*

2- A Comparative Study on the Electrodeposition of Tin from Two Different Ionic Liquids: Influence of the Anion on the Morphology of the Tin Deposits
*P. Giridhar, **A. M. Elbasiony**, S. Zein El Abedin, F. Endres, ChemElectroChem. (2014) 1: 1549–1556*

3- Electrodeposition of Zinc–Copper and Zinc–Tin Films and Free-Standing Nanowire Arrays from Ionic Liquids
*Z. Liu, **A. M. Elbasiony**, S. Zein El Abedin, F. Endres, ChemElectroChem. (2015) 2: 389–395*

4- Template-Free Electrodeposition of SnSi Nanowires from an Ionic Liquid
***A. M. Elbasiony**, S. Zein El Abedin, F. Endres, DOI: 10.1002/celc.201500124*

10.List of Abbreviations

$[BF_4]^-$	tetrafluoroborate
$[BMIm]BF_4$	1-butyl-3-methylimidazolium tetrafluoroborate
$[BMIm]PF_6$	1-Butyl-3-methylimidazolium hexafluorophosphate
[BMIm]TFSA	1-butyl-3-methyl-imidazolium bis(trifluoromethylsulfonyl)amide
$[BP^+ Cl]^-$	1-butylpyridinium chloride
CE	counter electrode
CV	cyclic voltammetry
$(CF_3SO_2)_3C^-$	tris(trifluoromethylsulfonyl)methide
$[(CF_3SO_2)_2N]^-$	bis(trifluoromethylsulfonyl)amide
$[CF_3SO_3]^-$	trifluoromethylsulfonate
$[DCA]^-$	dicyanamide
EDTA	ethylenediaminetetraacetic acid
EDX	energy dispersive X-ray (spectroscopy)
[EEMIm]TFSA	1,3-diethyl-5-methylimidazolium bis(trifluoromethylsulfonyl)amide
[EMIm]Cl	1-ethyl-3-methylimidazolium chloride
$[EMIm]Cl\text{-}BF_4$	1-ethyl-3-methylimidazolium chloride/tetrafluoroborate
[EMIm]DCA	1-ethyl-3-methylimidazolium dicyanamide
[EMIm]TFSA	1-ethyl-3-methyl imidazolium bis(trifluoromethylsulfonyl)amide
[EMMIm]TFSA	1-ethyl-2,3-dimethylimidazolium bis(trifluoromethylsulfonyl)amide
[EtPyBr]	1-ethylpyridinium bromide
HEDTA	(hydroxyethyl)ethylenediaminetriacetic acid
[HMIM]FAP	1-hexyl-3-methylimidazolium tris(pentafluoroethyl)trifluorophosphate
(Idranal VII)	*N*-(2-hydroxyethyl)ethylenediamine-*N*,*N'*,*N'*-triacetic acid trisodium salt

IR	infra-red spectroscopy
OCP	open circuit potential
PC	track-etched polycarbonate membranes
PEDOT	poly(3,4-ethylenedioxythiophene)
PPP	poly(p-phenylene)
PPV	Poly(p-phenylene vinylene)
PS	polystyrene
PT	polythiophene
[PF_6^-]	hexaflurophosphate
[$Py_{1,4}$] FAP	1-butyl-1-methylpyrrolidinium tris(pentafluoroethyl)trifluorophosphate
[$Py_{1,4}$]DCA	1-butyl-1-methylpyrrolidinium dicyanamide
[$Py_{1,4}$]TfO	1-butyl-1-methylpyrrolidinium trifluoromethylsulfonate
[$Py_{1,4}$]TFSA	1-butyl-1-methylpyrrolidinium bis(trifluoromethylsulfonyl)amide
RE	reference electrode
[RTILs]	room temperature ionic liquid
SEM	scanning electron microscopy
STM	in situ scanning tunneling microscope
[TMHA]TFSA	trimethyl-n-hexylammonium bis(trifluoromethylsulfonyl)amide
[TSIL]	task-specific ionic liquids
UPD	under potential deposition
WE	working electrode
XRD	X-ray diffraction analysis

11. Acknowledgement

First of All, Praise be to Allah, Who guided us to this; and in no way could we have been guided, unless Allah has guided us.

Staying at Clausthal University of Technology, Germany, has its own great inwardness not only in science but also in normal life. It gave me an opportunity to broaden my horizons, to learn a lot both in academic and everyday life and also to become a more tolerant and understanding personality so it's considered one of the most interesting and fantastic journeys in all my life.

I am deeply grateful to Prof. Dr. Frank Endres for his supervision, continuous support and valuable discussions. I am greatly indebted to him for giving me the opportunity to perform my Ph.D. under his supervision in his group on a highly interesting topic. I appreciate so much the fruitful discussions with him, not only in science, but also in everyday life as well.

I deeply thank him for offering in the working group an environment of trust and freedom which helps so much to do my work in a good way.

Also, I wish to express my deep thanks to Prof. Dr. S. Zein El Abedin for his great support and encouragement throughout the past period while doing my thesis from the inception phase till the end. I appreciate his support and advices during my stay in Clausthal which considered one of the most important steps in my life.

Many thanks to all our colleagues in the group for their kind help and warm feelings. As we have a very good team work who worked together as a family in an ideal working atmosphere.

Thanks to Dr. A. Prowald, Dr. P. Giridhar, Dipl.-Ing. S. Löffelholz and Mrs Karin Bode for making PS and PC templates, SEM/EDX measurements, XRD analysis and IR measurements.

I would like to express my deepest gratitude and appreciation to my parents, although they are no more alive, but their living sprits usually provide me the strength, support and love so I hope that they are satisfied and proud of me where they are and I ask Allah to bless them and shower them with mercy.

Finally, and to all of those, I would really like to say:

There are no words to match my gratitude.

Clausthal, 2015

Amr Mohamed Wahba El Basiony